UNITED STATES DEPARTMENT OF THE INTERIOR
GEOLOGICAL SURVEY

DATA SUMMARY FOR DENSE GEOS ARRAY OBSERVATIONS OF SEISMIC ACTIVITY ASSOCIATED WITH MAGMA TRANSPORT AT KILAUEA VOLCANO, HAWAII

by

Christopher Dietel [1], Bernard Chouet [1]

Keiiti Aki [2], Valerie Ferrazzini [2], Peter Roberts [2]

and

Robert Koyanagi [3]

Open-File Report 89-113

[1] *U.S. Geological Survey, Menlo Park, California*
[2] *University of Southern California, Los Angeles, California*
[3] *Hawaiian Volcano Observatory, Hawaii National Park, Hawaii*

January 30, 1989

CONTENTS

SUMMARY

From January 18 to February 28, 1988, the U.S. Geological Survey, Office of Earthquakes, Volcanoes and Engineering (OEVE) in cooperation with the University of Southern California (USC) and the Hawaiian Volcano Observatory (HVO) conducted a series of seismic experiments to monitor seismic activity associated with magma transport under Kilauea Volcano. A dense array of 11 six-channel digital recorders (GEOS) with an aperture of 0.8 by 0.8 km was deployed near Pu'u O'o on the east-rift of Kilauea Volcano and was operated from January 18 to 27. This network was reduced to a smaller, denser array of 12 GEOS recorders with an aperture of 120 m, which was operated from January 30 to February 20. In addition, four GEOS recorders were deployed and operated from February 20 to 28 near the summit of Kilauea to supplement six instruments deployed by the University of Southern California. This report gives a summary of the data obtained from the two arrays located on the east rift zone and from the four recorders located near the summit of Kilauea. Over 3000 minutes of harmonic tremor, gas-piston events, and earthquakes were recorded, yielding roughly 3.5 Gigabits of information.

A total of 16 preset windows, each of 3 minutes duration, was obtained on 10 or more GEOS instruments for periodic observations of harmonic tremor. While visually observing vigorous gas-piston activity in the Pu'u O'o vent, we recorded a 40-minute seismic record of tremor and two gas-piston events. In addition, 13 gas-piston events were recorded on 12 GEOS instruments operating in the trigger mode, and a second 40-minute window was recorded on 12 instruments to sample the seismicity after the vigor of the gas-piston activity within Pu'u O'o decreased. Our earthquake catalog includes 11 earthquakes with magnitudes ranging from M 1.8 to M 4.1 recorded on 10 or more instruments at Pu'u O'o and correlated to events in a Hawaiian Volcano Observatory CUSP listing. An additional 13 earthquakes with magnitudes ranging from M 1.4 to M 4.1 were recorded at the four GEOS stations located near the summit of Kilauea and correlated to events in a CUSP listing, and four long-period caldera events were recorded at the station located closest to Kilauea caldera.

The data shown in this report characterize the evolution of seismic activity induced by magma transport in the east rift zone of Kilauea Volcano. We have selected seismograms of harmonic tremor, gas-piston events, and earthquakes to characterize seismic wave coherence and propagation across the arrays. Seismograms, power spectra, moving window spectra, and three-dimensional plots of the wavefield generated by steady tremor and gas-piston activity in Pu'u O'o provide references for subsequent analysis.

Our report also describes the GEOS instrumentation and discusses the deployment, programming, and calibration procedures for the Hawaiian experiments. The Hawaiian data set proves the versatility of GEOS and its success in the recording of volcanically induced seismicity, and sets a precedent for future experiments on other volcanoes that require intensive seismic data aquisition.

INTRODUCTION

Knowledge of the dynamics of Hawaiian volcanoes can only be complete with an understanding of volcanic tremor. Koyanagi and others (1987) have shown that harmonic tremor, characterized by a regularly perturbed frequency pattern throughout its seismic signal, is associated with eruptive activity and below-surface magma movement in Hawaii. They have also shown that earthquake swarms, long-period events, and repetitive gas-piston events are often superimposed on backgrounds of volcanic tremor during eruption periods.

The continuing eruptive activity in the east rift of Kilauea has provided an excellent opportunity for a dense-array recording of harmonic tremor and other volcanically-induced ground motion. The GEOS data displayed in this report was obtained during the latest stage of relatively steady lava output in this sustained eruption of Kilauea.

A history of this eruptive activity, which began in January 1983, is given by Koyanagi and others (1987). Magma from beneath the summit of Kilauea moved into the east rift zone and erupted through linear fissure systems downrift from Napau crater. The eruptive fissures coalesced first to multiple vents, then to a single eruptive vent, later named Pu'u O'o, that produced repeated lava fountains.

The episodic high fountains, which alternated with longer repose periods, ended in July, 1986. The activity evolved into a continuous low-level outpouring of lava from a new vent (later named Kupaianaha) that opened nearly 3 km downrift. Pu'u O'o continued to degas, showing intermittent movements of lava within the vent and occasionally emitting pyroclastics during intervals of Strombolian activity. These lava movements, however, were mostly confined within the vent. Continuous low-level tremor indicated the persistent pressure oscillations from lava movement and degassing beneath Pu'u O'o. Similar, more localized signals were monitored at Kupaianaha, the active lava pond downrift. The temporal changes in the amplitude of the seismic signal from the HVO station STC, operated about 3 km west and uprift of Pu'u O'o, correlated with a variety of lava activity observed within the Pu'u O'o vent.

During the time of this experiment the main volume of lava was produced at Kupaianaha. The lava flowed downslope southeastward through a shallow tube system and

entered the sea near Kupapau Point, spreading occasionally along the coastal flats. The shallow tremor and related seismicity was localized beneath Pu'u O'o, at Kupaianaha, at points along the tube system extending from Kupaianaha, and at Kupapau Point where lava entered the sea.

As the Pu'u O'o vent widened, episodes of lava activity were accompanied by seismic events that occurred repeatedly during low-amplitude background tremor. Spindle-shaped envelopes of high signal amplitude with no clear shear-wave arrivals were linked to the vigorous bursting of gas slugs and collapse of the lava column in the volcanic conduit. This type of repetitive lava activity was termed "gas-piston activity" by Swanson, who observed a similar phenomenon during the eruption of Mauna Ulu (Swanson, 1979).

At the begining of our experiments in January, 1988, a steady harmonic tremor along the east rift zone was observed from HVO station STC. Visual observations were also conducted at Kupaianaha, indicating an almost constant flow of lava from the pond into the tube system leading to the sea.

Our objectives were to record tremor in sufficient detail to interpret the excitation mechanisms of tremor, and to record long-period events and earthquakes to determine the source mechanisms of deeper volcanic events beneath Kilauea. Three seismic arrays were set up on Kilauea Volcano, including two dense arrays near the base of Pu'u O'o on the east rift zone, and a broad array near the summit caldera. High-quality digital records of sustained tremor, gas-piston events, and earthquakes were obtained from the Pu'u O'o arrays, and gas-piston events were observed from the rim of the Pu'u O'o crater and compared with seismic recordings. The GEOS instruments deployed near the summit caldera supplemented the six instruments deployed by the University of Southern California; earthquakes and long-period events recorded with this network are also discussed in this report.

The Pu'u O'o experiment is the first to obtain recordings of volcanic tremor from a dense array of instruments, and it is the first to use the GEOS instruments in a configuration designed specifically to record volcanic seismicity, achieving accurate timing to within one millisecond. The 3.5 Gigabits of data collected offer an exceptional range of information, which will be used to study source mechanisms associated with magmatic

activity and to test new theories of the origin of volcanic tremor.

FIELD INSTRUMENTATION

A detailed description of the GEOS instrument (GEOS; General Earthquake Observation System) used to collect the data presented in this report is provided by Borcherdt and others (1985). This report provides only a general summary of instrumentation given in Appendix A. Subsequent chapters provide specific parameters and calibration procedures selected to record the Hawaiian data.

Timing Scheme

For the small, dense arrays used on the east rift zone, an accurate timing scheme was essential. In a design by Gary Maxwell, the internal clocks of the GEOS units were allowed to operate independently. The units in the array setups were interconnected with RG–174 wiring, custom-made with BNC and Bendix connectors, and cut in 12 sections with lengths of 500 to 1500 m to fit the special configuration of the initial array. A 1-Hz pulse was tapped from the "master" unit (pin S on the side panel monitoring plug) and fed into a power amplifier clock driver, which strengthened and divided the signal to reach the other "slave" units. The slave units received the 1-Hz pulse (pin G on the side panel monitor plug) and were programmed to treat the pulse as an external WWVB radio signal time code. Since the GEOS units take time corrections on only the initial rise of a WWVB time code, only a 1-Hz pulse from the master was necessary for an accurate time correction. The slave units determined the discrepancies between their own clocks and the master clock and were programmed to record these time corrections to magnetic tape every hour, achieving accurate time to within one millisecond. All timing corrections have been applied to the data presented in this report.

Sensors and Sensor Cabling

The two types of velocity sensors chosen for the Hawaiian experiments were the Mark Products three-component L–22–3D (natural frequency of 2 Hz and sensitivity of 0.5 V/cm/s) and the Mark Products vertical component L–4C (natural frequency of 2 Hz

and sensitivity of 1.0 V/cm/s). Connector plugs of both the L–4C and L–22–3D sensors are equipped with shunting resistors to standardize sensor sensitivity and damping. L–4C sensors are normally used with digital cassette recorders that have an imput impedance of 10kΩ. Since the GEOS recorders have a higher imput impedance of 100kΩ, it was necessary to reduce the resistance on the sensor output signals. This was achieved by adding an 11kΩ resistor to the plug shunt-resistor circuit (see Fig. 68) for the L–4C sensors.

Special sensor cables of 50 and 250 m lengths were designed by Gary Maxwell and Joe Sena, and assembled by Don Ritchey. Cables for single vertical component L–4C sensors were 250 m long, and plugs were spliced in at 50, 150, and 250 m from the GEOS recorder connector. Cables for the three-component L-22 sensors were 50 m long. No extra-length cables were necessary for stations deployed on the Kilauea summit.

FIELD PROCEDURES

Site Selection

A flat expanse of ponded lava flow covering approximately 0.5 km^2 was chosen for the setup of the two GEOS arrays deployed near Pu'u O'o. Figure 1 is a map showing the Kilauea summit-caldera and the location of the site chosen for the arrays on the east rift zone. The four stations OUT, MOB, MOA, and YNG deployed later near the Kilauea summit, and the six USC stations HVO, KEA, ESC, NEN, HIL, and PUO are also shown. The array site, located about 15 km east of the Kilauea caldera, consists of a fractured surface of hard, vesicular basalt formed when a massive pahoehoe flow from an eruption in 1986 ponded and cooled. The fringes of the site are broken up with pressure ridges caused by irregular flow. Tephra mounds and spatter cones line cracks and fissures on the southern edge of the site along the rift zone. The rift zone is delineated by two sets of fissures: those developed during the initial stage of the eruption, and later fissures developed during the thirty-fifth episode of the Pu'u O'o sequence (see map in Fig. 2). The vent of the nearly 300-m-high Pu'u O'o spatter cone is located on the rift zone approximately 1 km east of the array sites.

Repeated lava flows and pyroclastic deposits from 48 episodes of the eruption have buried forests and given the site its present elevation. A few skeletal trees remain at

Pu'u Kamoamoa, the high ground (once the top of a cinder cone) between the array locations and Pu'u O'o. Tension cracks on the flatter surface of the ponded flow have variable widths reaching 0.25 m in some places. Solid basalt can be seen extending to a depth of several meters in some cracks, indicating that the ponded flow is fairly thick. Some of the cracks emit steam and gases, especially after rainfall. Steam vents on the rift zone are suggestive of shallow subsurface magma.

Setup of First Array

Figure 2 shows the configurations of the two seismic arrays deployed near Pu'u O'o. In the figure, the grid of the larger array shows the triangulation lines used to survey the seismic stations positioned in reference to a bench mark (BM 79–102) located on the January, 1983 eruption fissures (also shown in the inset to Fig 2), and the stations of the smaller, second array are unlabeled and indicated by dots. Station lines for the first array were surveyed using heavy string, sited roughly parallel and perpendicular to the east-west trending fissures of the rift zone. Sensor locations were then pinpointed with measuring tape and marked with labeled flagging nailed to the basalt with masonry nails. Because of the care taken to place array lines and sensors on the most homogeneous parts of the flow, sensor spacing varies from 50 to 160 m, and the pattern of the array is asymmetrical. Pahoehoe bubbles and flakes formed at the surface of the flow during cooling were scraped off before coupling the sensors to the basalt with plaster of Paris. The three-component sensors were oriented with positive radial motion to the north (perpendicular to the rift zone) and positive transverse motion to the east (parallel to the rift zone).

Sensor cabling was unrolled and laid by hand, and connectors were wrapped with electrical tape to minimize water penetration. Plastic buckets were placed over sensors to minimize exposure to sun, wind, and rain. The buckets were partially covered with debris from the flow and held in place with heavy blocks of lava.

The thin RG–174 timing wire was carefully laid from each GEOS to the clock driver, which was protected by a spare GEOS case and located at the center of the array. The "master clock" GEOS was sited a few meters from the clock driver.

The GEOS recorders were set within plastic cases equipped with foam insulation and

small doors for cable inputs. Custom rain coats were used to cover the recorders and clock driver.

As shown in Figure 2, the first array configuration covered an area of about 0.8 by 0.8 km. It extended over the entire surface of the flatter, consolidated flow and over portions of the surrounding, more broken-up flow. The seismic array consisted of 11 lines (designated A through K in Fig. 2) with each line occupied by a single GEOS and two sensor cables (one cable input allocated to channels 1 through 3, and one cable input allocated to channels 4 through 6). In this report, the so-called Pu'u O'o stations refer to locations of individual sensors. For example, station A1 of the first array refers to the location of the single-component vertical sensor that provides input to channel 1 of the GEOS instrument on line A, and station B1,2,3 of this array refers to the location of the three-component sensor that provides input to channels 1, 2, and 3 of the GEOS instrument on line B (see Fig. 2). Line A of the first array extended along the lower southwest portion of the site between the two major fissures of the rift zone (see Fig. 2). Sensors for this line were buried, rather than plastered, in tephra deposits. The line was slightly angled with its westernmost end intersecting the January, 1983 fissure. Line E on the southern end of the array crossed the episode 35 eruption fissures along a profile normal to those fissures.

Setup of Second Array

Initial analysis of tremor data acquired from our first array indicated the necessity to tighten the network to an aperture of 120 m. Figure 3 depicts the configuration of the second, smaller array. The center of the flatter, solid portion of the flow was chosen for the setup of that array (see location in Fig. 2) consisting of 12 GEOS instruments and shaped in the form of a spoked half-circle specifically designed for the study of the wave-type, polarization and phase velocity of a random wavefield (Aki, 1958). Rotating horizontal sensor orientations (shown in Fig. 3) were chosen for this purpose. Close 10-m sensor spacing minimized the effects of scattering and optimized seismic wave phase coherence across the array. Sensor locations were surveyed with nylon string and measuring tape to a precision of 20 cm. Cabling was carefully laid using the procedure followed for the larger array; sensors were coupled to the ground using plaster of Paris and covered with buckets

for protection from the environment.

INSTRUMENT PROGRAMMING

Since the GEOS instruments are usually deployed for earthquake and refraction studies, programming the units to record ground motion from volcanic sources offered a unique challenge. A portable MEQ/800 recorder was deployed at the array site for quick visual inspection of the seismicity near Pu'u O'o. Sustained harmonic tremor of constant amplitude was observed following the setup of the initial array.

GEOS units were first programmed to record periodic 3-minute windows (5-minute and 15-minute windows were also used) to obtain daily samplings of harmonic tremor. Since banded tremor of increasing and decreasing amplitudes had been observed at station STC of the Hawaiian Volcano Seismic Network in the weeks preceding the experiment, the units were also programmed to trigger on a sustained increase in amplitude expected from an increase in tremor activity. The primary goal was to obtain periodic windows of tremor, hence tape-consuming false triggers such as frequent helicopter and plane noise, and weather noise, could not be tolerated. A Short-Term Average (STA) of five seconds was programmed into the trigger algorithm to ensure triggering on a sustained increase in ground-motion amplitude and to minimize false triggers.

Table 1 lists the GEOS parameters for the six data collection periods used with the first array. Gains of 42 and 48 dB were selected to record harmonic tremor with high resolution and to account for a possible increase in tremor amplitude. When tremor amplitudes remained low and constant, the units were programmed to record one 15-minute window and several 3-minute windows at a maximum gain of 60 dB for optimum resolution. The tremor amplitudes, in fact, showed little fluctuation during the full recording period of the first array, which extended over two weeks from January 18 to 27. All systems recorded six channels of velocity at 200 samples/second/channel. Corner frequencies for the GEOS seven-pole Butterworth anti-aliasing filters were selected at 50 Hz. The master timing GEOS unit was synchronized with a master clock to Greenwich Mean Time (GMT, Coordinated Universal Time), and the slave units were programmed to record time corrections every hour.

The primary interest of the Pu'u O'o experiment was to record ground motion due to volcanic tremor, and recording parameters were selected accordingly. Since gains were set high to record the low-amplitude tremor, two large earthquakes of magnitudes M 3.9 and M 4.1 saturated the GEOS amplifiers. For smaller earthquakes with emergent signatures, P arrivals were often missed when the instruments triggered only on the S waves from those events. STA windows were decreased from 5.0 to 2.0 seconds to allow earthquakes with sufficiently high amplitudes to trigger units more rapidly. This allowed enough time (2.5 s) for pre-event memories to record initial arrivals. Even with decreased STA windows, however, the units often triggered only on S waves of small, emergent earthquakes.

Table 2 lists the GEOS parameters chosen for the nine data collection periods used with the second, denser array. For some data collection periods when the instruments operated in trigger mode, only a few preset time windows were programmed for samplings of tremor because gas-piston events that developed during this time period were triggering units frequently and filling data tapes. If array tapes were found to be less than full during a field visit, a single preset window was recorded to fill the tapes.

Trigger sensitivities were varied according to the vigor of gas-piston activity and the anticipated lengths of the time intervals between visits to the array. STA windows were lowered from 2.0 to 1.0 second and finally to 0.5 second with the goal of recording the emergent onsets of gas-piston events. When the playbacks of data demonstrated that it was not possible to fully record these events with GEOS units in trigger mode because of the limited pre-event memory, a long 40-minute window was manually recorded to obtain a sequence containing two complete gas-piston events. The sample rate of this recording (and a later 40-minute recording) was decreased to 100 samples/second/channel to double the recording time. A 40-minute recording was necessary since the roughly one-minute-long events occurred at intervals varying from 10 to 40 minutes.

The small number of earthquakes recorded during this period may be due to gas-piston activity in the Pu'u O'o vent increasing the long-term average (LTA) amplitudes in the GEOS trigger algorithm. With the larger long-term average amplitudes, larger short-term average (STA) amplitudes would have been necessary to exceed the algorithm trigger ratio (STA/LTA), and smaller earthquakes would possibly not trigger the instruments.

LTA windows could have been decreased, but this may have inhibited the recording of smaller gas-piston events preceded by a high background of tremor. (Either a high or low background of tremor was observed preceding gas-piston events depending on the phase of cyclic activity in the Pu'u O'o vent.)

INSTRUMENT PERFORMANCE

The Pu'u O'o experiments have shown that the GEOS digital seismic recorders can be used in a dense array configuration with the timing scheme developed by Gary Maxwell to record the details in space and time of the elastic wavefield associated with volcanic seismicity. Implementation of an extended, pre-event memory will obviously aid the recording of extended emergent events in future experiments. Although the timing scheme leaves clock adjustments for post-experiment computer work, the field setup and operation is easy and reliable. The clock driver operated continuously for the duration of both arrays on just one pair of 12-volt batteries, and the GEOS units continuously recorded reliable clock corrections on tape.

One hardware malfunction, traced to a tape controller board synchronization problem, was responsible for the loss of some data on all GEOS data tapes. A modification to the tape controller has been developed by Mark Kennedy and Gary Maxwell to alleviate the problem.

The extreme Hawaiian climatic environment along the east rift zone, with rain, humidity, heat, and volcanic gases, did not affect the operation of the GEOS instruments. Dessicant packs placed inside the instruments kept moisture levels down, and raincoats were placed over the plastic GEOS carrying and deployment cases. Water seepage into sensor plug connections shorted wires, causing some false triggers, but this problem was restricted to only a few instruments during short intervals. Some site conditions were favorable; porous rock soaked up rain water, and the barrenness of the site allowed sunshine and wind to rapidly dry sensor plugs.

SEISMOGRAMS RECORDED ON THE PU'U O'O ARRAYS

Harmonic Tremor and Earthquakes Recorded with the First Array

Figures 4 through 7 show sample seismograms of harmonic tremor and sample seismograms of one earthquake recorded with the first array.

The best samplings of sustained tremor were obtained in nine three-minute windows and one five-minute window recorded on ten GEOS units, and one 15-minute window recorded on nine units. Table 3 lists the start times (given in Greenwich Mean Time) of the preset recording windows of harmonic tremor from the six data collection periods of the first array.

Figure 4 displays three minutes of typical sustained tremor recorded on the first array. Array stations are listed at the left of the figure, and the time histories are presented in record-section format. The horizontal axis at the top of the figure gives the time into the trace in seconds. The origin time, which is the start time of the recording, is shown at the right of the figure in Greenwich Mean Time to the nearest second. (The format is DDD+HH:MM:SS where D = Day, H = Hour, M = Minute, and S = Second.) The amplitudes of the various traces are normalized to the maximum amplitude in the record section.

Table 4 lists the earthquakes recorded on the first array and the number of units that recorded each event. One earthquake of magnitude M 2.2 that was fully recorded on all 11 GEOS units did not saturate on any of the 66 components. Figure 5 depicts this earthquake in record-section format similar to Figure 4, above. Stations are listed at the left of the figure. The horizontal axis at the top of the figure shows the time into the trace in seconds, and the start time for this event is shown at the right of the figure in Greenwich Mean Time to the nearest second. Amplitudes of individual traces are normalized to the maximum amplitude in the record section. In Figure 6, we have selected the first 3 seconds of this earthquake for the vertical components only to depict the details of the wave forms. In Figure 7, we have selected a window of 1-second duration, starting at 0.25 seconds into the record of Figure 6, to show wave coherence and propagation.

A total of 17 out of the 30 recorded earthquakes were correlated with events of the

Hawaiian Volcano Observatory CUSP listing; these events are listed in Table 5. Their magnitudes range from M 1.3 to M 4.1.

Harmonic Tremor, Gas-Piston Events, and Earthquakes Recorded with the Second Array

Figures 8 through 17 show sample seismograms of harmonic tremor and sample seismograms of one earthquake recorded with the second array. Sample seismograms of gas-piston events and correlation of visually observed gas-piston activity with recorded seismic data are provided in the following chapter.

The best samples of sustained tremor from the second array were obtained in the two 40-minute windows and in seven three-minute windows recorded on at least ten units. Table 6 lists the start times (in Greenwich Mean Time) of the preset recording windows of harmonic tremor for the nine data collection periods of the second array.

Presented in record section format similar to Figure 4, Figure 8 displays 3 minutes of tremor recorded on the second array. Amplitude fluctuations are coherent across the entire array. For a closer look, Figure 9 shows 20 seconds of this tremor depicting the details of the wave forms. The start time in Figure 9 is taken 1 second into the record of Figure 8. In Figure 10 we have taken the traces of the vertical components of ground motion from Figure 9 to show the coherence of these wave forms, and in Figure 11 we have displayed 3 seconds of the tremor from the records in Figure 10 to show the wave propagation characteristics. The start time in Figure 11 is taken 12 seconds into the record of Figure 8. In Figure 12 we display the vertical traces along the lines A and G including station L1 (see Fig. 3) to illustrate wave coherence and wave propagation along a linear profile of the array; 20 seconds of the data are shown, and the start time is 13 seconds into the record of Figure 8. Finally, for the most detailed display of the wave forms, in Figure 13 we show 3 seconds of data from this linear profile with the start time set 12 seconds into the record of Figure 8, and in Figure 14 we show 1 second of this data with start time set 13 seconds into the record of Figure 8. In Figures 13 and 14, a low-pass filter with corner at 30 Hz has been applied, as indicated, to improve the apparent signal-to-noise ratio.

Table 7 provides a list of triggered recording times for gas-piston events obtained with the second array. A total of 13 triggered recordings of gas-piston events were obtained

on all 12 GEOS units, and 26 additional events were recorded on at least 10 units. The two 40-minute seismograms obtained during this period, the first of which contains two complete gas-piston events, are shown in Figures 22 and 32 and are discussed in detail in the following chapter.

Table 8 lists the recording times in Greenwich Mean Time of the ten earthquakes recorded on the second array, and the number of GEOS units that recorded each event. Of the ten recorded earthquakes, seven were correlated to events of the Hawaiian Volcano Observatory CUSP earthquake listing, and these events of magnitudes ranging from M 1.7 to M 4.1 are listed in Table 9. One earthquake with well-recorded P arrivals is shown in Figure 15. This recording is shown in record-section format as described for Figure 4 above. In Figure 16 we display 3 seconds of the vertical components for this recording, starting 0.5 seconds into the record of Figure 15, to illustrate wave coherence and wave propagation characteristics.

In Figure 17 we have selected the time history of ground velocity recorded on the three-component L–22 sensor at station A1,2,3 (Fig. 3) for the earthquake shown in Figure 15. Each trace is labeled on the left with its corresponding component of ground motion. Trace 1 represents vertical motion, trace 2 represents horizontal radial motion, and trace 3 represents horizontal transverse motion (see Fig. 3 for orientation). The horizontal axis shows the time into the trace in seconds with the starting time (in Greenwich Mean Time) indicated at the top right in GEOS format. (GEOS, or NSMDC, format is explained on p. 34 in Appendix B. The seven numerals refer to the Julian day, hour, and minute of the start time of the recording, T is a letter code for seconds, and A is the letter code for channels 1, 2, and 3.) The starting second to the nearest millisecond is indicated at the left of the time axis. Maximum ground motion is shown in cm/s at the upper left of each trace; amplitudes in the record have been normalized to a peak velocity of $6.51 \cdot 10^{-2}$ cm/s. Maximum digital counts are shown at the lower left of these traces.

In Figures 18, 19, and 20 we have taken Fourier amplitude spectra (not corrected for instrument response) of ground velocity computed for each component depicted in Figure 17. These are obtained over the window labeled L–L in Figure 17, which has been cosine tapered over 10% of its duration at both ends to remove bias caused by window

end points that fall on wave forms with amplitude values other than zero. The spectra are plotted on a log–log scale with amplitude in cm on the vertical axis and frequency in Hz on the horizontal axis. The spectra show corner frequencies in the range of 6 to 10 Hz for this earthquake.

For a general view of earthquake locations, Figure 21 shows the epicenters of located earthquakes recorded on the two Pu'u O'o arrays.

A SUMMARY AND PRELIMINARY ANALYSIS OF VOLCANIC SEISMICITY RECORDED AND OBSERVED AT PU'U O'O

During the two-month period of the Pu'u O'o experiment, an exceptional evolution of magma dynamics was observed. From January 18 to 27, the persistent harmonic tremor recorded on the initial array indicated that magmatic activity was relatively constant. From January 30 to February 4, spindle-shaped envelopes of signal amplitude recorded across the smaller dense array correlated in time with gas-piston events, some of which were observed from the Pu'u O'o crater rim. Gas-piston activity ceased from the afternoon of February 4, to February 11. From February 12 to 20, GEOS records showed periodic three-minute spindle-shaped events of lesser amplitudes than those of the gas-piston events observed earlier. Less vigorous gas-piston activity was observed from the Pu'u O'o crater rim on February 14, during the recording of the second 40-minute record. Steady steam and gas emissions restricted later observations of the Pu'u O'o vent, and by the end of the Pu'u O'o experiment, the seismograms indicated a return to steady tremor.

A glance at the record sections of some of the long windows of harmonic tremor obtained on the first array reveals pulses of increased amplitudes that are coherent throughout the array (see Fig. 4). A closer look, however, reveals that there is little phase coherence between wave forms across the array due to scattering from local heterogeneities in the underlying complex of pahoehoe and aa flows and tephra deposits. Earthquake coda recorded on the first array may be useful for the investigation of the scattering properties of the medium near Pu'u O'o.

The initial array was tightened to a smaller dense array with a spacing of 10 to 15 m between stations to investigate the details of the wavefield of harmonic tremor near Pu'u O'o. Visual inspection of the first data playbacks showed excellent local coherence of

wave propagation (see Figs. 9 through 14). The spoked half-circle array was designed to investigate wave propagation properties and source parameters.

The onset of gas-pistoning at Pu'u O'o on January 30 provided an excellent opportunity to correlate visual lava activity with the recorded seismicity. The first visual sign of that activity (besides repeated instrument triggering) was a change in steam and gas emissions from the Pu'u O'o vent. Brown, billowing gas clouds were repeatedly followed by clearing, which allowed observation of the activity within the vent.

Gas-piston activity as described by Swanson (1979) occurs when trapped, pressurized slugs of gases ascend in the volcanic conduit and expand with decreasing confining pressure. These gas pockets break through the ponded lava surface in orange-domed upwellings, each gas-slug burst abruptly reducing the confining pressure and triggering a chain reaction of vigorous fountaining activity followed by a rapid drainback of lava deeper into the volcanic conduit.

At the time of the experiment, the Pu'u O'o crater had a diameter of 150 m and an estimated depth of about 150 m. The southwest half of the crater floor was elevated roughly 20 m above its northeast counterpart. Two conduits were visible at the northeast and southwest perimeter of the crater floor, and observations during the two periods of gas-piston activities in February showed that both of these conduits acted interchangeably as inlet and outlet to lava movement in the crater. The character of the activity within the vent appeared to change daily.

Figure 22 is a sample of the 40-minute window obtained across the small array on February 4. This figure shows time histories of ground velocity recorded on the three-component L–22 sensor at station A1,2,3 (see Fig. 3). Each trace is labeled at the left with its corresponding component of ground motion. Trace 1 represents the vertical component of ground velocity, trace 2 is the horizontal radial component, and trace 3 is the horizontal transverse component of motion (see Fig. 3 for sensor orientation). The horizontal axis shows the time into the trace in minutes. The starting time is shown at the upper right with the first three numerals indicating Julian day, followed by hour and minute (GMT) (see p. 35). The starting second to the nearest millisecond is indicated at the left of the time axis. Maximum ground motion is shown in cm/s at the upper

left of each trace; amplitudes in the record have been normalized to a peak velocity of $5.38 \cdot 10^{-3}$ cm/s. The activity within the Pu'u O'o vent during this recording was observed from the crater rim and was later correlated in time with the seismic record. The seismogram shows two bursts of higher amplitude that occur at approximately 9 and 35 minutes into the record. These events correspond to the times of observed gas-piston events in the Pu'u O'o vent.

Location A in Figure 22 is a period of relatively high amplitude tremor. Figure 23 is a seismogram of 50 seconds of this tremor for the vertical component of motion recorded at station L1 (see Fig. 3). This 50-second window corresponds in time to a 50-second window of the 40-minute record shown in Figure 22, starting 7 minutes 10 seconds into the record. The peak velocity of the 50-second seismogram is $5.52 \cdot 10^{-4}$ cm/s, listed above the corresponding amplitude. Observed from the crater rim at this time was a river of lava steadily flowing into the southwest conduit. Location B in Figure 22 roughly correlates with the most vigorous activity of the first gas-piston event that occurred within the 40-minute window. This event began as lava in the northeast inlet conduit choked and ponded, and domed upwellings of the surface of the ponded lava increased in size, bursting into a fully developed storm of superheated volcanic gases. Figure 24 is a seismogram showing 100 seconds of this gas-piston event recorded on the vertical component of ground velocity at station L1. This 100-second window corresponds to a 100-second window of the 40-minute record shown in Figure 22, starting 8 minutes 50 seconds into the record. The record shows a peak velocity of $3.14 \cdot 10^{-3}$ cm/s. The large gas emission of less than one-minute duration was immediately followed by a complete drainback of the pond into the northeast conduit.

Activity on the crater floor decreased, and lava began to rapidly rise from the northeast conduit. The ponded lava rose an estimated 10 m above the highest point of the crater floor. This passive filling of the crater floor is correlated to the relatively aseismic time period shown at C in Figure 22. A small rise in amplitudes soon after C may be associated with observed gas-piston activity at the Kupaianaha lava pond.

Location D correlates with the most vigorous activity of the second gas-piston event. Domed upwellings broke through a passive surface of cooling crust, releasing larger and

more vigorous lava bursts than during the first event. Figures 25 through 28 are seismograms showing 100 seconds of this gas-piston event recorded on the vertical components of ground velocity at stations A1, D1, G1, and L1. The 100-second windows correspond to a 100-second window in the 40-minute record in Figure 22, starting 34 minutes 20 seconds into the record. Figure 29 depicts the horizontal component 2 (see Fig. 3) of ground velocity recorded at station L2, and Figure 30 depicts the horizontal component 3 of ground velocity recorded at station L3 for that event. The peak ground velocity generated by this gas-piston event is $5.50 \cdot 10^{-3}$ cm/s on component 2 of velocity recorded at station L2. The maximum amplitude of the record corresponds to the burst of the largest gas bubble immediately followed by the rapid drainback of lava into the northeast conduit, which totally emptied the crater.

Following that event lava began to rise from the northeast conduit, and at point E, a river of lava flowing from the northeast into the southwest conduit was again observed on the crater floor. Figure 31 is a seismogram showing 50 seconds of the tremor recorded on the vertical component of ground velocity at station L1 following this gas-piston event. This 50-second window corresponds to a 50-second window of the 40-minute record in Figure 22, starting 36 minutes 30 seconds into the record. The peak ground velocity in this 50-second window is $2.02 \cdot 10^{-4}$ cm/s.

Gas-piston activity at Pu'u O'o lasted about two weeks separated by a week of cyclic tremor. Events observed after February 12 were of lower amplitudes. Figure 32 is a sample of the 40-minute window obtained with the small array on February 14. This record from station A1,2,3 (see Fig. 3) shows fluctuating amplitudes with a periodicity of 3 minutes, which can also be observed in the preset three-minute records. Observations on February 14 showed that the gas-piston activity in the Pu'u O'o vent was less vigorous and limited to the lower half of the crater floor above the northeast conduit.

The spectral characteristics of selected tremor windows and gas-piston events are shown in Figures 33 through 54. Four types of analyses are considered including: (1) power spectra obtained by the segment averaging method (Yuen, 1978) applied to individual events at selected stations; (2) moving window spectra obtained by shifting a window of fixed duration through an individual event observed at selected stations; (3) power spectra

obtained by stacking and averaging over a group of similar events observed at a single station; and (4) power spectra obtained by stacking and averaging the spectra of a given event over many stations.

Examples of power spectra obtained by the segment averaging method are displayed in Figures 33 through 41. A power spectrum was derived by stacking and averaging the power spectra obtained over 71 segments of 20.48 s duration shifted by constant increments of 1 s through the record of an event. The resulting average spectrum was then smoothed using a Hanning window. This analysis was applied to the events displayed in Figures 23 through 31 to generate spectra in the band of 1 to 20 Hz with a frequency resolution of 0.05 Hz. Figure 33 shows the power spectrum of the vertical component of ground velocity at station L1 for tremor preceding a gas-piston event on February 4, 1988 (see position "A" in the sequence of Fig. 22). The seismogram from which this spectrum was derived is shown in Figure 23; the record interval selected for the spectrum ranges from 240.00 to 330.48 s. The peak spectral amplitude is $1.3 \cdot 10^{-7}$ cm^2/s at the frequency of 3.0 Hz. The spectrum displays many narrow-band peaks in the band from 2 to 10 Hz; the spectrum below 2 Hz is not well resolved due to the limited bandwidth of the instrument (see Fig. A2 in Appendix A). Selected spectral peaks are indicated by arrows and are listed at the upper right.

Figure 34 shows the power spectrum of the vertical component of ground velocity at the same station for a gas-piston event superimposed on a background of tremor recorded on February 4, 1988 (see position "B" in the sequence of Fig. 22). The time interval used to generate this spectrum extends from 360.00 to 450.48 s in the record displayed in Figure 24. Selected dominant and subdominant frequencies are indicated by arrows and are listed at the upper right. Two dominant frequencies are observed at 3.0 and 3.7 Hz. The peak spectral amplitude is $1.9 \cdot 10^{-6}$ cm^2/s at 3.0 Hz; this dominant frequency coincides with the dominant frequency of tremor obtained in Figure 33.

Power spectra of a gas-piston event recorded on February 4, 1988 (see position "D" in the sequence of Fig. 22) at stations A1, D1, G1, and L1, L2, L3 are displayed in Figures 35 through 40. These spectra were derived using the same time interval starting at 95.00 s and ending at 185.48 s in the records displayed in Figures 25 through 30. Selected

resonant frequencies are indicated by arrows and are listed at the upper right of each plot. Figures 35, 36, and 37 show the results for the vertical component of ground velocity at stations A1, D1, G1 (displayed in Figs. 25, 26, 27). Comparison between these spectra shows that the resonant frequencies at 2.3, 3.2, 3.6, and 4.5 Hz are independent of station position, suggesting that these frequencies represent a source rather than a path effect. The dominant frequency depends on the station position, showing a value of 3.6 Hz at station A1, 4.0 Hz at station D1, and 3.8 Hz at station G1. The peak spectral amplitudes are $1.9 \cdot 10^{-6}$, $3.3 \cdot 10^{-6}$, and $4.0 \cdot 10^{-6}$ cm^2/s at A1, D1, and G1, respectively.

Figures 38 through 40 show the power spectra for the same gas-piston event obtained on the three components of ground velocity recorded at station L. Figure 38 displays the result for the vertical component shown in Figure 28, Figure 39 represents the horizontal component 2 in Figure 29 (approximately transverse to the direction from the Pu'u O'o crater), and Figure 40 represents the horizontal component 3 in Figure 30 (approximately radial to the Pu'u O'o crater). The peak spectral amplitudes are $2.1 \cdot 10^{-6}$ cm^2/s at the frequency of 4.5 Hz on L1, $7.3 \cdot 10^{-6}$ cm^2/s at the same frequency on L2, and $5.5 \cdot 10^{-6}$ cm^2/s at 3.6 Hz on L3. The strong spectral peak at 4.5 Hz is common to the three components of motion.

Finally, in Figure 41 we show the power spectrum of the vertical component of ground velocity at station L1 for tremor following the gas-piston event just discussed (see position "E" in the sequence of Fig. 22). The record of this tremor is shown in Figure 31 and the time interval considered for the spectrum extends from 200.00 to 290.48 s. Selected resonant frequencies are indicated by arrows and are listed at the upper right. Two dominant frequencies are observed at 3.2 and 3.9 Hz with a common peak spectral amplitude of $1.4 \cdot 10^{-8}$ cm^2/s. The resonant frequencies for this event are observed to be different from those obtained for the preceding gas-piston event (compare Fig. 41 with Fig. 38).

A more detailed view of the temporal characteristics of these events is obtained using the moving window spectrum technique. This approach is similar to that used above, but instead of stacking the power spectra obtained over individual windows we compute the spectrum of ground velocity for each window and consider the evolution of this spectrum in time as the window is moved through the record of the event under study. The result

can be displayed as a three-dimensional plot or contour plot of the spectral amplitude of ground velocity versus time and frequency. Examples of moving window spectra obtained for the events considered above are given in Figures 42 through 52.

A three-dimensional representation of the spectral amplitude of ground velocity versus frequency and time is given in Figure 42. The plot represents the vertical component of ground motion recorded at station L1 for the gas-piston event shown in Figure 28 and was obtained by computing spectra over 101 windows of 5.12 s duration shifted by constant increments of 1 s through the record of this event. The record interval considered extends from 82.56 to 182.56 s (see Fig. 28) and the bandwidth ranges from 0 to 10.1 Hz with a frequency resolution of 0.2 Hz. A two-dimensional gridding interpolation scheme was applied to the matrix of spectral densities to increase the number of grids in the plot for a more pleasing result. The plot shows the partition of energy among various dominant frequencies throughout the history of the event and clearly indicates the presence of a dominant frequency at 4.5 Hz with a peak spectral amplitude of $2.4 \cdot 10^{-3}$ cm at 124 s. This peak coincides with the paroxysm of activity observed in the crater over the course of this event (see Figs. 22 and 28).

A more detailed picture of the above three-dimensional spectrum is provided in Figure 43 where the window considered has been reduced to include only the main part of the event extending from 97.5 to 167.5 s, and the bandwidth has been narrowed to the range of 2.1 to 8.0 Hz. The two-dimensional gridding scheme used in Figure 42 was again applied to increase the number of grids in this plot. The figure shows the complexity of the pattern of excitation of ground motion produced during the main energy release from that event. We shall take another look at this event using the contour plots discussed below.

Contour plots of the spectral amplitude of ground velocity versus frequency and time are given in Figures 44 through 52 for the events displayed in Figures 23–31. These plots were obtained using 71 windows of 5.12 s duration shifted by constant increments of 1 s across the seismogram of an event. The bandwidth considered ranges from 2.1 to 8.0 Hz and the frequency resolution is 0.2 Hz. As for the plots described in Figures 42 and 43, we used a two-dimensional gridding interpolation scheme to stretch the plots for ease in viewing. A magnification factor was applied to the spectral amplitudes in each plot prior

to contouring; the magnification is $5 \cdot 10^4$ in Figure 44, 10^4 in Figures 45–51, and 10^5 in Figure 52. Contour intervals (after magnification) are 1 cm and bold contours are used every 5 cm. The spectral amplitudes ranging from 5 to 10 cm are shaded grey and spectral amplitudes larger than 10 cm are marked with a dot pattern in those plots.

Figure 44 is a spectral map of the record shown in Figure 23. The time interval considered ranges from 242.5 to 312.5 s. Dominant frequencies are found in the band of 2.7 to 3.3 Hz, which coincides with the peak spectral amplitude found in Figure 33. The peak amplitude is $2.8 \cdot 10^{-4}$ cm and occurs 296 s into the record.

Figure 45 gives a spectral representation of the data displayed in Figure 24. The section of record considered for the plot ranges from 362.5 to 432.5 s. Dominant frequencies are found in the range of 2.9 to 3.7 Hz (see Fig. 34). The peak energy release occurs in the time interval 380–410 s and the peak spectral amplitude is $1.7 \cdot 10^{-3}$ cm 396 s into the event (compare with Fig. 24).

Spectral maps of the gas-piston event shown in Figures 25–30 are given in Figures 46 through 51. The same time interval was used for each plot extending from 97.5 to 167.5 s in the records shown in Figures 25–30. Figures 46 through 48 display the vertical component of ground velocity recorded at stations A1, D1, and G1, respectively. The dependence of ground excitation on station position is obvious in these figures, although some of the spectral features appear to be common to the three stations including the peak at 4.5 Hz, which dominates the spectrum near 124 s in those plots. Most of the energy in the ground motion is concentrated in the band of 3.0 to 5.0 Hz in the time interval 110–140 s (compare with Figs. 35–37). The peak spectral amplitudes are $1.8 \cdot 10^{-3}$ cm at station A1, $2.1 \cdot 10^{-3}$ cm at station D1, and $2.3 \cdot 10^{-3}$ cm at station G1.

Maps of the spectral amplitudes for the three components of motion obtained at station L for this event are given in Figures 49 through 51. Figure 49 represents the vertical component of ground velocity shown in Figure 28 and is the contour version of the three-dimensional perspective shown in Figure 43. The dominant peak at 4.5 Hz seen in the earlier plot is the most important feature seen near 124 s, lasting approximately 8 s. Note also the spectral peak at 3.7 Hz in the time interval 128–135 s, which corresponds to the second highest peak seen in Figure 43. Figure 50 represents the horizontal component

2 of ground velocity shown in Figure 29 (see Fig. 3 for orientation of station L1,2,3), and Figure 51 shows a spectral map of the horizontal component 3 given in Figure 30. The peak spectral amplitude at 4.5 Hz near 124 s is common to the three components of motion displayed in Figures 49–51. The amplitudes of this peak are $2.4 \cdot 10^{-3}$ cm on the vertical component (Fig. 49), $4.0 \cdot 10^{-3}$ cm on the horizontal component 2 (Fig. 50), and $2.6 \cdot 10^{-3}$ cm on the horizontal component 3.

Figure 52 is a spectral map of the record of tremor shown in Figure 31. The time interval considered ranges from 202.5 to 272.5 s in this record. Peak spectral amplitudes are found in the range of 3.0 to 5.0 Hz and appear to be evenly distributed over the interval considered. The dominant spectral peak occurs at the frequency of 4.7 Hz and has the value of $9.8 \cdot 10^{-5}$ cm (compare with Fig. 41).

A comparison between the power spectra of tremor and gas-piston events is made in Figures 53 and 54 using the spectral stacking technique applied to a suite of records. The top of Figure 53 shows a stack obtained from the vertical component of ground velocity for suites of tremor recorded in the period of January 22–25, 1988 at station K2 of the first array deployed at Pu'u O'o (see Fig. 2). The bottom of Figure 53 shows a similar stack obtained from the vertical component of ground velocity for gas-piston events recorded on February 2, 1988 at station L4 of the second array at Pu'u O'o (see Fig. 3). These results were derived by stacking and averaging the power spectra obtained over 10 windows of 40.96 s duration taken through 10 individual events. The resulting average spectrum was then smoothed using a Hanning window. The bandwidth considered ranges from 1 to 20 Hz and the frequency resolution is 0.02 Hz. The list of events analyzed is given at the upper right of the plots. As both stations occupy the same location these spectra offer a direct comparison of the nature of these two persistent sources of volcanic activity. The overall spectral shapes are similar but the amplitudes differ by an order of magnitude. Three spectral peaks, including the two dominant peaks, are common to both spectra at frequencies below 4 Hz as indicated by the arrows in those plots. No precise alignment in the spectral peaks of the two sources can be seen above 4 Hz. As the source of gas-piston activity was observed to occur within Pu'u O'o, we may infer from this data that the source of persistent tremor is also linked to activity within that vent. However, the presence of two

orifices in the crater of Pu'u O'o suggests that the geometry of the underlying feeder may be complex and, as we shall demonstrate below, the excitation mechanisms of tremor and gas-piston events can be markedly different even though they apparently share a similar source region.

Figure 54 compares stacks of power spectra for one section of tremor and one gas-piston event obtained over 47 vertical components of ground velocity including all but one station in the dense array (station L4 was not considered; see Fig. 3). These results were derived by stacking the spectra obtained in windows of 81.92 s duration, followed by averaging and smoothing with a Hanning window. The bandwidth extends from 1 to 20 Hz and the frequency resolution is 0.01 Hz. The tremor window considered starts 270 s into the file displayed in Figure 22, and the gas-piston selected is the second event in that file (see position "D" in this record). A seismogram of the vertical component of ground velocity obtained at station L1 for this event is shown in Figure 28; the time interval considered ranges from 90.00 to 171.92 s covering the entire event history. This type of stack smoothes out the path effects and strengthens the spectral peaks due to the source. The results show the presence of very narrow peaks in both spectra that must represent the source effects, but the peaks occur at different frequencies in the tremor and gas-piston event. The peak spectral amplitude of tremor is roughly an order of magnitude smaller than that obtained for the gas-piston event.

The dense array deployed in the second phase of our experiment at Pu'u O'o provided records with good phase correlation across the network (see example in Fig. 14), suggesting that such records may be used to reconstruct the elastic wavefield over the surface encompassed by the array. To obtain a snapshot of the ground motion over the array, three steps of calculation are needed. First, an absolute time is selected and clock corrections (see discussion p. 5) are applied to each station to line up all the records along a common time; second, we select a time for the snapshot and apply a cubic interpolation spline (Wiggins, 1976) to the digitized records to calculate the amplitude of motion at that time for each station (because of the necessary clock corrections the snapshot time usually falls between samples); and third, we apply a two-dimensional gridding interpolation scheme to the matrix of observed amplitudes to obtain a dense rectangular mesh that gives a smooth

representation of the ground motion over the array.

Due to the fan-like distribution of stations used in the layout of the network (see Fig. 3), some distortion is expected in the shape of the wavefield reconstructed in this manner. However, as long as the wavefield is smooth over the scale of the network this distortion should present a minor problem. An example with synthetic data, shown in Figure 55, provides a qualitative measure of this distortion. This figure represents a plane wave with wavelength of 80 m moving across the network along an azimuth of N47°E. Gridding was applied to the initial set of 47 amplitudes calculated for this wave at the known station positions. The result shows a slight undulation in the amplitude of the wave in the direction normal to the propagation path, suggesting that this type of reconstruction should provide a fairly accurate picture of the actual wavefield. This method was applied to a section taken through the 47 seismograms of the vertical component of ground velocity obtained for the gas-piston event depicted in Figure 28. Figures 56 and 57 show a sequence of 11 snapshots sampling 0.1 s of this event at constant intervals of 0.01 s starting at 22:34:2.996 GMT on February 4, 1988, that is approximately 123 s into the seismogram depicted in Figure 28. A longer sampling of this event is offered in Figures 58 through 63, which show a sequence of 31 snapshots sampling 3 s of ground motion at constant intervals of 0.1 s starting at the same time as the previous sequence. These snapshots demonstrate the stochastic nature of the wavefield resulting from the complexities of the source and propagation medium. This suggests that a statistical investigation of the temporal and spatial characteristics of the wavefield will be required to investigate the nature of those complicated waves, as well as the nature of the propagation medium (*e.g.,* Aki, 1958).

SITE LOCATIONS, RECORDING PARAMETERS, AND RECORDED SEISMOGRAMS AT FOUR STATIONS LOCATED NEAR THE KILAUEA SUMMIT

Four sites were selected near the Kilauea summit caldera to record long-period events and earthquakes associated with magmatic activity beneath Kilauea. These stations supplemented other digital recorders deployed near the summit by the University of Southern California. Figure 1 shows the locations of the GEOS stations in relation to the Kilauea summit.

Immediately south of the summit caldera was GEOS station OUT, located near station Outlet of the Hawaiian Volcano Observatory. The GEOS instrument was deployed at the edge of a recent lava flow in the Kau Desert south of the Kilauea summit, and the sensor was buried in gravel soil. Station MOB was deployed on the Mauna Loa access road about 8 km northwest of the intersection of Mauna Loa road and Highway 11, and the sensor was placed in sandy soil about 50 m east of the road. Station MOA was deployed at the end of Mauna Loa road approximately 15 km northwest of the Kilauea summit. The sensor was buried in sandy soil about 10 m east of a structure used by HVO to house tiltmeters (Uwekahuna vault) and other instrumentation. Station YNG was deployed approximately 5 km northeast of the Kilauea summit at a residence near the end of Wright Road (Highway 148) north of the town of Volcano. The sensor was buried in damp, silty soil approximately 50 m west of the highway.

Table 10 lists the locations of the GEOS summit stations along with the U.S.C. stations. Each GEOS unit recorded three components of velocity at 200 samples/second/channel with a Mark Products L–22–3D velocity sensor. The three-component sensors were oriented with positive radial motion to the north and positive transverse motion to the east. The anti-aliasing filters were set at 50 Hz. The units were synchronized to Greenwich Mean Time (GMT) with a master clock, and corrections were taken from a master clock every other day. The units were programmed for trigger mode with an STA of 0.5 s. Trigger sensitivities were increased as the seismic activity near the summit of Kilauea decreased. The GEOS instrument at station OUT was programmed to record one 90–minute tape at 100 samples/second/channel at a gain of 60 dB to obtain a series of low-amplitude long-period events. With the exception of this recording, gains and trigger thresholds were selected according to site characteristics.

The four GEOS units were deployed following the observation of several relatively large long-period events by the Hawaiian Volcano Seismic Network. Four long-period events recorded at station OUT, one of which was also recorded at Station MOB, exhibit low frequencies in the 1–6 Hz range and have been correlated with the preliminary HVO CUSP listing of Long-Period Caldera (LPC) events. These events have magnitudes ranging from M 1.8 to M 2.0. Emergent initial arrivals were missed because of the late trigger. Fig-

ure 64 depicts a three-component seismogram of an LPC event recorded at station OUT. The record shows 31 seconds of ground velocity in the same format described for Figure 17 in a previous chapter. Within one day of the installation of the GEOS units, these events became shallower, and their wave forms displayed smaller amplitudes that became less well-defined. A sampling of these shallower events was obtained in the 90–minute window obtained at a gain of 60 dB. Figure 65 shows 22 seconds of this record starting approximately 74 minutes into the 90–minute record, or, more precisely, at a GMT of 053:20:34:00 plus 85.00 seconds (see Figure 17 for format). Signal-to-noise ratio is poor; frequencies of the larger amplitudes range from 1 to 6 Hz. Due to attenuation and the rapid decay of amplitude with distance, no long-period events were recorded at stations MOA, and YNG.

A total of 13 earthquakes were recorded on the four stations, all of which were correlated with events in the HVO CUSP listing. Table 11 lists these events with magnitudes ranging from M 1.4 to M 4.1. (The LPC events recorded at station OUT on Feb. 19 are also listed.) The recorded seismograms of the earthquakes show well-defined initial P arrivals. Figure 66 displays a 30-second window for an earthquake recorded on the four summit stations. The traces are shown in record-section format (as explained for Figure 4 in a previous chapter). Each trace is listed on the left with its 3-component letter station code followed by a number identifying the component of motion, where 1 is vertical motion, 2 is north-south horizontal motion, and 3 is east-west horizontal motion. An additional 12 earthquakes with magnitudes ranging from M 1.2 to M 2.2 were recorded on three stations and are listed in Table 12. Figure 67 shows the epicenters of located earthquakes recorded on the GEOS summit stations. Many other small earthquakes were recorded on one or two stations only, and are not listed.

CALIBRATION PROCEDURES

Calibration signals for the sensors and GEOS instruments were recorded prior to the dismantling of each of the Pu'u O'o arrays and in the laboratory following the experiment for the stations deployed near the summit of Kilauea Volcano. Tables 13 and 14 list the recording times and parameters for the calibration of each instrument on the Pu'u O'o arrays. Table 15 lists the recording times and parameters for the calibration of the instru-

ments deployed near the summit of Kilauea. A general description of the calibration of the GEOS instrumentation is given in Appendix A.

Because of the location and configuration of the sensor coil shunt resistors, a unique procedure was used to calibrate the instrumentation on the two Pu'u O'o arrays. The shunt resistors are located in the sensor cable connector plugs. Figure 68 shows schematic diagrams of the sensor coils and cabling used for the two types of sensors deployed on the two arrays. The shunt resistors labled "S" and "T" in the figure are in a T–network with the sensor coil. Without the S and T resistors, the sensitivity of the sensor coil would be a function of the resistance and natural frequency of the coil, which vary for individual sensors. Each sensor plug is equipped with S and T resistors with the specific values that provide a damping factor of 0.8 and a standard coil sensitivity of 0.5 V/cm/s for L–22–3D sensors and 1.0 V/cm/s for L–4C sensors.

During *in situ* calibration of a GEOS network, the sensor input signal is applied with the use of one additional conductor pair per component used specifically for calibration. These calibration conductor pairs were omitted from the custom cables assembled for the two arrays to keep the cost and the bulk of the cables manageable.

Since the custom cables lacked the extra conductor pairs, the GEOS calibration input signal to the sensor coil was applied at the junction of the S and T resistors, rather than at the junction of the T resistor and sensor coil as in a normal calibration (see Figure 68). The resulting input signal to the sensor coil is reduced by the S and T resistor bridge, and the resulting sensor output calibration pulses are thus reduced in amplitude. To adjust the *in situ* calibrations recorded on the arrays, two calibrations were performed in the laboratory. The first was performed with the same cable and sensor configurations used in the field, and the second was performed with short, test cables wired for normal calibration (four conductors per component). Comparison of the two calibrations yielded factors to be applied to each component of the *in situ* calibrations to remove the effect of the reduced input signal to the sensor coils due to the S and T resistors. Values of these factors are given in Tables 16 and 17. Tables 18 and 19 list the sensor types and the sensor numbers (according to the U.S.G.S. numbering system) used for each station on the Pu'u O'o arrays.

The data from five of the single-component vertical L–4C sensors were found to have

excessively high amplitudes. On investigation it was found that a broken wire (joining pins A and E in the sensor plug) eliminated the effect of the S resistor, causing underdamped amplitudes. Calibration tests performed in the laboratory on these sensors before and after rewiring indicated the necessity to apply a reduction factor of 0.56 to the recorded amplitudes for those sensors. Header values for sensor coil constants (sensitivity) were then changed from 1.0 V/cm/s to 1.78 V/cm/s (1.0/0.56) on those five components.

APPENDIX A: GENERAL DESCRIPTION OF GEOS INSTRUMENTATION AND CALIBRATION

The GEOS recording system was developed by the U.S. Geological Survey for use in a wide variety of seismic experiments. The digital data acquisition system operates under control of a central microprocessor, which permits adaptation of the system for a variety of field experiments including seismic refraction, and studies of near-source high-frequency strong motion, teleseismic earth structure, earth tidal strains, and free oscillation.

The power consumption in record-mode is approximately two and a half Watt. The system may be used as a portable recorder in remote locations or as a permanent recorder in an observatory setting with inexpensive 24V DC backup power sources. Figure A1 shows the GEOS system with two sets of three-component sensors (force-balance accelerometer, velocity transducer) and an external WWVB antenna commonly used for controlled-source, and local-regional earthquake experiments. (See Borcherdt and others, 1985, for a description of the hardware modules comprising the system.)

The GEOS has six channels of signal conditioning modules for amplification and filtering. Selectable under software control, they permit acquisition of seismic signals ranging in amplitude from slightly above seismic background noise to 2 g in acceleration for ground motions near large events. The analog-to-digital conversion module is equipped with a 16-bit CMOS analog-to-digital converter, which provides 96 dB of linear dynamic range or signal resolution. With two sets of sensors, this implies an effective system dynamic range of about 180 dB. A data buffer with direct memory access capabilities allows for maximum throughput rates of 1200 samples/second. With sampling rates software selectable as any integral quotient of 1200, broad and variable system bandwidth ranging from 10^{-5}–$6 \cdot 10^{2}$ Hz has been achieved by using the recorders with a wide variety of sensor types (*e.g.,* Borcherdt and others, 1985).

The GEOS instruments use high-density compact tape cartridges that store large data sets in ANSI standard format, which allows minicomputer systems to easily access data (1600 bpi, 2.5 Mbyte tape cartridges were used for the Hawaiian experiments.)

The GEOS instruments are equipped with internal WWVB receivers, and the GEOS internal clocks can be synchronized with WWVB or external standards such as GOES

satellite, master clock, or conventional digital clocks. The GEOS can be programmed to determine time corrections with respect to any time standard. This capability permits especially accurate correction for conventional drift of internal clocks.

In situ calibration of GEOS deployments improves data accuracy and allows on-site evaluation of instrument and sensor performance. The calibration module in the GEOS allows calibration of the signal-conditioning modules and three types of sensors: velocity transducers with calibration coils, those without the coils, and force-balance accelerometers. The system response with current velocity transducers (Mark Products L–22 and L–4 sensors) allows broad-band signals (0.5–400 Hz) to be recorded on scale with high resolution.

Calibration signals, automatically generated by GEOS, provide a reference for accurate calibration of ground motion as recorded at the GEOS sensor locations. Two signals are used as calibration for the data recorded on the velocity sensors. Shut off of a known DC voltage applied to the sensor coil is used as a calibration signal for the complete sensor-recording system, and an impulse in voltage applied at the input of the recording system provides a spiked calibration signal for the recording system independent of the sensors. The GEOS instrument selects one voltage value for both of these signals based on the active channel with the highest gain setting. Table A1 lists these voltages. Analysis of both of these calibration signals can determine the response of the recorder as well as the response of the recorder-sensor combination.

The DC voltage input signal applied to the sensor coil simulates a step-function in ground acceleration applied to the mass of the sensor. The unit impulse response of the complete sensor-recording system to ground velocity can then be estimated from the Fourier transform of the step accleration response multiplied by the square of angular frequency. The left-hand side of Figure A2 shows the Fourier amplitude spectra of the velocity response computed for three channels of the GEOS unit, with the sensors included, for stations J1, J2, and J3 of the second array at Pu'u O'o. The low-frequency roll-off is controlled by the sensor response, which rolls off proportional to ω^3 at low frequencies; the high-frequency limit is imposed by the corner frequency of the selected anti-aliasing filter.

The impulse applied at the input of the recording system is automatically selected by

GEOS to be one sample in duration. The right-hand side of Figure A2 shows the Fourier amplitude spectra computed from the resulting output signal of the three channels of the GEOS unit, without the sensors, for stations J1, J2, and J3 of the second array at Pu'u O'o. These spectra provide an estimate of the amplitude response of the signal conditioning system alone in terms of ground velocity. The frequency response of the recording system can be estimated for frequencies greater than a low-frequency limit imposed by the relative strength of the applied impulse voltage for the selected gain setting.

The analysis of the recorded calibration signals provides an estimate of the overall instrumental response to ground velocity for each GEOS deployment location.

A complete record of recording system parameters is saved on each tape together with calibration signals for both the sensors and the recorders. These records assure rapid and accurate signal interpretation, both in the field and in the laboratory with computers.

Data can be played back in either an analog or digital format in the field using the read capability of the GEOS mass-storage module. Data can also be played back using portable mini-computer systems configured with appropriate cartridge tape readers (see Borcherdt and others, 1985, for details). For the Hawaiian experiments, analog playbacks on light-sensitive paper were used in the field to identify seismic events and trigger parameters, analyze seismic wave coherence, and evaluate instrument performance. Digital playback of the data was conducted with a Tandberg serpentine tape drive attached to a DEC PDP 11/70 at the National Strong Motion Data Center in Menlo Park. Software packages, developed by G. Maxwell, E. Cranswick, C. Mueller, A. Converse, and B. Chouet were used to play back and process the data set.

APPENDIX B: GEOS DATA FORMATS

For processing and analysis of the GEOS data at the U.S. Geological Survey, we conventionally use the data in what is termed NSMDC (National Strong Motion Data Center) format (also termed "GEOS" or "DR–100" format). For distribution of the data set by the IRIS Data Management Center and to facilitate its usage by other centers, the data can be presented in SEG–Y format (Barry and others, 1985). For a detailed description of the SEG–Y format see Barry and others (1985).

Data Format for GEOS Tape Cartridges

The GEOS recording unit writes data onto a 1/4–inch digital magnetic tape cartridge conforming to ANSI specification X3.55–1977. The tape drive writes four tracks of data, one track at a time, in a "serpentine" manner. When one track of data has been completed, the tape drive writes the subsequent track of data in the opposite direction. The tape drives used for this study write data at a density of 1600 bits/inch.

Data on a tape cartridge are organized into events. An event is organized as one or more records of data, followed by a tape file mark. Two types of events are recognized: clock events, which provide time standard information, and seismic data events, including calibrations.

Each data record is composed of 512 16-bit words, or 1024 8-bit bytes. A seismic data record contains a time stamp followed by a stream of multiplexed digitized samples from all active channels. For example, a typical seismic data record for one event with channels 4, 5 and 6 active would be organized as follows:

Word	1:	Year (last two digits)
Word	2:	Julian day of year
Word	3:	Hour of day
Word	4:	Minutes
Word	5:	Seconds
Word	6:	Milliseconds
Word	7:	Channel 4 data
Word	8:	Channel 5 data
Word	9:	Channel 6 data
Word	10:	Channel 4 data
Word	11:	Channel 5 data
	⋮	
Word	508:	Channel 4 data
Word	509:	Channel 5 data
Word	510:	Channel 6 data

The time stamp in each data record is directly associated with the first sample in the data record. Note that some words out of a data record may not be used; such free words may be used for other purposes in future versions of the GEOS software.

The first data record of an event contains a special block of data, called an event header. (Event header information is subject to change in future releases of the GEOS software.) When the GEOS begins writing data to the cartridge tape, it overwrites the seismic data already sampled into the first part of the first data record with the event header. With this method, the time stamp that precedes the event header applies to forty-nine data samples that have been overwritten. In the data analysis procedures, this time is adjusted to correctly reflect the time of the first sample, which can be used from the first data record. The format of a GEOS event header as presently defined is given in Table B1.

National Strong Motion Data Center Format

Data recorded by GEOS currently are read and analyzed by a Digital Equipment Corporation PDP–11/70 minicomputer, which runs the RSX–11M–Plus operating system. The data is demultiplexed and stored as disk-resident time series files, which conform to a data format (NSMDC format) developed initially by Jon B. Fletcher and Joanne Vinton.

A single GEOS seismic event is converted to one or more files under the NSMDC format. Each NSMDC format file contains digitized data from a single component of motion. Therefore, a single GEOS seismic event can generate between one and six NSMDC format files.

Each NSMDC file contains header information regarding the physical and electronic aspects of the digitized data. Although this causes some redundant information to be included with each component file from one seismic event, each component may be processed separately and independently from all other components of the same event.

A file is composed of 16-bit signed integer values and 32-bit floating-point values in PDP–11 floating-point format. Data may be represented in either integer or floating-point format, but only one format may be used in one file. GEOS data is always stored in integer format.

Each file is organized into 512-byte records. This record size was chosen because it is the blocksize of a PDP–11 or VAX disk block. Data may then be processed by using efficient read and write requests.

Each file is organized as follows:

Record	1:	Header record (integer)
Record	2:	Header record (floating point)
Record	3:	Data record number 1
	⋮	
Record 2+n:		Data record number n

The ability to define extra header records has been incorporated into the data format to allow for storage of additional information. If used, these header records would follow the floating-point header record.

The NSMDC has a rigid file naming format. The file name is generated from the following information: the time the first data sample in the file was recorded, the particular component the file represents, and the three-character station name where the GEOS recorder or motion sensor was located.

Specifically, a NSMDC file name has the following form:

JJJHHMMSC.STA

where "JJJ" is the Julian day of the year, "HH" is the hour in 24-hour format, "MM" is the minute of the hour, "S" is a letter code from A to T, which represents the three-second interval of the minute, "C" is the component number, and "STA" is the 3-letter station name.

The following conventions have been established for the specific fields of the file name. The time must be normalized to Coordinated Universal Time (Greenwich Mean Time). By convention, components 1 through 3 are reserved for acceleration motion, 4 through 6 are used for velocity motion, and 7 through 9 are reserved for displacement. (In the Hawaiian experiments components 1 through 6 were used for velocity motion.) Components 1, 4, and 7 represent the vertical component of motion; 2, 5 and 8 represent a horizontal component (typically true north); 3, 6, and 9 represent a horizontal component (typically true east). The exact orientation of each component can be specified within the header data for each file.

The header offsets that are used for data recorded by GEOS are presented in Tables B2 and B3. Headers are usually edited in subsequent processing. Furthermore, data recorded

by other instruments may not require the use of some of these offsets in the headers. The absence of data in a particular header field is indicated by the use of the "undefined value" in such fields. The "undefined value" is usually the most negative integer which can be represented with 16 bits (−32768) or the smallest representable 32-bit floating-point number in PDP–11 floating-point format ($1.7 \cdot 10^{-38}$).

ACKNOWLEDGMENTS

The authors wish to acknowledge Tom Wright, Reggie Okamura, Jennifer Nakata, Christina Heliker, James Griggs, and many others at the Hawaiian Volcano Observatory for their invaluable assistance in the Hawaiian array experiments. Mr. and Mrs. Dallas Jackson provided excellent accommodations. John McRaney of the University of Southern California provided the travel logistics for both the USC and USGS crews, and Michelle Robertson and Aaron Martin provided needed assistance packing up at the end of our experiment.

Several people of the USGS in Menlo Park are to be acknowledged. Gary Maxwell offered his expertise and hours of his time developing the timing, calibration, and general operation procedures for the GEOS instruments in an array configuration. Joe Sena helped design the array sensor cables and test and modify the GEOS instruments specially for the objectives of the Hawaiian array experiment and for the Hawaiian environment. Don Ritchey constructed array sensor cables and designed special equipment that assisted array setup in the field. Chuck Mueller provided us with computer playouts in Menlo Park during the initial analysis of the data tapes from the first array . Software developed by G. Maxwell, E. Cranswick, J. Vinton, C. Mueller, G. Glassmoyer, B. Chouet, A. Converse, and C. Dietel facilitated the processing and analysis of the data presented in this report. Ray Eis drafted many of the figures in this report, and Cynthia Ramseyer assisted in much of the typing. Carol Sullivan provided her talents with TEX to produce readable text.

Special thanks are due to David Okita of Volcano Heli-Tours who provided us with superb helicopter assistance, useful information and advice concerning the conditions at Pu'u O'o, and a constant helping hand during our experiments.

REFERENCES CITED

Aki, K., Space and time spectra of stationary stochastic waves, with special reference to microtremors, *Bull. Earthq. Res. Inst. Tokyo Univ.*, **35**, 415–456, 1958.

Aki, K., and Richards, P., *Quantitative Seismology, Theory and Methods*, **1**, 497, 1980.

Barry, K. M., Cavers, D., and Kneale, C., Recommended standards for digital tape formats, *Geophysics*, **40**, 344–352, 1985.

Borcherdt, R. D., Fletcher, J., Jensen, E., Maxwell, G., Van Schaack, J., Warrick, R., Cranswick, E., Johnston, M., and McClearn, R., A General Earthquake Observation System (GEOS), *Seismological Society of America Bulletin*, **75**, 1783–1823, 1985.

Koyanagi, R.Y., Chouet, B., and Aki, K., Origin of volcanic tremor in Hawaii, *U.S. Geological Survey Professional Paper* **1350,** 2, 1221–1257, 1987.

Swanson, D. A., Duffield W., Jackson, D., and Peterson, D., Chronological narrative of the 1969–71 Mauna Ulu eruption, Kilauea Volcano, Hawaii, *U.S. Geological Survey Professional Paper* **1056,** 55 p., 1979.

Wiggins, R. A., Interpolation of digitized curves, *Bull. Seismol. Soc. Am.*, **66**, 2077–2081, 1976.

Yuen, C.K., Quadratic windowing in the segment averaging method for power spectrum computation, *Technometrics*, **20**, 195–200, 1978.

Table 1. Recording parameters—first array.

Data Collection Period (GMT: HR:MN)	Recording Mode	Ratio	Station	Gain	Sample Rate
1: 18:19–19:21	3–Min. Preset Windows 2–Hr. Period	–	–	42	200
2: 19:18–20:01	15–Min. Preset Window One Window (19:21:59)	–	–	60	200
3: 19:22–22:03	3–Min. Preset Windows 5–Hr. Period Triggers	2**3	5.0	42	200
4: 21:23–23:01	3–Min. Preset Windows 2–Hr. Period Triggers	2**2	5.0	60	200
5: 22:19–26:00	5–Min. Preset Windows 12–Hr. Period Triggers	2**2	5.0	48	200
6: 25:20–27:22	5–Min. Preset Windows One Window (27:14:59) Triggers	2**2	2.0	48	200

Table 2. Recording parameters—second array.

Data Collection Period (GMT: HR:MN)	Recording Mode	Ratio	Station	Gain	Sample Rate
7: 29:21–33:00	3–Min. Preset Windows 12–Hr. Period Triggers	2**2	2.0	48	200
8: 32:19–34:22	3–Min. Preset Windows 12–Hr. Period Triggers	2**3*	2.0*	48	200
9: 34:18–35:22	Triggers One Preset Window (35:18:44)	2**4	1.0	48	200
10: 35:21–36:01	One Manual Continuous Record	–	–	48	100
11: 36:01–43:23	Triggers One Preset Window (43:20:59)	2**3	0.5	48	200
12: 43:21–45:20	3–Min. Preset Windows 12–Hr. Period Triggers	2**3	0.5	48	200
13: 45:18–46:00	One Manual Continuous Record	–	–	48	100
14: 45:22–48:21	3–Min. Preset Windows 12–Hr. Period Triggers (+ One Additional Preset: 48:19:59)	2**4	0.5	48	200
15: 48:20–51:21	3–Min. Preset Windows 24–Hr. Period Triggers (+ One Additional Preset: 51:19:59)	2**2	0.5	42	200

*Sta = 1.0, Ratio = 2**2, for events 32:22:27, 33:00:19

Table 3. Preset recordings of harmonic tremor—first array.

Data Collection Period	Recording Start Time (GMT: DAY:HR:MN)	Window Length	Number of Units that Recorded
1	019 02 59	3 Minutes	8
	019 04 59		8
	019 06 59		9*
	019 08 59		9*
	019 10 59		8
	019 12 59		8*
	019 14 59		8
	019 16 59		8
2	019 21 59	15 Minutes	11*
3	020 05 59	3 Minutes	11*
	020 10 59		11*+
	020 15 59		10+
	020 20 59		11*+
	020 01 59		10*
	021 06 59		10*
	021 11 59		9*
	021 16 59		9*
4	022 03 59	3 Minutes	11*+
	022 05 59		11+
	022 07 59		11*
	022 09 59		11+
	022 11 59		11*+
	022 13 59		11*
	022 15 59		10*
	022 17 59		6*
5	023 09 59	5 Minutes	11*
	024 09 59		11*+
	025 09 59		11*+
6	027 14 59	5 Minutes	11*+

*One or more GEOS instruments obtained only partial recordings of window.

+Ten or more GEOS instruments obtained full recordings of at least 3 minutes.

Table 4. Earthquakes recorded with the first array.

Data Collection Period	Recording Start Time (GMT: DAY:HR:MN)	# of Units that Recorded
3	021 15 49	8
4	022 03 30	11
	022 15 43	10
	022 17 04	10
5	023 09 36	10
	023 12 23	8
	023 12 52	5
	024 03 26	8
	024 09 39	9
	024 20 24	3
	024 21 48	8
	024 23 59	11
	025 03 26	6
	025 03 30	5
	025 07 43	6
	025 20 33	4
6	026 06 25	11
	026 07 28	11
	026 08 09	3
	026 11 23	4
	026 19 21	6
	026 19 41	2
	026 21 50	5
	027 01 24	11
	027 02 49	10
	027 05 17	10
	027 05 22	6
	027 05 35	5
	027 09 44	9
	027 15 05	4

Table 5. Earthquakes recorded with GEOS and correlated with determinations from the HVO CUSP network—first array.

Date	Time (GMT) (HR:MN:SEC)	Latitude	Longitude	Magnitude	# of Units that Recorded
88 Jan 22	15:43:47.15	19 19.96	155 07.56	2.0	10
88 Jan 22	17:04:18.43	19 23.40	154 42.29	4.1	10
88 Jan 23	09:36:37.14	19 20.37	155 07.14	1.8	10
88 Jan 23	12:52:23.24	19 21.81	155 03.50	1.7	5
88 Jan 24	09:39:06.00	19 21.83	155 04.55	1.7	9
88 Jan 25	03:26:31.72	19 16.67	155 06.02	1.3	6
88 Jan 25	03:30:28.33	19 19.83	155 12.57	2.0	5
88 Jan 25	07:43:40:84	19 20.95	155 03.38	1.8	6
88 Jan 26	07:28:56.22	19 20.72	155 07.70	2.2	11
88 Jan 26	08:09:43.64	19 19.94	155 08.28	1.4	3
88 Jan 26	19:21:42.42	19 19.71	155 07.54	1.6	6
88 Jan 27	01:24:35.97	19 19.49	155 03.43	3.9	11
88 Jan 27	02:49:04.48	19 20.89	155 03.75	2.0	10
88 Jan 27	05:17:15.13	19 21.49	155 11.41	2.0	10
88 Jan 27	05:22:46.74	19 21.25	155 10.85	1.9	6
88 Jan 27	05:35:16.35	19 22.12	155 03.89	1.6	5
88 Jan 27	15:05:57.60	19 20.08	155 03.56	1.6	4

Table 6. Preset recordings of harmonic tremor—second array.

Data Collection Period		Recording Start Time (GMT: DAY:HR:MN)	Window Length	Number of Units that Recorded
7		030 02 59	3 Minutes	12^{++}
		030 14 59		12^{++}
		031 02 59		10*
		031 14 59		8*
		032 02 59		6*
8		033 02 59	3 Minutes	12^{++}
		033 14 59		9*
9		035 18 44	2 Minutes Minimum	10*
Array Line:				
10	A:	035 21 58	40 Minutes	12^{++}
	B:	035 21 59	(each line manu-	
	C:	035 21 59	ually started)	
	D:	035 22 01		
	E:	035 22 00		
	F:	035 22 01		
	G:	035 22 01		
	H:	035 21 59		
	I:	035 21 59		
	J:	035 22 00		
	K:	035 22 01		
	L:	035 22 00		
11		043 20 59		11^{+}
12		043 23 59		12^{*+}
		044 11 59		9
Array Line:				
13	A:	045 21 07	40 Minutes	12^{++}
	B:	045 21 08	(each line manu-	
	C:	045 21 08	ually started)	
	D:	045 21 08		
	E:	045 21 09		
	F:	045 21 10		

(Continued)

Table 6 (Continued). Preset recordings of harmonic tremor—second array.

Data Collection Period	Recording Start Time (GMT: DAY:HR:MN)	Window Length	Number of Units that Recorded
	H: 045 21 07		
	I: 045 21 08		
	J: 045 21 09		
	K: 045 21 09		
	L: 045 21 10		
14	046 11 59	3 Minutes	12++
	046 23 59		11*
	047 11 59		11+
	047 23 59		11*
	048 19 59		9*
15	050 11 59	3 Minutes	7
	051 11 59		7
	051 19 59		7*

*One or more GEOS instruments obtained only partial recordings of window.

+Ten or more GEOS instruments obtained full recordings of at least 3 minutes.

++12 GEOS instruments obtained full recordings of at least 3 minutes.

Table 7. Triggered recordings of gas-piston events.
(seven or more GEOS unit triggers)

Data Collection Period	Recording Start Time (GMT: DAY:HR:MN)	# of Units that Recorded
7	031 10 13	8
8	033 03 19	12
	033 03 55	12
	033 04 25	12
	033 04 49	12
	033 05 21	12
	033 06 00	12
	033 06 34	12
	033 07 00	11
	033 08 04	10
	033 09 20	10
	033 09 46	10
	033 10 12	7
	033 10 32	8
	033 10 49	10
	033 11 10	10
	033 14 26	7
9	Note: ten or more triggers only:	
	035 00 11	10
	035 01 14	10
	035 01 51	10
	035 02 38	12
	035 04 26	12
	035 05 32	12
	035 06 44	12
	035 08 45	11
	035 09 11	11
	035 09 51	11
	035 13 04	10
	035 15 24	10
	035 16 01	12
11	(043 06 32)	(6)

(Continued)

Table 7 (Continued). Triggered recordings of gas-piston events.
(seven or more GEOS unit triggers)

Data Collection Period	Recording Start Time (GMT: DAY:HR:MN)	# of Units that Recorded
12	044 17 51	10
	044 17 55	10
	044 18 25	7
	044 18 32	10
	044 18 38	9
	044 18 44	10
	044 18 50	10
	044 18 58	10
	044 19 04	10
	044 19 11	10
	044 19 17	10
	044 19 23	10
	044 19 54	10
	044 20 04	9
	044 20 28	9
	044 20 35	8
14	046 06 19	12
	046 16 22	8
	046 18 19	7
	046 19 48	9
	047 01 31	11
	047 07 10	8

Table 8. Earthquakes recorded with the second array.

Data Collection Period	Recording Start Time (GMT: DAY:HR:MN)	# of Units that Recorded
7	030 18 36	11
	031 00 28	4
	031 09 56	8
8	033 00 19	7
11	040 15 09	5
	041 13 26	10
	043 11 03	4
12	044 07 55	10
	044 08 48	10
15	051 04 47	7

Table 9. Earthquakes recorded with GEOS and correlated with determinations from the HVO CUSP network—second array.

Date	Time (GMT) (HR:MN:SEC)	Latitude	Longitude	Magnitude	# of Units that Recorded
88 Jan 30	18:36:20.76	19 21.66	155 05.84	1.8	11
88 Jan 31	09:56:21.43	19 21.38	155 02.65	1.7	8
88 Feb 09	15:09:59.15	19 20.32	155 06.47	1.9	5
88 Feb 10	13:26:57.64	19 21.10	155 02.49	3.4	10
88 Feb 13	07:55:29.73	19 17.61	155 12.84	2.7	10
88 Feb 13	08:48:34.41	19 16.71	155 13.01	3.0	10
88 Feb 20	04:47:04.74	19 21.21	155 01.58	4.1	7*

*Also recorded on the 4 summit stations

Table 10. Station locations near the Kilauea summit.

Station	Instrument	Latitude	Longitude
		GEOS Stations	
OUT	39	19 23.6N	155 17.3W
MOB	46	19 27.2N	155 20.0W
MOA	26	19 29.8N	155 23.3W
YNG	6	19 28.7N	155 16.0W
		U.S.C. Stations	
ESC	6	19 22.5N	155 13.1W
HIL	4	19 18.1N	155 18.7W
HVO	5	19 25.4N	155 17.6W
KEA	3	19 24.3N	155 15.2W
NEN	1	19 20.6N	155 16.6W
PUO	2	19 23.5N	155 06.6W

Table 11. Earthquakes recorded with GEOS at four summit stations correlated with determinations from the HVO CUSP network.

Date	Time (GMT)	Latitude	Longitude	Magnitude
88 Feb 19	00:00:21.60*	19 25.70	155 16.06	2.0
88 Feb 19	03:39:45.70*	19 23.28	155 17.80	1.8
88 Feb 19	04:58:59.33*	19 24.72	155 16.56	1.9
88 Feb 19	07:00:17.60*	19 27.16	155 13.61	1.8
88 Feb 20	04:47:04.74**	19 21.21	155 01.58	4.1
88 Feb 20	04:50:31.84	19 21.99	155 01.81	2.8
88 Feb 20	06:25:26.39	19 20.91	155 01.08	2.8
88 Feb 21	00:55:02.12	19 22.28	155 30.08	2.4
88 Feb 24	14:00:31.82	19 25.69	155 20.43	2.1
88 Feb 24	14:45:28.69	19 26.00	155 20.01	1.7
88 Feb 24	14:51:51.17	19 25.74	155 20.16	1.5
88 Feb 24	15:27:38.38	19 26.02	155 20.13	2.5
88 Feb 24	15:29:10.97	19 26.29	155 19.60	1.8
88 Feb 28	08:03:17.19	19 22.41	155 29.98	1.7
88 Feb 28	14:43:59.75	19 25.09	155 16.18	1.5
88 Feb 28	16:51:41.46	19 22.38	155 29.96	2.2
88 Feb 28	17:34:31.26	19 24.87	155 19.34	1.4

*LPC event recorded on station OUT only.

**Also recorded on 7 Pu'u O'o array units.

Table 12. Earthquakes recorded with GEOS at three summit stations and correlated with determinations from the HVO CUSP network.

Date	Time (GMT)	Latitude	Longitude	Magnitude
88 Feb 24	14:02:21.69	19 25.99	155 20.15	1.5
88 Feb 24	15:23:24.35	19 26.70	155 19.49	1.3
88 Feb 24	16:13:50.17	19 25.58	155 19.82	1.2
88 Feb 24	17:54:16.57	19 26.28	155 19.82	1.4
88 Feb 24	19:37:12.57	19 26.05	155 19.46	1.5
88 Feb 24	20:52:43.21	19 25.94	155 19.84	1.5
88 Feb 24	21:05:02.96	19 26.16	155 19.26	1.4
88 Feb 24	23:23:22.60	19 26.02	155 19.00	1.6
88 Feb 24	23:35:45.70	19 25.73	155 19.74	2.2
88 Feb 24	23:43:12.62	19 26.03	155 19.44	1.3
88 Feb 28	08:11:31.37	19 31.19	155 20.86	1.3
88 Feb 28	14:37:49.31	19 58.15	155 28.85	2.1

Table 13. Calibration recording parameters—first array.

Array Line	Channels	Recording Time (GMT: DAY:HR:MN)	Gain (dB)	Sample Rate (s/s/chan.)
A	1–6	001 00 04*	42	200
	1–6	001 00 05*		
B	1–6	018 21 39	42	200
	1–6	018 21 40		
C	1–6	018 21 12	42	200
	1–6	018 21 12		
D	1–6	018 22 01	42	200
	1–6	018 22 02		
E	1–3	019 00 43	42	200
	1–3	019 00 44		
	4–6	019 00 46		
	4–6	019 00 47		
F	1–6	018 19 51	42	200
	1–6	018 19 51		
G	1–3	018 22 36	42	200
	1–3	018 22 37		
	4–6	018 22 39		
	4–6	018 22 40		
H	1–3	019 01 49	42	200
	1–3	019 01 50		200
	4–6	019 01 51		100
	4–6	019 01 52		100
I	1–6	018 23 21	42	200
	1–6	018 23 21		
J	1–6	027 20 48	48	200
	1–6	027 20 49		
K	1–6	018 23 43	42	200
	1–6	018 23 44		

*Corrupt header time (record 0–K).

Table 14. Calibration recording parameters—second array.

Array Line	Channels	Recording Time (GMT: DAY:HR:MN)	Gain (dB)	Sample Rate (s/s/chan.)
A	1–6	051 19 07	42	200
	1–6	051 19 07		
B	1–6	048 21 53	48	200
	1–6	048 21 54		
C	1–6	048 22 29	48	200
	1–6	048 22 29		
D	1–6	051 19 32	42	200
	1–6	051 19 33		
E	1–6	048 22 38	48	200
	1–6	048 22 38		
F	1–6	088 00 48*	48	200
	1–6	003 01 03*		
G	1–6	051 19 43	42	200
	1–6	051 19 44		
H	1–6	051 19 15^	42	200
	1–6	051 19 16^		
I	1–3	051 19 28	42	200
	1–3	051 19 29		
	4–6	051 19 25		
	4–6	051 19 26		
J	1–6	051 19 38	42	200
	1–6	051 19 39		
K	1–6	051 20 11^	42	200
	1–6	051 20 11^		
L	1–3	051 19 52	42	200
	1–3	051 19 53		200
	4–6	051 19 50		100
	4–6	051 19 50		100

*Corrupt header time (record 0–K).

^Bad record.

Table 15. Calibration recording parameters—summit stations.

Station	Channels	Recording Time (GMT: DAY:HR:MN)	Gain (dB)	Sample Rate (s/s/chan.)
OUT	4–6	074 23 31	42	100
	4–6	074 23 32	42	100
MOA	4–6	074 23 04	42	100
	4–6	074 23 05	42	100
MOB	4–6	074 23 00	42	100
	4–6	074 23 01	42	100
YNG	4–6	074 23 00	42	100
	4–6	074 23 01	42	100

Table 16. Calibration factors for L–4C sensors.

L–4C #	Factor	L–4C #	Factor
81	1.22	101	1.22
82	1.22	102	1.23
83	1.22	103	1.23
84	1.22	104	1.25
85	1.20	105	1.23
86	1.22	106	1.27
87	1.23	107	1.28
88	1.22	108	1.24
89	1.24	109	1.20
90	1.25	110	1.25
91	1.21	111	1.22
92	1.22	112	1.21
93	1.23	113	1.22
94	1.22	114	1.22
95	1.26	115	1.23
96	1.21	116	1.23
97	1.25	117	1.22
98	1.21	118	1.21
99	1.22	119	1.21
100	1.23	120	1.23

Table 17. Calibration factors for L–22–3D sensors.

L–22–3D #	Component	Factor	L–22–3D #	Component	Factor
157	V	2.32	199	V	2.68
	N	–		N	3.07
	E	2.33		E	3.21
162	V	1.91	302	V	2.33
	N	2.23		N	2.46
	E	2.26		E	1.53
189	V	2.19	304	V	1.81
	N	2.29		N	2.53
	E	2.01		E	2.16
190	V	1.84	305	V	2.02
	N	1.69		N	1.64
	E	1.81		E	2.30
196	V	2.17	310	V	2.05
	N	2.49		N	2.07
	E	2.35		E	1.75
197	V	2.57	311	V	2.01
	N	3.12		N	1.92
	E	2.81		E	1.86

Table 18. Instrument–sensor array configurations—first array.

Array Line Letter Code	Instrument #	Sensor Type	Channel	Sensor # 1	2	3	4	5	6
A	42	L–4		87	104	91	77	89	82
B	10	L–22/L–4		–	162	–	112	116	108
C	15	L–22/L–4		–	311	–	83	118	99
D	43	L–4		113	84	101	98	105	85
E	6	L–22		–	190	–	–	191	–
F	13	L–22		–	310	–	–	305	–
G	40	L–22		–	?	–	–	196	–
H	11	L–22/L–4		–	?	–	?	?	?
I	26	L–4		?	?	?	?	?	?
J	41,19	L–4/L–22		?	?	?	?	?	?
K	39	L–4		?	?	?	?	?	?

Table 19. Instrument–sensor array configurations—second array.

Array Line Letter Code	Instrument #	Sensor Type	Channel	Sensor # 1	2	3	4	5	6
A	13	L–22/L–4		–	199	–	95	119	116?
B	26	L–22		–	190	–	–	162	–
C	6	L–22		–	196	–	–	302	–
D	43	L–22/L–4		–	310	–	112	108	116?
E	39	L–22		–	305	–	–	189	–
F	46	L–22		–	304	–	–	197	–
G	10	L–22/L–4		–	157	–	114	111	93
H	42	L–4		82	97	91	87	104	89
I	40	L–4		84	85	113	98	105	101
J	19	L–4		81	107	109	103	106	83
K	15	L–4		96	90	92	110	100	86
L	11	L–22/L–4		–	311	–	102	118	99

Table A1. Calibration signal voltage values.

Gain (dB)	Value (volts)
0	+2.56000
6	+2.56000
12	+1.64000
18	+0.82000
24	+0.41000
30	+0.20500
36	+0.10250
42	+0.05125
48	+0.02625
54	+0.01375
60	+0.00750

Table B1. GEOS seismic event header description.

Word 1:	Year (last two digits)
Word 2:	Julian day of year
Word 3:	Hour of day
Word 4:	Minutes
Word 5:	Seconds
Word 6:	Milliseconds
Word 7:	Station number
Word 8:	Experiment number
Word 9:	GEOS serial number
Word 10:	Event sequence number
Word 11:	Event type code
Word 12:	Lowest active channel number
Word 13:	Highest active channel number
Word 14:	Channel 1 sensor type
Word 15:	Channel 1 amplifier gain (dB)
Word 16:	Channel 1 anti-alias filter (Hz)
Word 17:	Channel 2 sensor type
Word 18:	Channel 2 amplifier gain (dB)
Word 19:	Channel 2 anti-alias filter (Hz)
Word 20:	Channel 3 sensor type
Word 21:	Channel 3 amplifier gain (dB)
Word 22:	Channel 3 anti-alias filter (Hz)
Word 23:	Channel 4 sensor type
Word 24:	Channel 4 amplifier gain (dB)
Word 25:	Channel 4 anti-alias filter (Hz)
Word 26:	Channel 5 sensor type
Word 27:	Channel 5 amplifier gain (dB)
Word 28:	Channel 5 anti-alias filter (Hz)
Word 29:	Channel 6 sensor type
Word 30:	Channel 6 amplifier gain (dB)
Word 31:	Channel 6 anti-alias filter (Hz)
Word 32:	Aggregate sample rate (Hz)
Word 33:	Number of pre-event records
Word 34:	Number of samples per record
Word 35:	Time standard code
Word 36:	Clock correction block (8 words)
Word 44:	-(Remaining free correction words)
Word 45:	Trigger channel number
Word 46:	Trigger short-term average interval
Word 47:	Trigger long-term average interval
Word 48:	Trigger short-term/long-term ratio
Word 49:	Battery voltage (encoded)

Table B2. Definition of GEOS header offsets for first header record.

First Header Record: 256 16-bit integers

(1)	Number of optional integer header records in use
(2)	Number of optional ASCII header records in use
(3)	"Undefined value" used to flag unused offsets
(4)	*Data type flag*: if positive, data are in floating point format; if negative, data are in integer format. The absolute value of this offset specified the number of bytes per data point. *Special cases*: if 1, then 32-bit floating point format; if "undefined," then 16-bit integer format.
(10)	Year of the event
(11)	Julian day
(12)	Hours
(13)	Minutes
(14)	Seconds
(15)	Milliseconds
(16)	Microseconds number
(17)	Sample number of first time mark
(18)	Detection amplitude of tickmark
(19)	Number of tickmarks detected
(20)	Serial number of recording unit
(21)	Event sequence number
(27)	Number of first active channel recorded by unit
(28)	Recorder channel number used for this component
(29)	Number of active channels recorded by unit
(30)	Number of components recorded under this component's station name
(31)	Number of data records (excluding headers)
(32)	Index of the last sample in the last data record
(33)	Total samples per data record recorded by unit
(34)	Playback program identification code
(35)	Playback program major version number
(36)	Playback program minor version number
(37)	Recording unit type identification code
(38)	Major version number of recording unit software
(39)	Minor version number of recording unit software
(40)	Sensor serial number
(41)	Vertical orientation, in degrees
(42)	Horizontal orientation, in degrees
(43–49)	Sensor model ID (14 ASCII characters)
(50)	Station location number
(51)	Experiment or tape number

(Continued)

Table B2 (Continued). Definition of GEOS header offsets for first header record.

First Header Record: 256 16-bit integers (Continued)	
(52)	Trigger algorithm identification code
(53)	Trigger short-term average interval (tenths of seconds)
(54)	Trigger long-term average interval (seconds)
(55)	Trigger STA/LTA ratio (powers of 2)
(56)	Trigger channel number
(57)	Pre-event memory size (tenths of seconds)
(58)	Post-trigger record duration (seconds)
(101–200)	Processing history (ASCII)
(208)	Data file directory I.D.
(209)	Data file sub-directory I.D.
(210–216)	ASCII filename
(217–219)	ASCII study name

Notes: The GEOS does not record tickmarks.
Header record 1, offset 41: vertical orientation is expressed as a number from 0 to 90, with 0 representing true vertical and 90 representing true horizontal.
Header record 1, offset 42: horizontal orientation is expressed as a number from 0 to 359, with 0 representing true north, and 90 representing true east.

Table B3. Definition of GEOS header offsets for second header record.

Second Header Record: 128 32-bit floating point values	
(1)	Number of optional reel header blocks in use
(2)	"Undefined value" to flag unused offsets
(5)	Component sampling rate, in samples per second
(6)	Component sample lag, in seconds
(39)	Transducer type (four ASCII characters)
(40)	Sensor latitude (decimal degrees)
(41)	Sensor local x-coordinate (meters)
(42)	Sensor longitude (decimal degrees)
(43)	Sensor local y-coordinate (meters)
(44)	Sensor elevation (meters)
(45)	Sensor local z-coordinate (meters)
(46)	Digitizing constant, digital counts per volt
(47)	Anti-alias corner frequency
(48)	Poles of anti-alias filter
(49)	Sensor natural frequency (hertz)
(50)	Sensor damping coefficient
(51)	Sensor motion constant (volts per motion-unit)
(52)	Amplifier gain
(60)	Clock correction
(61)	Seconds since last clock correction
(62)	Instrument battery voltage
(63)	Desired trigger algorithm STA/LTA ratio
(64)	Actual value at trigger moment
(65)	Actual LTA value at trigger moment
(66)	Maximum value of STA/LTA ratio during event

Notes: Header record 2, offset 48: filter roll-off equals 6 dB per pole indicated.

Header record 2, offset 52: gain expressed in dB if Header record 1, offset 5 is equal to one (1); otherwise, gain expressed as an algebraic factor.

Header record 2, offset 60: the clock correction is subtracted from the time specified in Header record 1 to generate the corrected time.

Figure 1. Map showing Kilauea caldera, the east and southwest rift zones of Kilauea Volcano, and the locations of the seismic stations deployed for the Hawaiian experiments. The USGS GEOS arrays, and the USC station PUO, are shown as a single triangle located about 15 km east of Kilauea caldera. The GEOS stations MOA, MOB, YNG, and OUT (open triangles) were deployed in late February to supplement the USC stations HVO, KEA, ESC, HIL, and NEN (solid triangles).

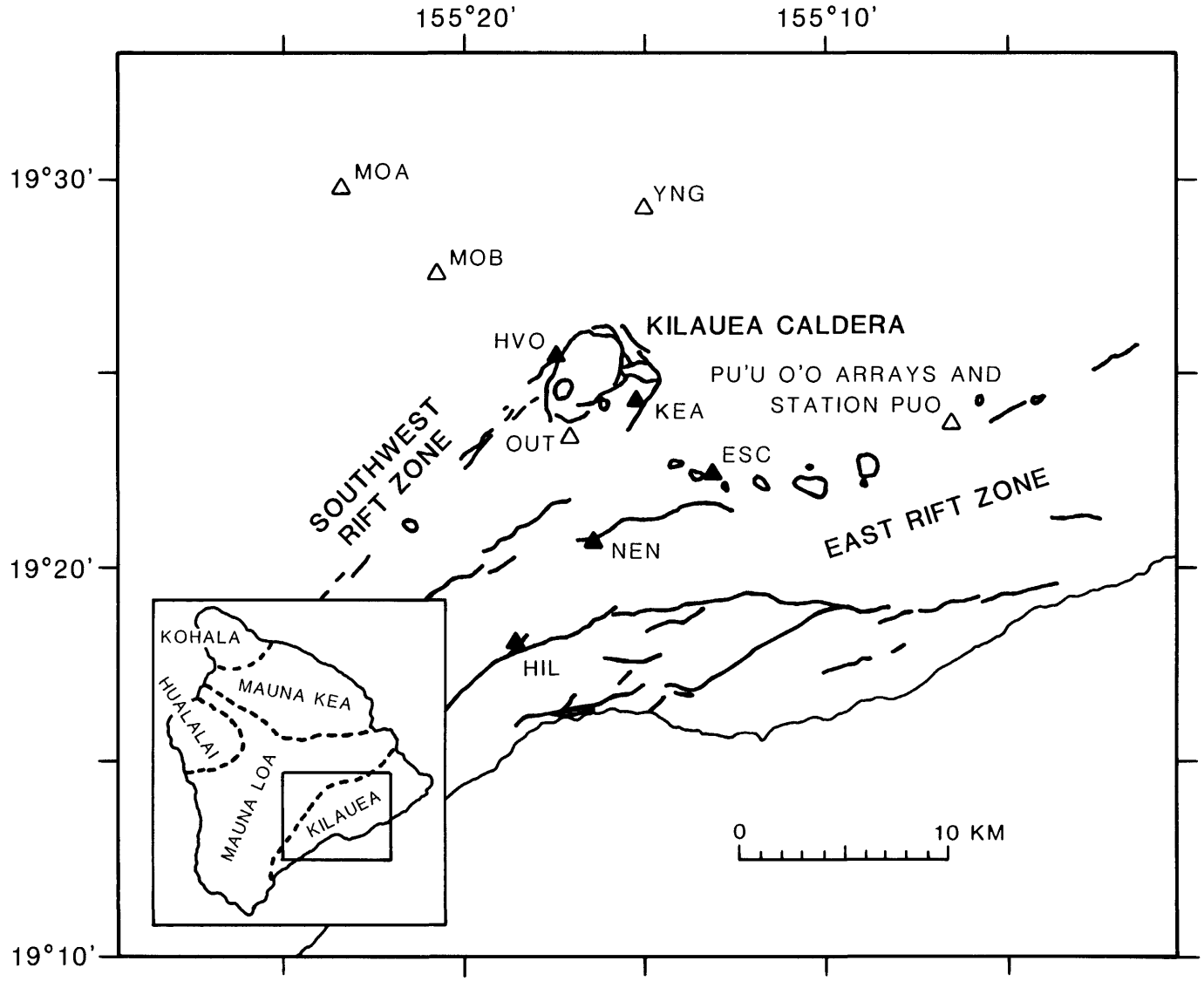
155°20'
155°10'
19°30'
19°20'
19°10'
MOA
YNG
MOB
KILAUEA CALDERA
HVO
PU'U O'O ARRAYS AND
STATION PUO
KEA
OUT
ESC
SOUTHWEST
RIFT ZONE
EAST RIFT ZONE
NEN
HIL
KOHALA
MAUNA KEA
HUALALAI
MAUNA LOA
KILAUEA
0
10 KM

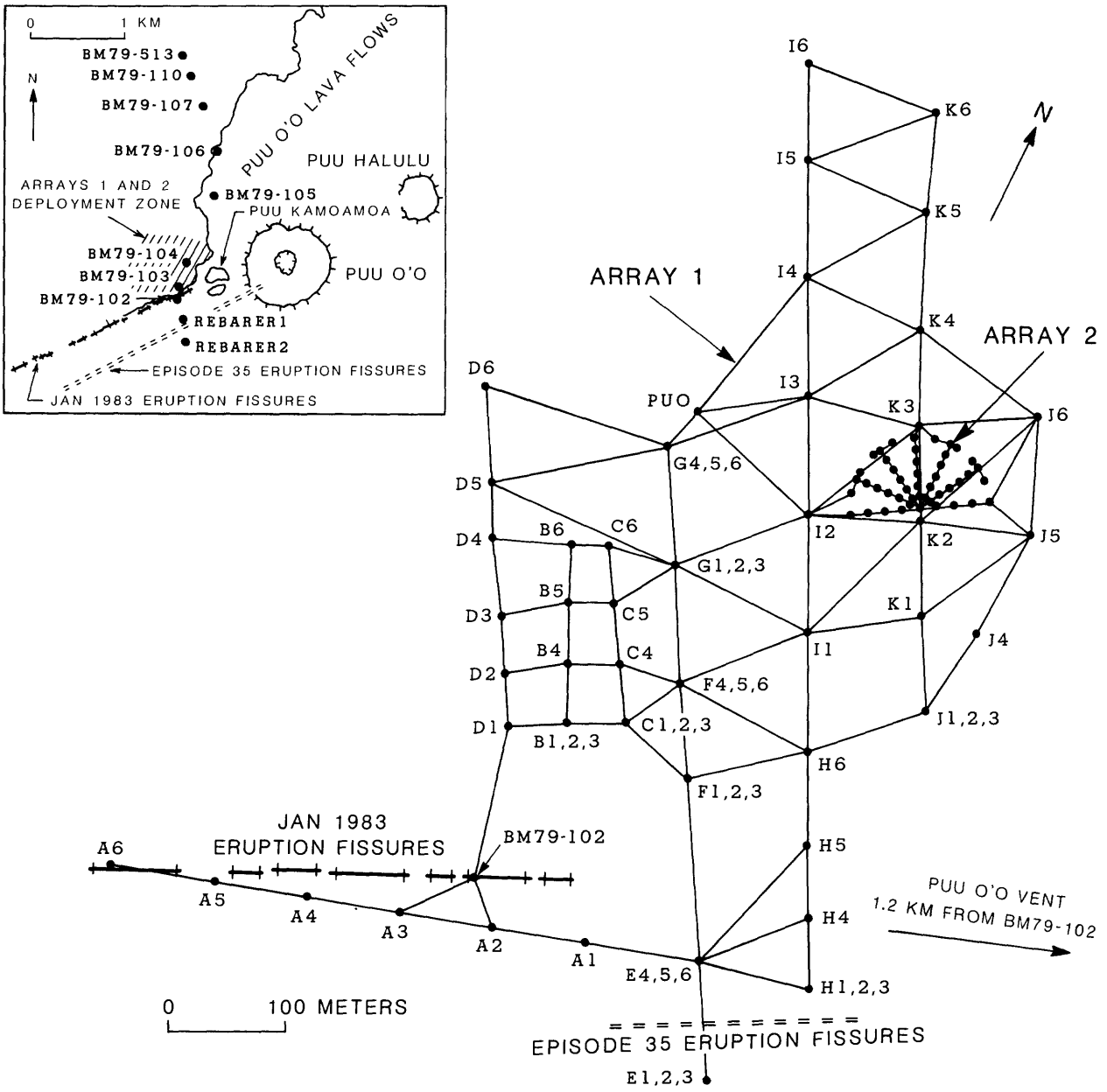

Figure 2. Map showing the configurations of the two GEOS arrays near Pu'u O'o in relation to bench mark BM 79-102 and the eruption fissures of January, 1983, and episode 35. Solid dots depict sensor locations, which are labeled for Array 1 only (see Fig. 3 for sensors of Array 2). The 3-component sensors on Array 1 were oriented with positive radial motion to the north and positive transverse motion to the east. The USC station PUO is shown near sensor G4,5,6. The inset map at the upper left of the figure shows the Arrays 1 and 2 deployment zone in relation to Pu'u O'o, Pu'u Kamoamoa, and local bench marks.

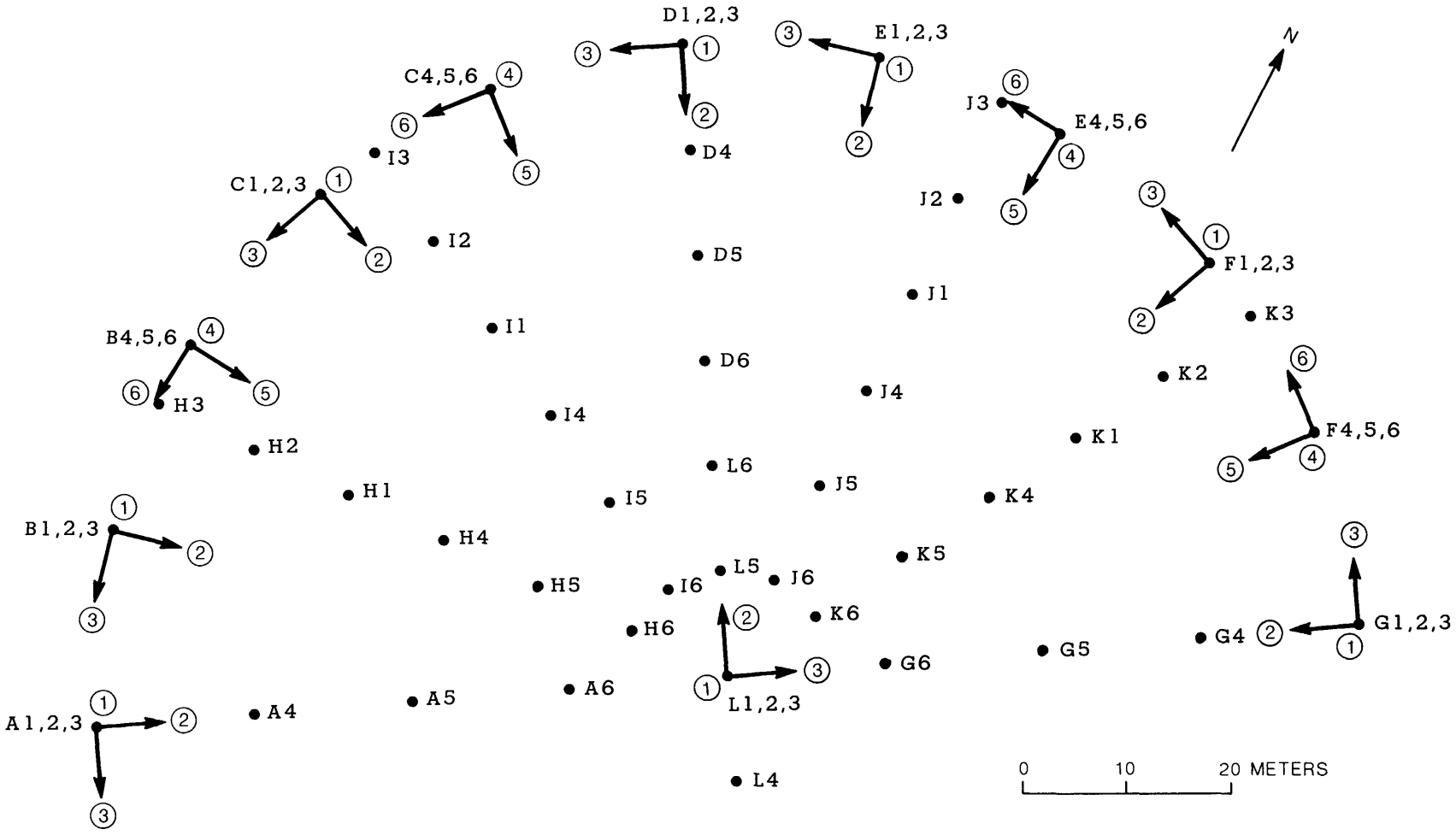

Figure 3. Map showing the configuration of the second GEOS array near Pu'u O'o. Solid dots depict sensor locations. Horizontal-component sensor orientations are indicated by arrows. The arrow directions give the positive directions of motion. Circled numbers represent GEOS channel-number inputs.

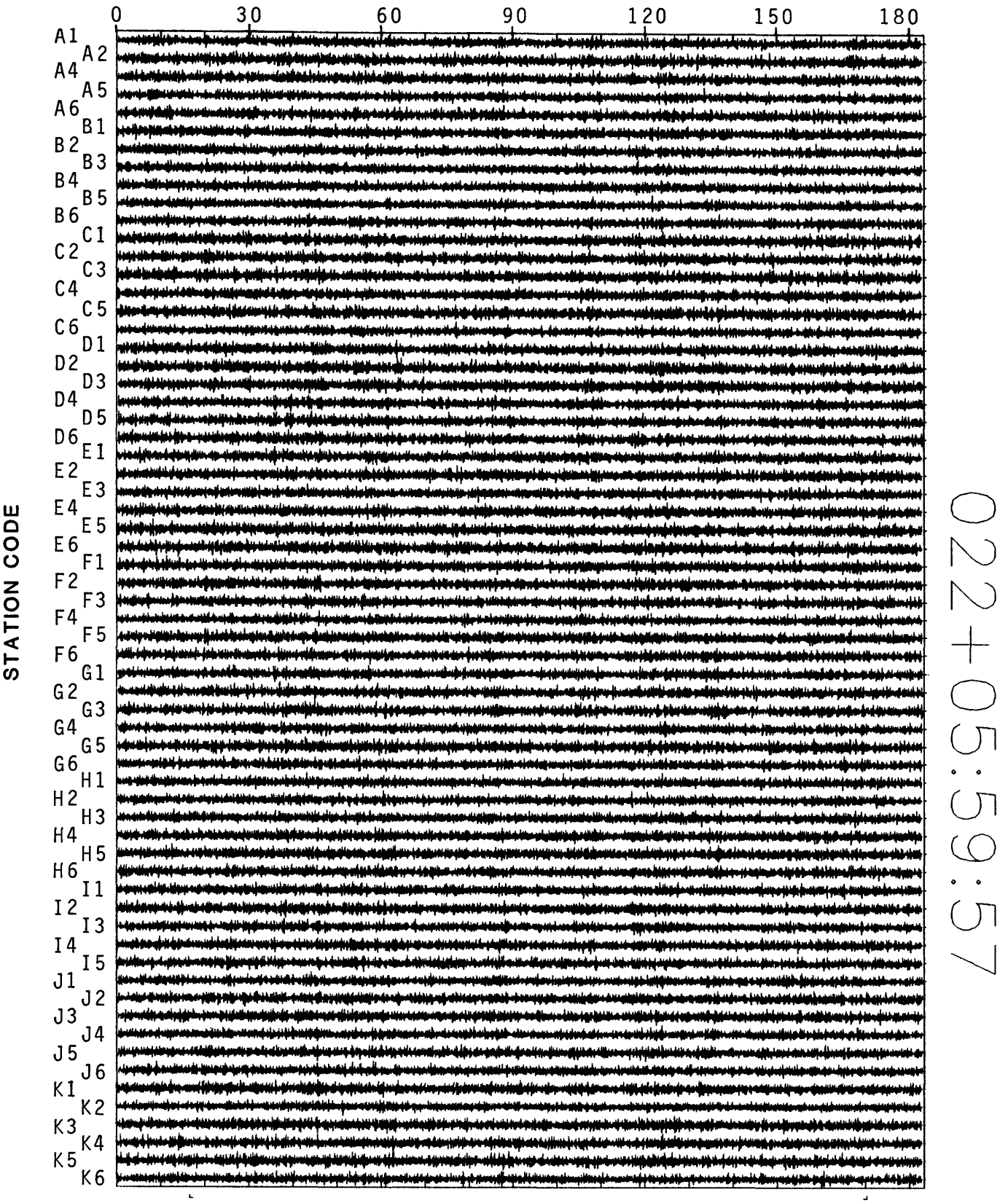

Figure 4. Record section showing 3 minutes of ground velocity for tremor recorded with the first array (components A3 and I6 are not shown).

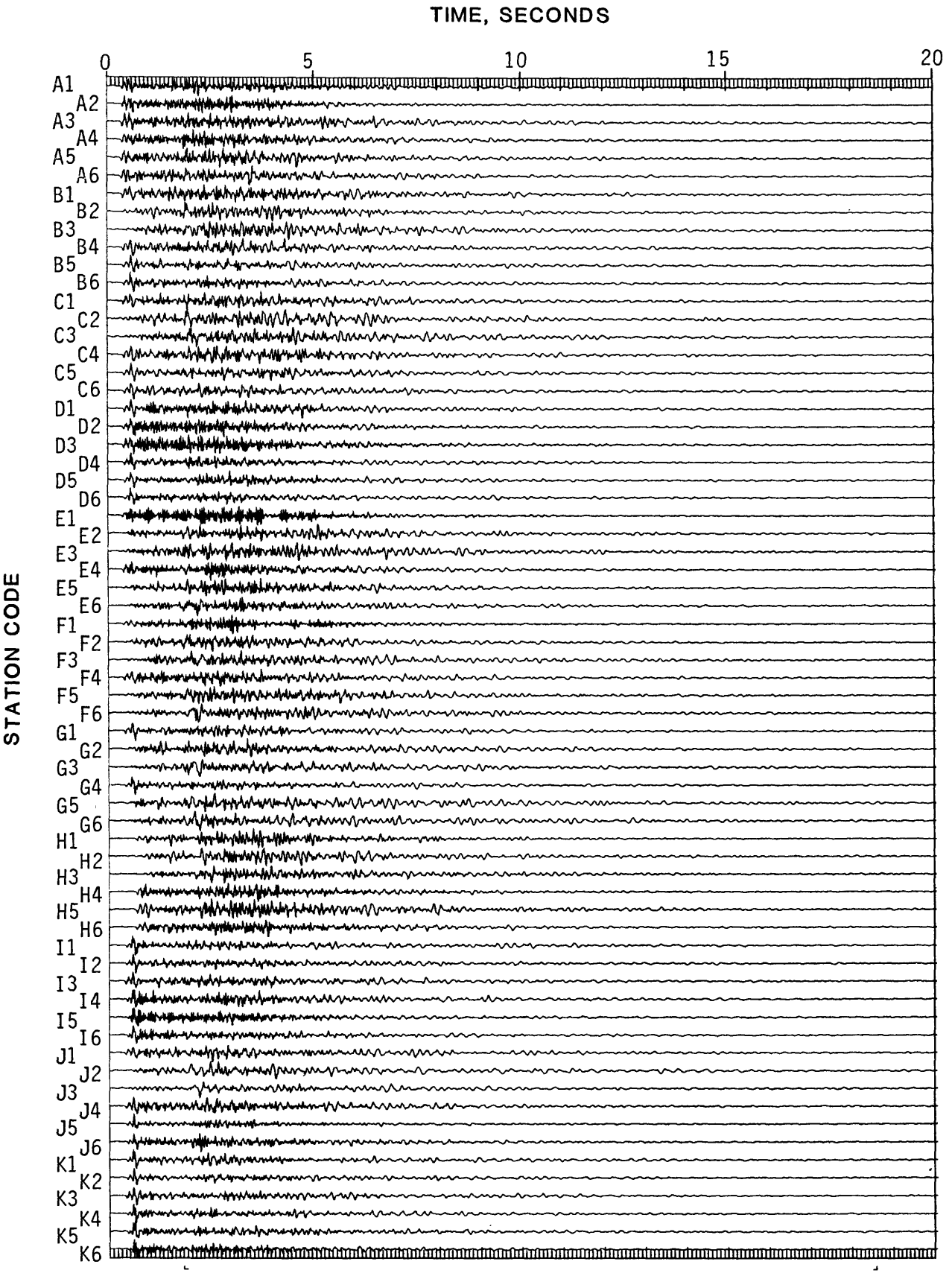

Figure 5. Record section showing 20 seconds of ground velocity for a M 2.2 earthquake recorded with the first array.

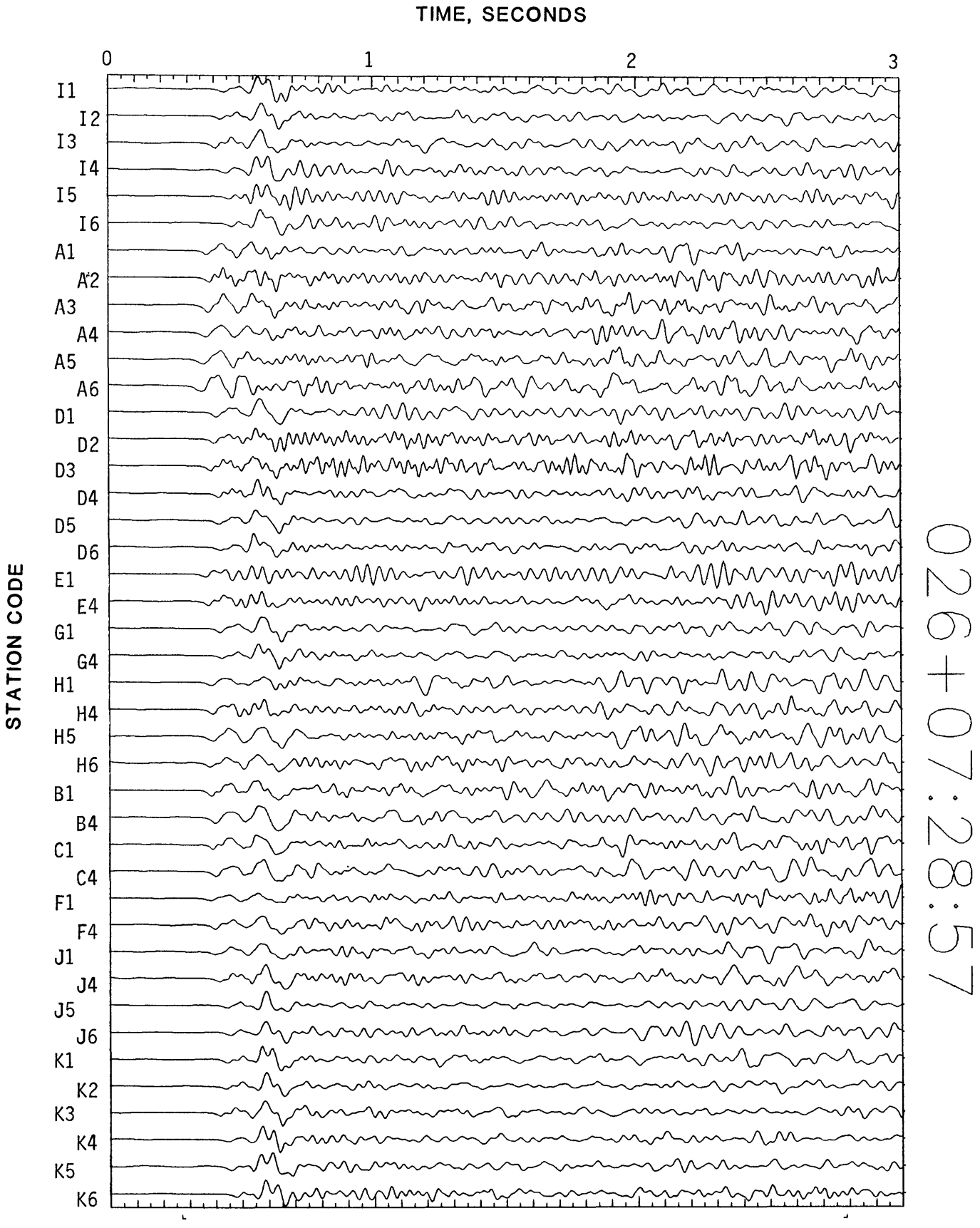

Figure 6. Record section showing the first 3 seconds of vertical ground velocity for the M 2.2 earthquake depicted in Figure 5.

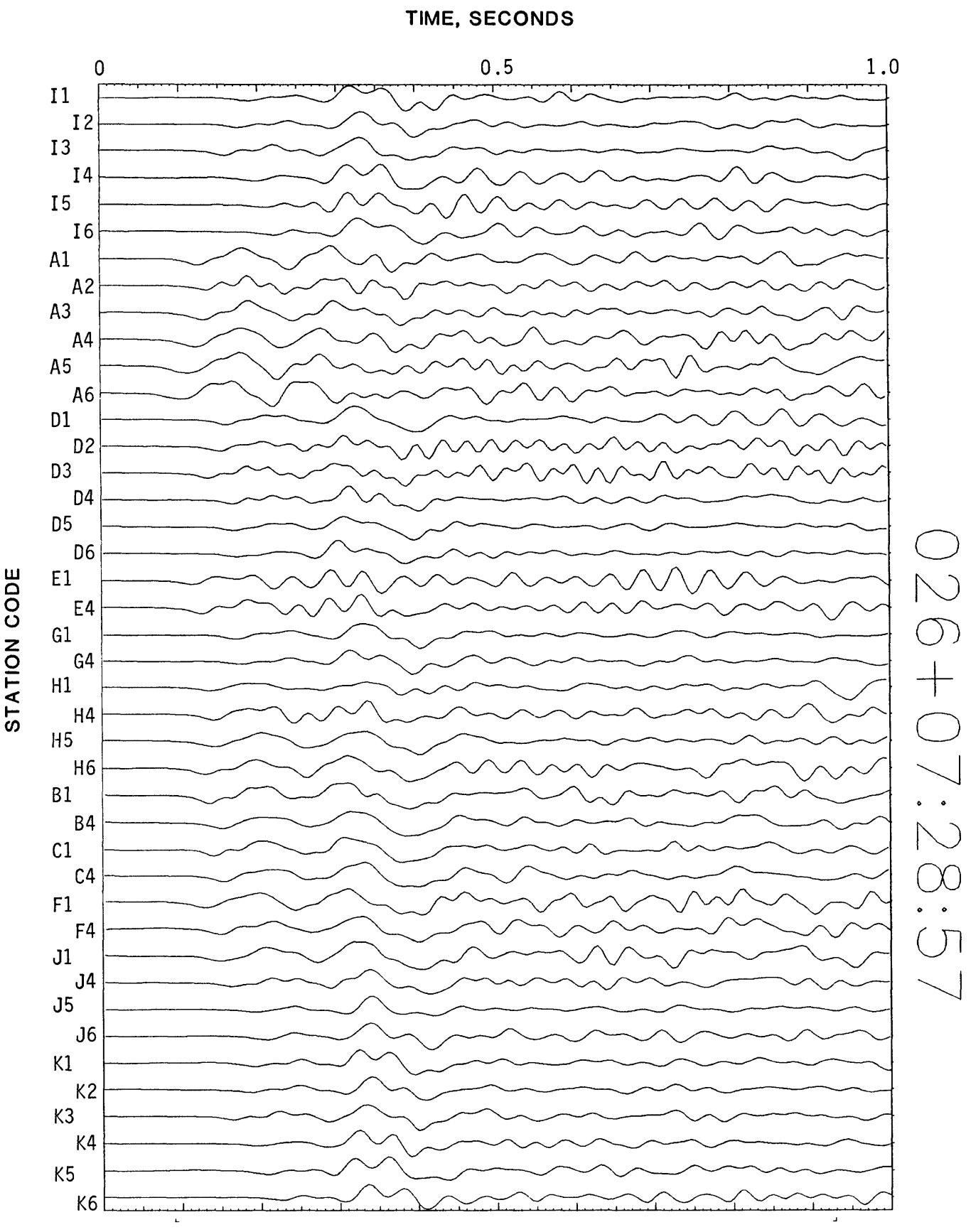

Figure 7. Record section showing 1 second of vertical ground velocity for the M 2.2 earthquake depicted in Figure 5.

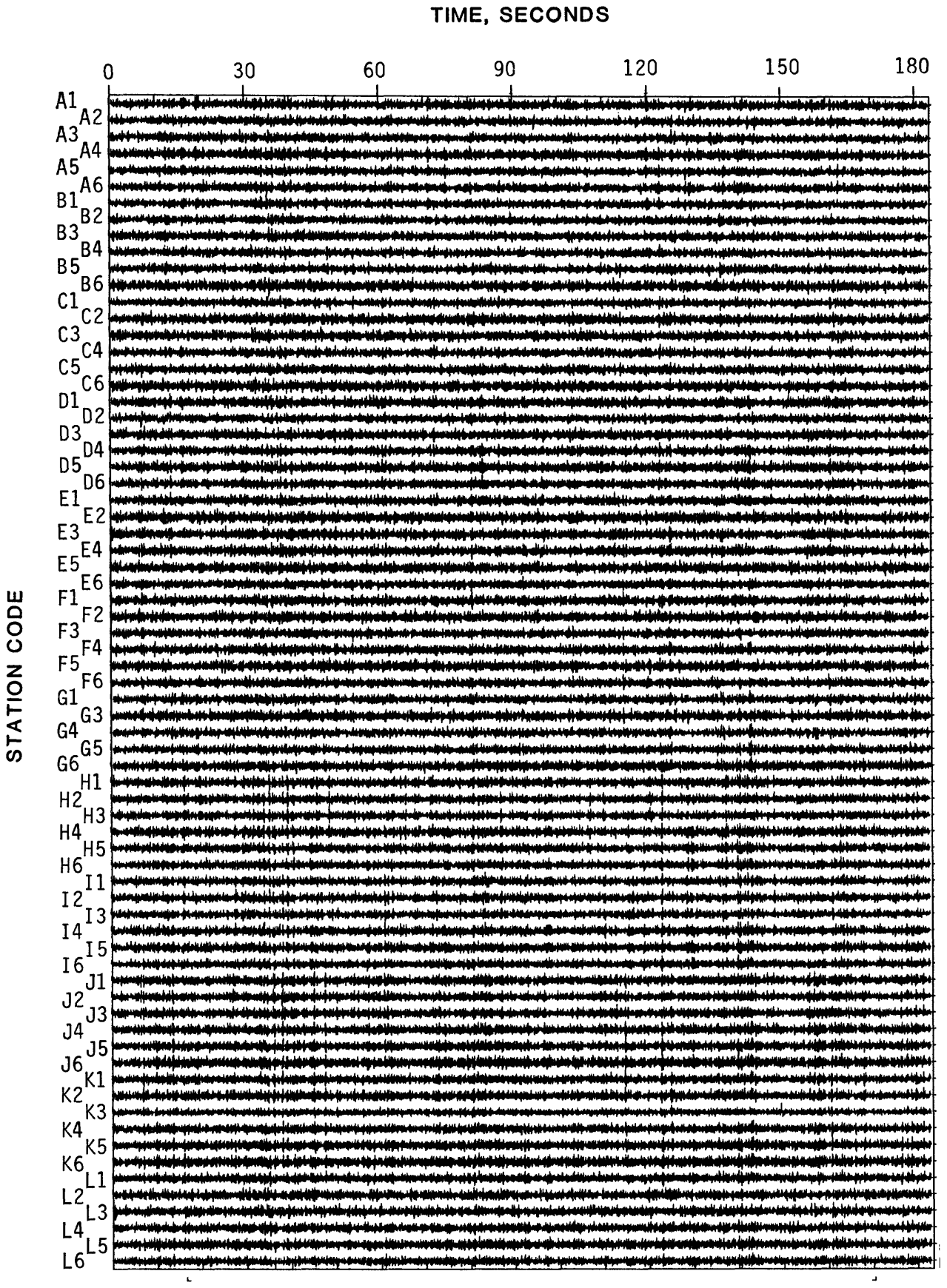

Figure 8. Record section showing 3 minutes of ground velocity for tremor recorded with the second array (component G2 is not shown).

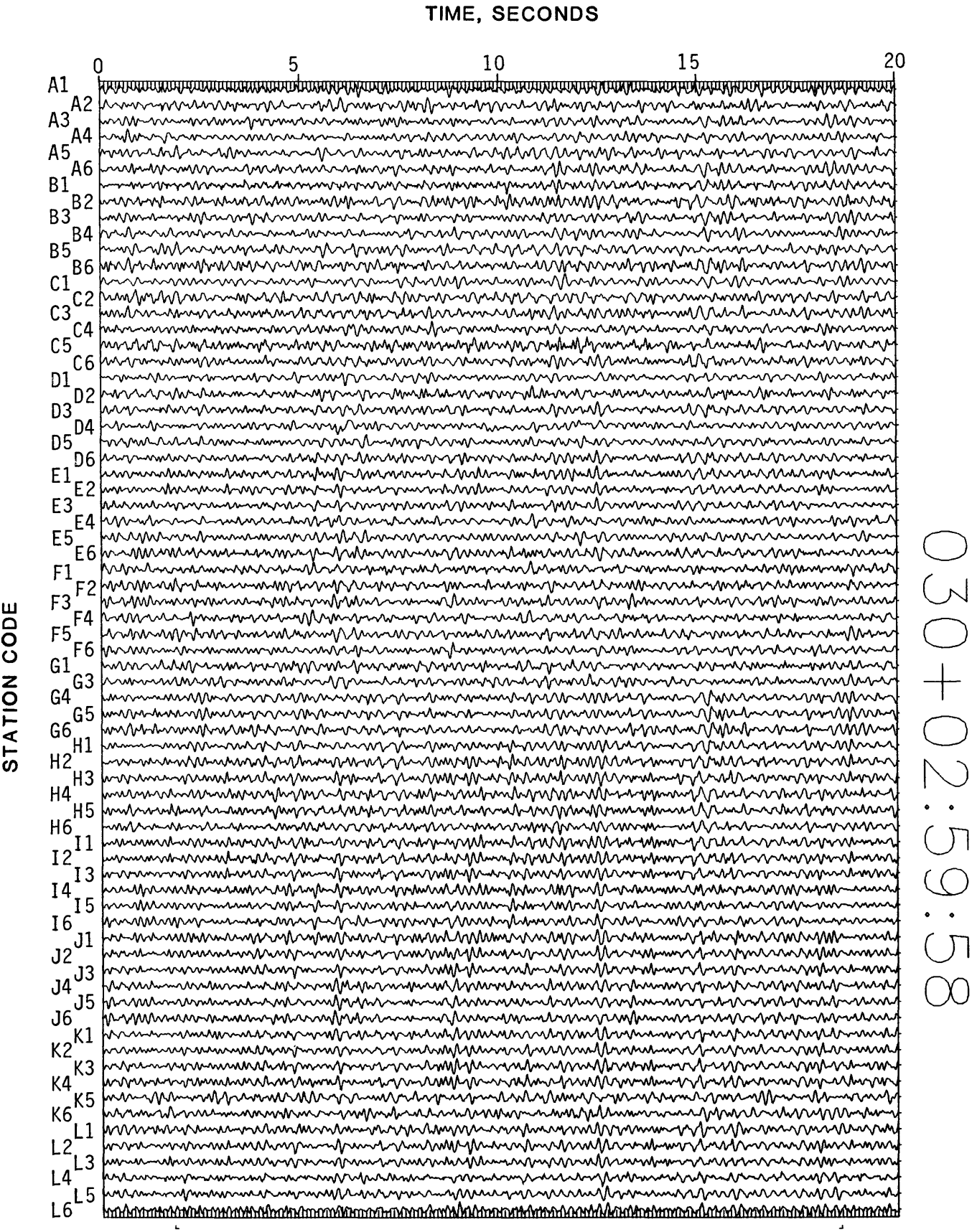

Figure 9. Record section showing 20 seconds of ground velocity for the tremor depicted in Figure 8 (component G2 is not shown).

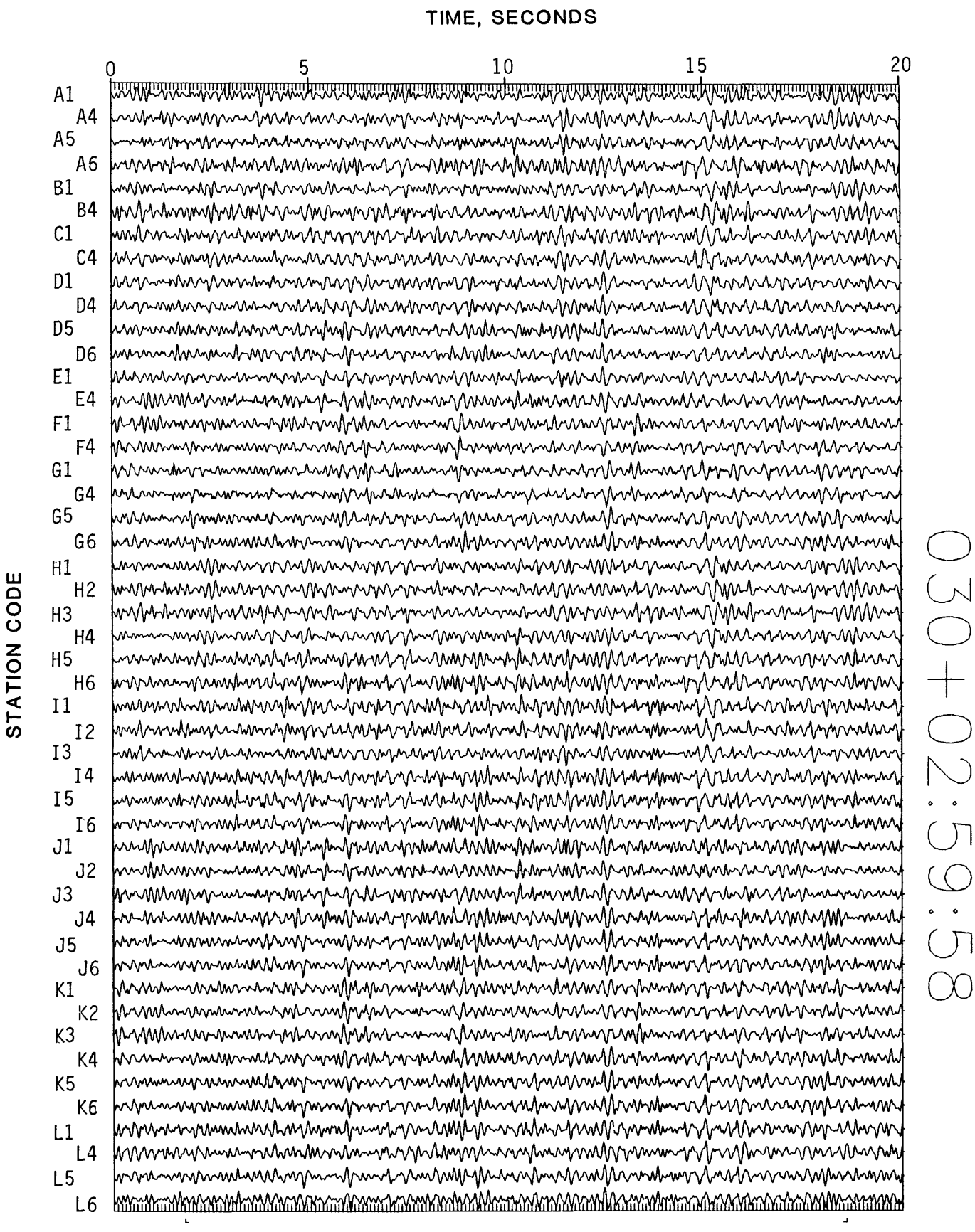

Figure 10. Record section showing 20 seconds of vertical ground velocity for the tremor depicted in Figure 8.

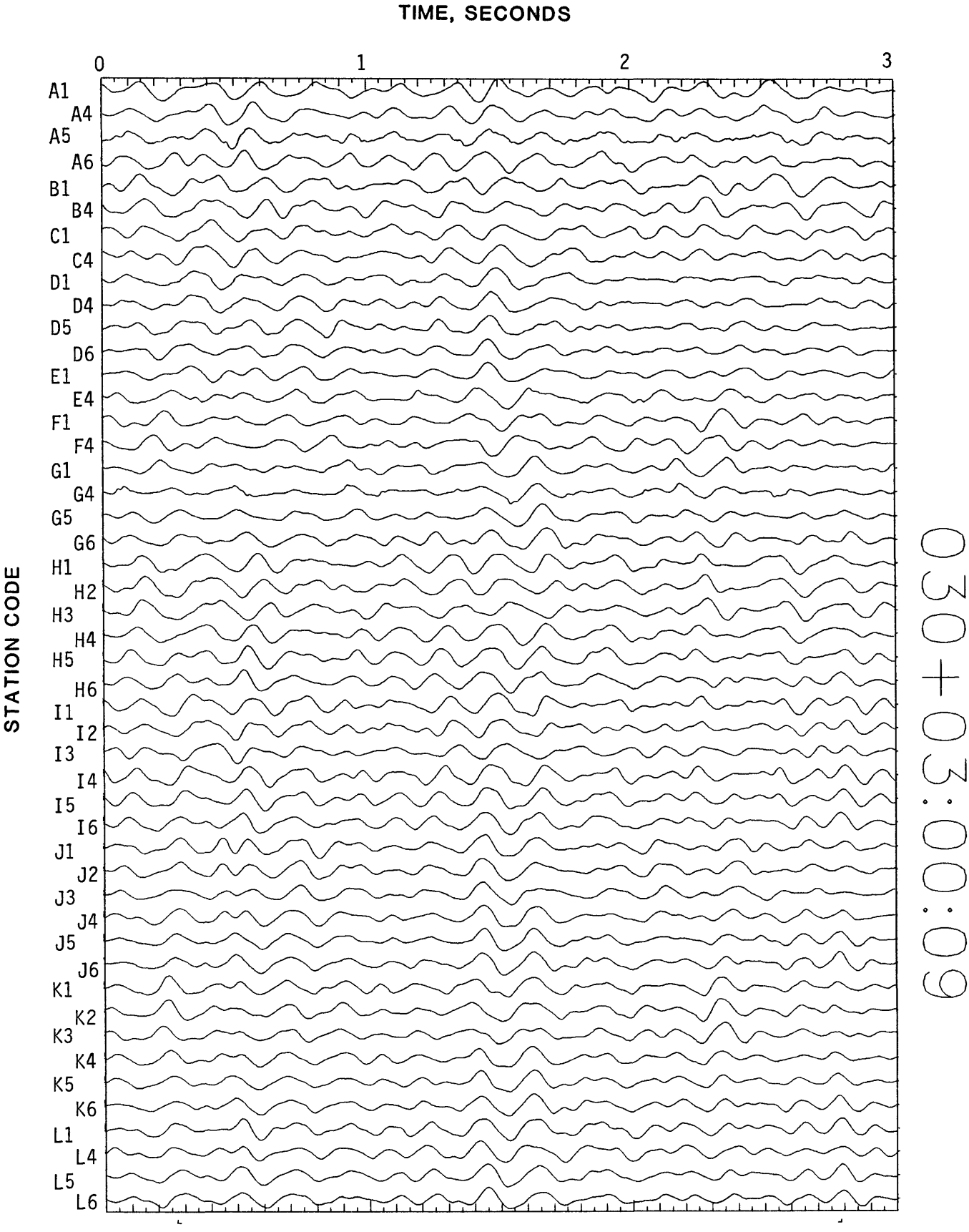

Figure 11. Record section showing 3 seconds of vertical ground velocity for the tremor depicted in Figure 8.

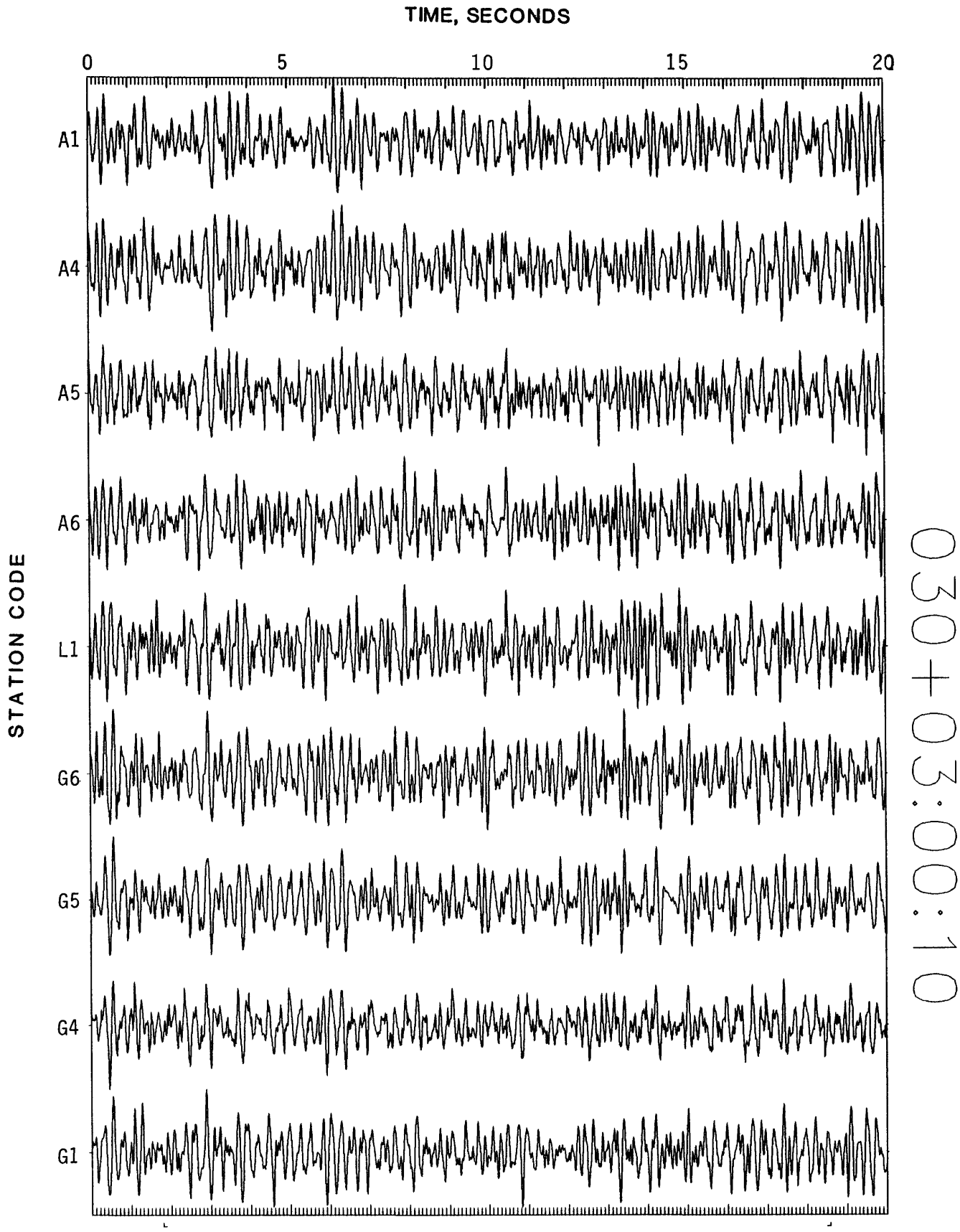

Figure 12. Record section showing 20 seconds of vertical ground velocity for tremor along a linear profile of the second array.

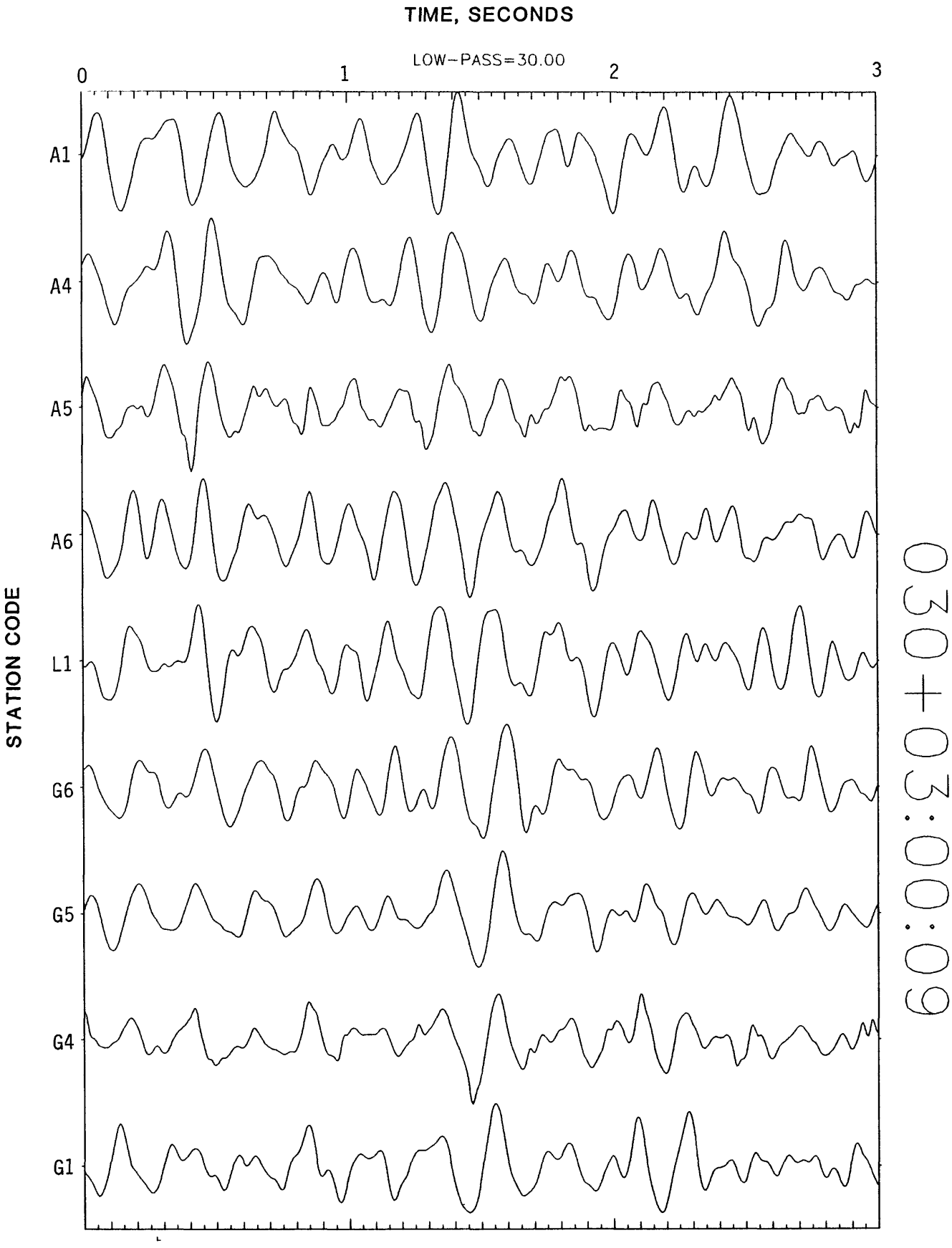

Figure 13. Record section showing 3 seconds of vertical ground velocity for the tremor depicted in Figure 12.

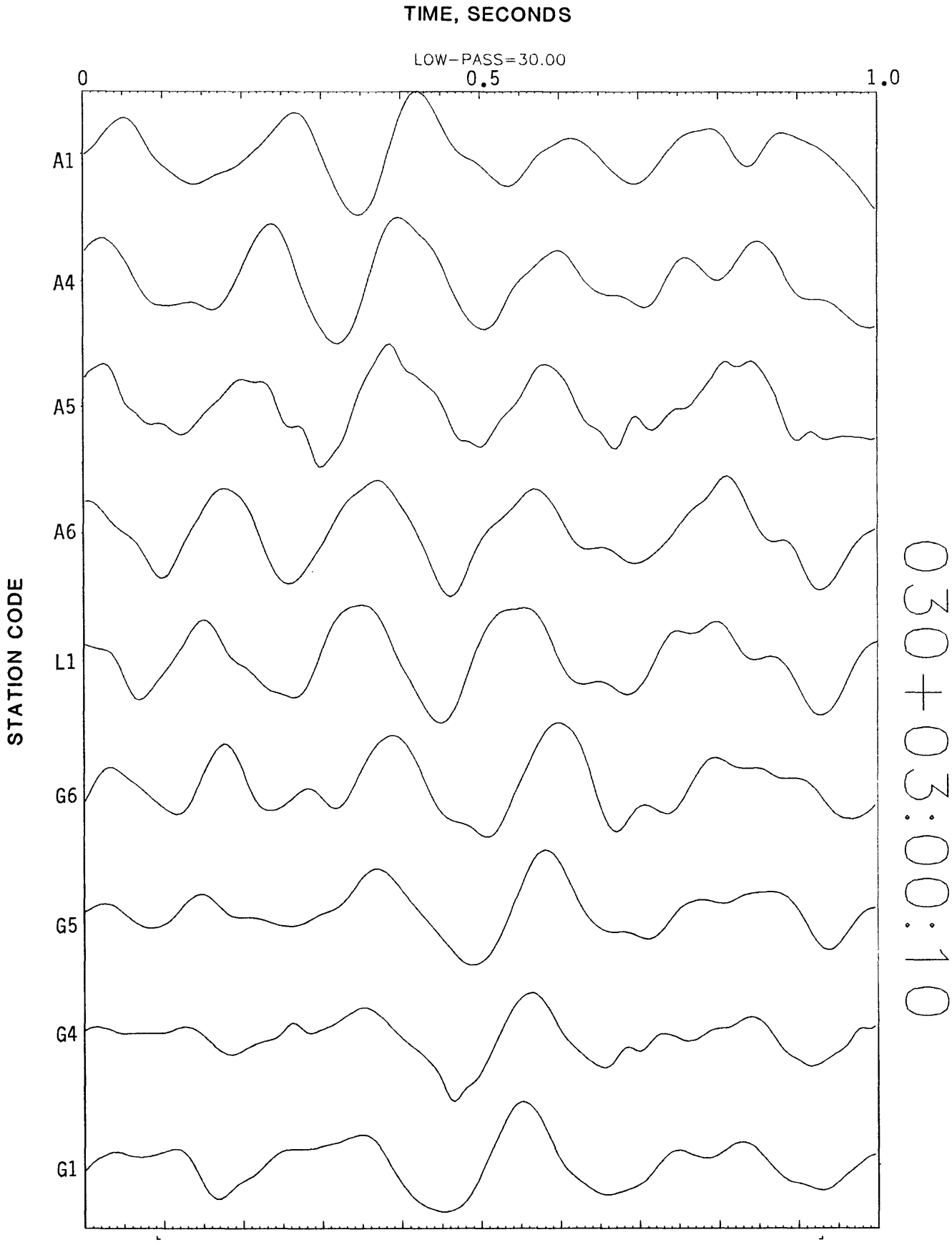

Figure 14. Record section showing 1 second of vertical ground velocity for the tremor depicted in Figure 12.

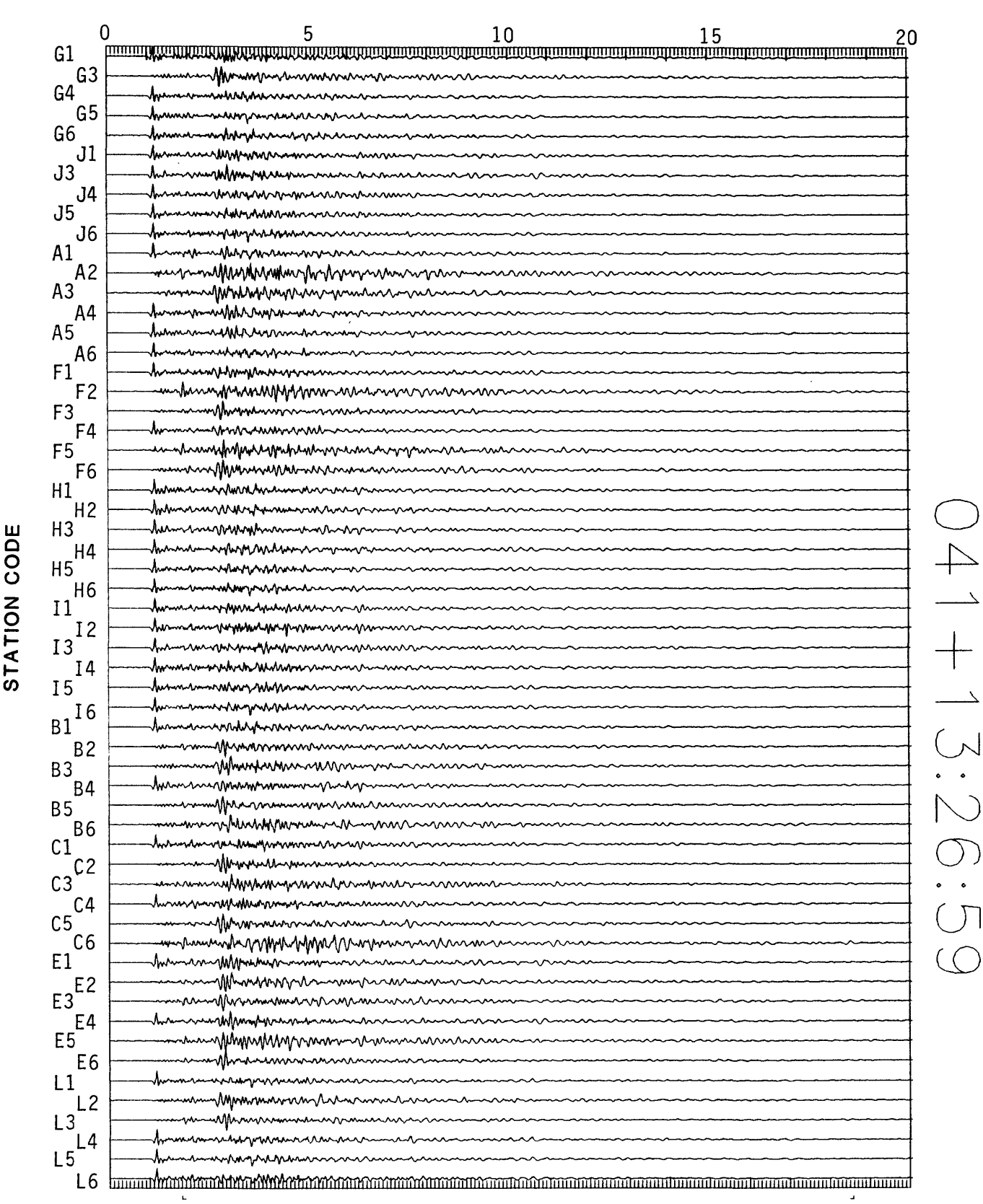

Figure 15. Record section showing 20 seconds of ground velocity for a M 3.4 earthquake recorded with the second array (components G2 and J2 are not shown).

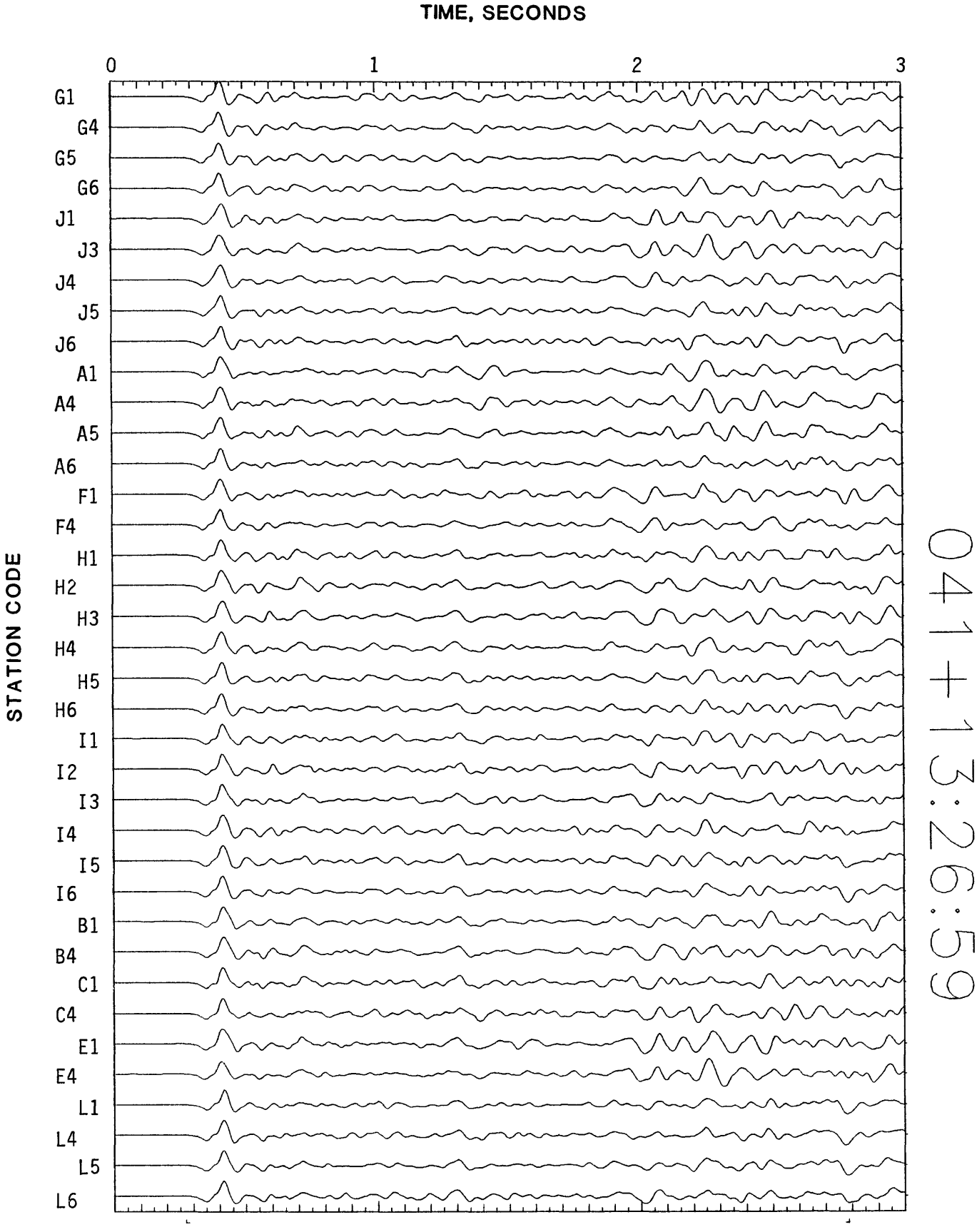

Figure 16. Record section showing 3 seconds of vertical ground velocity for the M 3.4 earthquake depicted in Figure 15 (component J2 is not shown).

Figure 17. Three-component velocity seismograms recorded at station A1,2,3 on the second array, showing 15 seconds of the M 3.4 earthquake depicted in Figure 15. Vertical dashed lines define boundaries for a selection of spectral windows; the largest window, labeled L-L, was selected for the spectra shown in Figures 18-20.

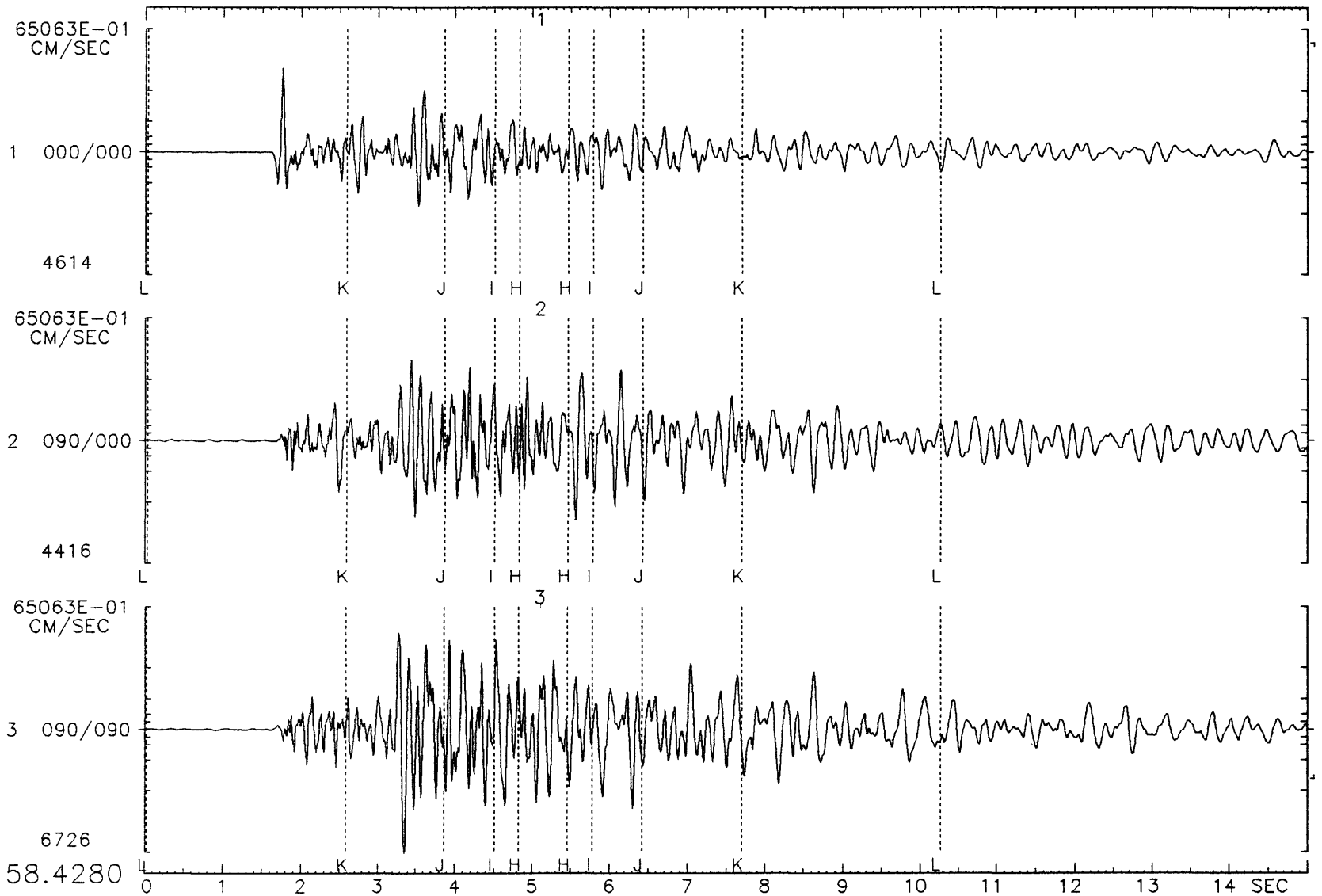
0411326TA.AAA
65063E-01
CM/SEC
1 000/000
4614
65063E-01
CM/SEC
2 090/000
4416
65063E-01
CM/SEC
3 090/090
6726
58.4280
L K J I H H I J K L
0 1 2 3 4 5 6 7 8 9 10 11 12 13 14 SEC
TIME, SECONDS

Figure 18. Fourier amplitude spectrum computed for the vertical component of ground velocity (component 1) depicted in window L-L in Figure 17.

MOTION=VELOCITY S/S=200. SAM=04096 04132GTA.AAA
NUMERATOR AMPLITUDE (CENTIMETER)
-3
-4
3.13
6.25
12.5
25.0
FREQUENCY, HZ

Figure 19. Fourier amplitude spectrum computed for the component 2 horizontal ground velocity depicted in window L-L in Figure 17.

MOTION=VELOCITY S/S=200. SAM=04096 041326TA.AAA
NUMERATOR AMPLITUDE (CENTIMETER)
-2
-3
-4
3.13
6.25
12.5
25.0
FREQUENCY, HZ

Figure 20. Fourier amplitude spectrum computed for the component 3 horizontal ground velocity depicted in window L-L in Figure 17.

MOTION=VELOCITY S/S=200. SAM=04096 041326TA.AAA
NUMERATOR AMPLITUDE (CENTIMETER)
-2
-3
-4
3.13
6.25
12.5
25.0
FREQUENCY, HZ

Figure 21. Map showing the epicenters of 23 earthquakes taken from an HVO CUSP listing and correlated with earthquakes recorded on the two Pu'u O'o arrays. The epicenter of the M 4.1 earthquake listed in Table 5 (22:17:04 GMT) falls outside the map boundary.

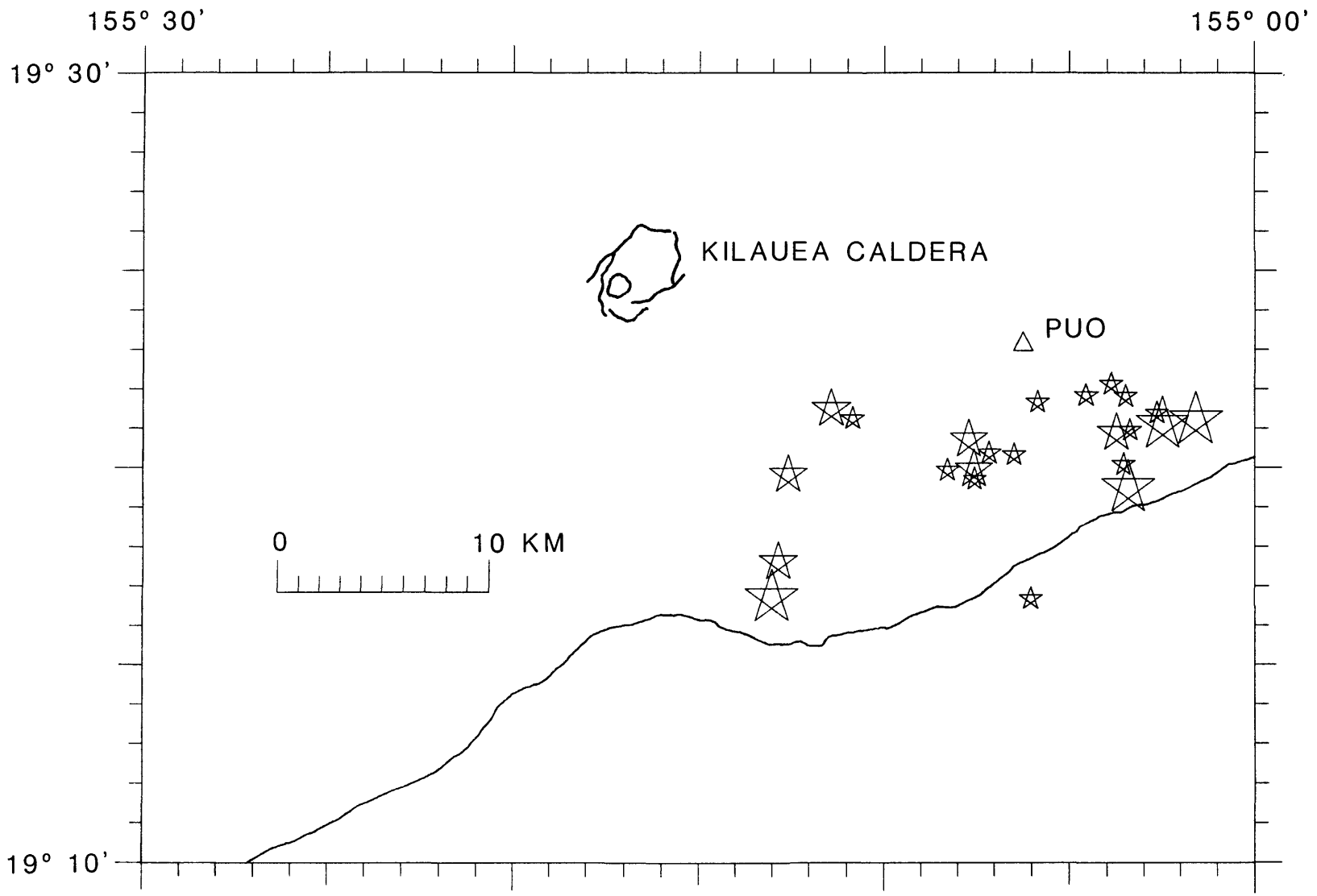
155° 30'
155° 00'
19° 30'
19° 10'
KILAUEA CALDERA
PUO
0
10 KM

Figure 22. Three-component velocity seismograms recorded at station A1,2,3 on the second array showing 40 minutes of tremor with two gas-piston events that were visually observed from the rim of Pu'u O'o. See text for a description of the visual observations that correlate with points A-E.

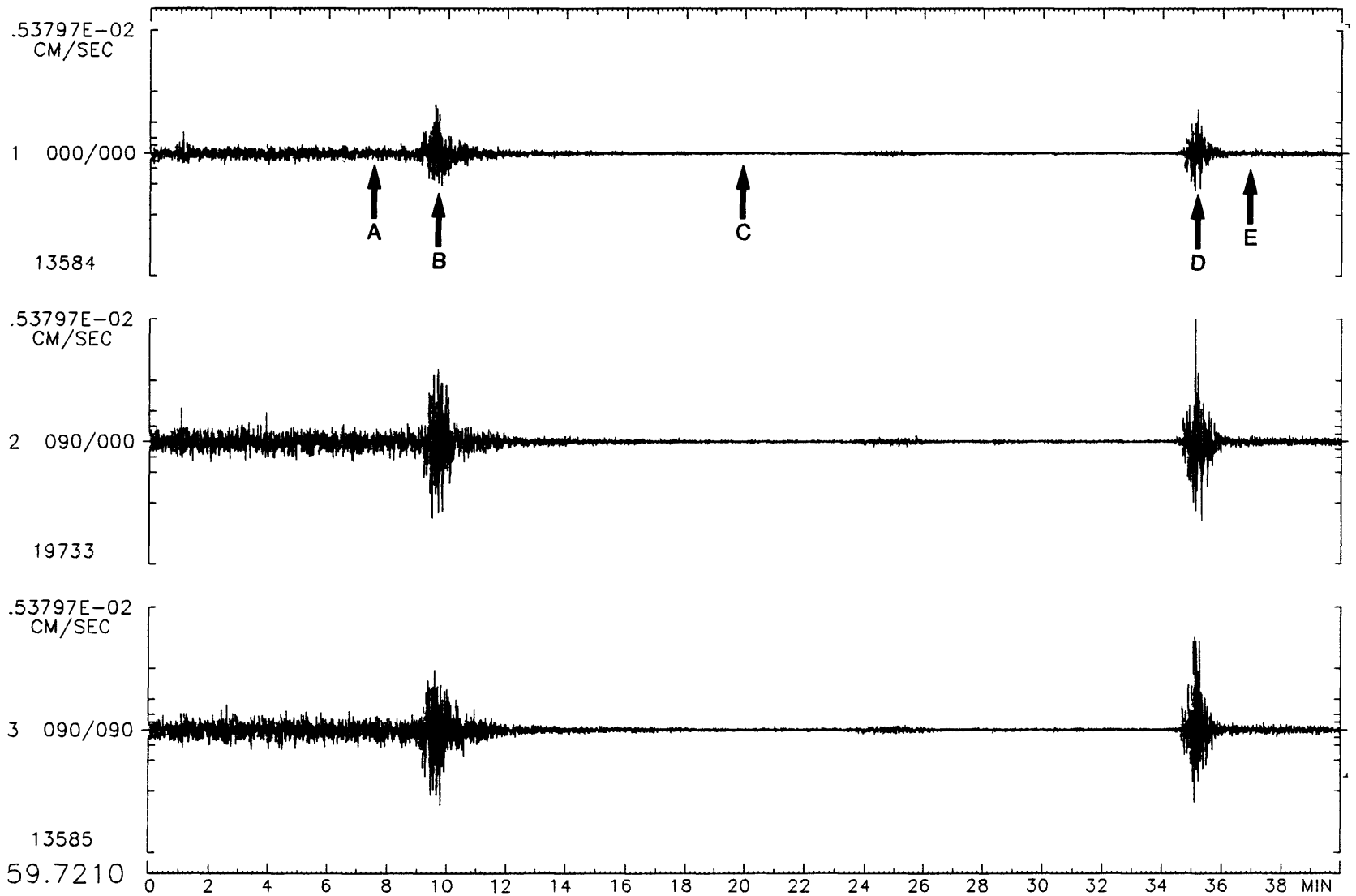
0352158TA.AAA
.53797E-02
CM/SEC
1 000/000
A
B
C
D
E
13584
.53797E-02
CM/SEC
2 090/000
19733
.53797E-02
CM/SEC
3 090/090
13585
59.7210
0 2 4 6 8 10 12 14 16 18 20 22 24 26 28 30 32 34 36 38 MIN
TIME, MINUTES

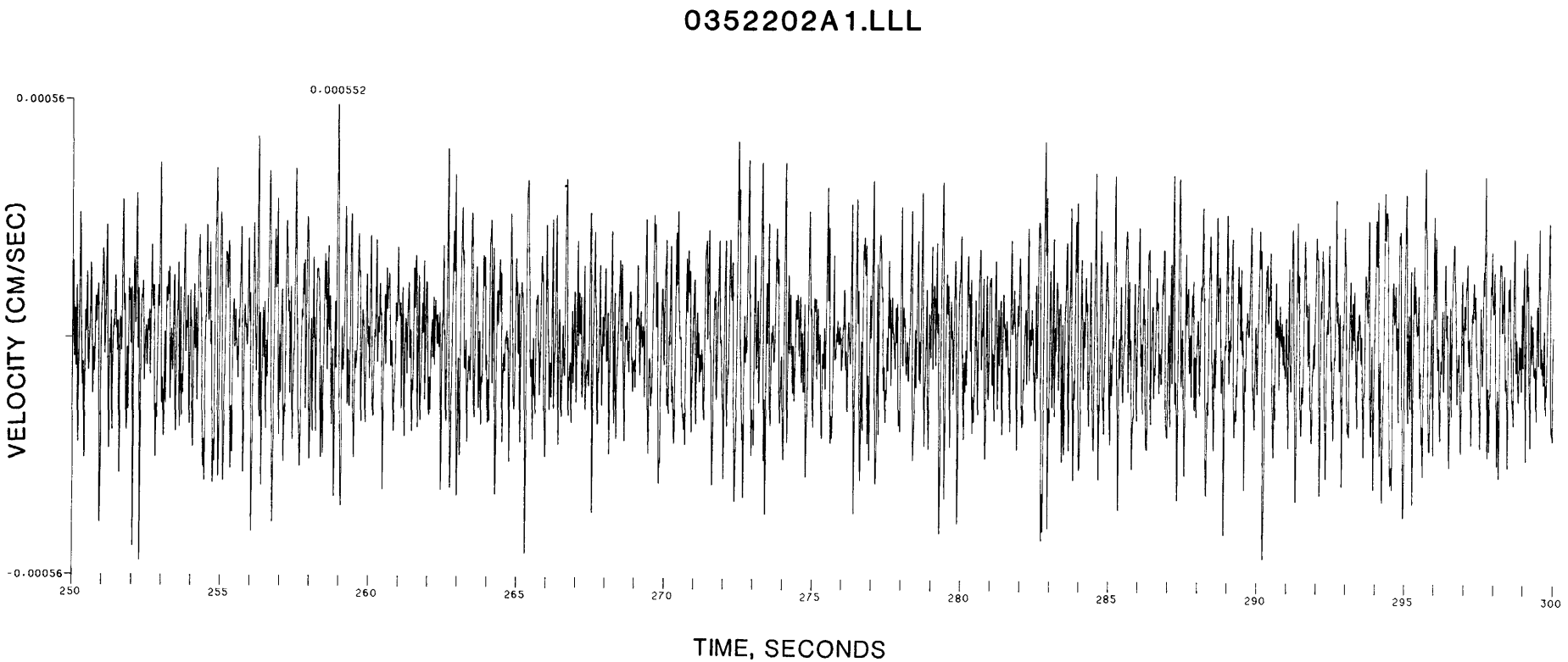

Figure 23. Seismogram recorded at station L1 showing 50 seconds of vertical ground velocity for tremor at position A in the record of Figure 22.

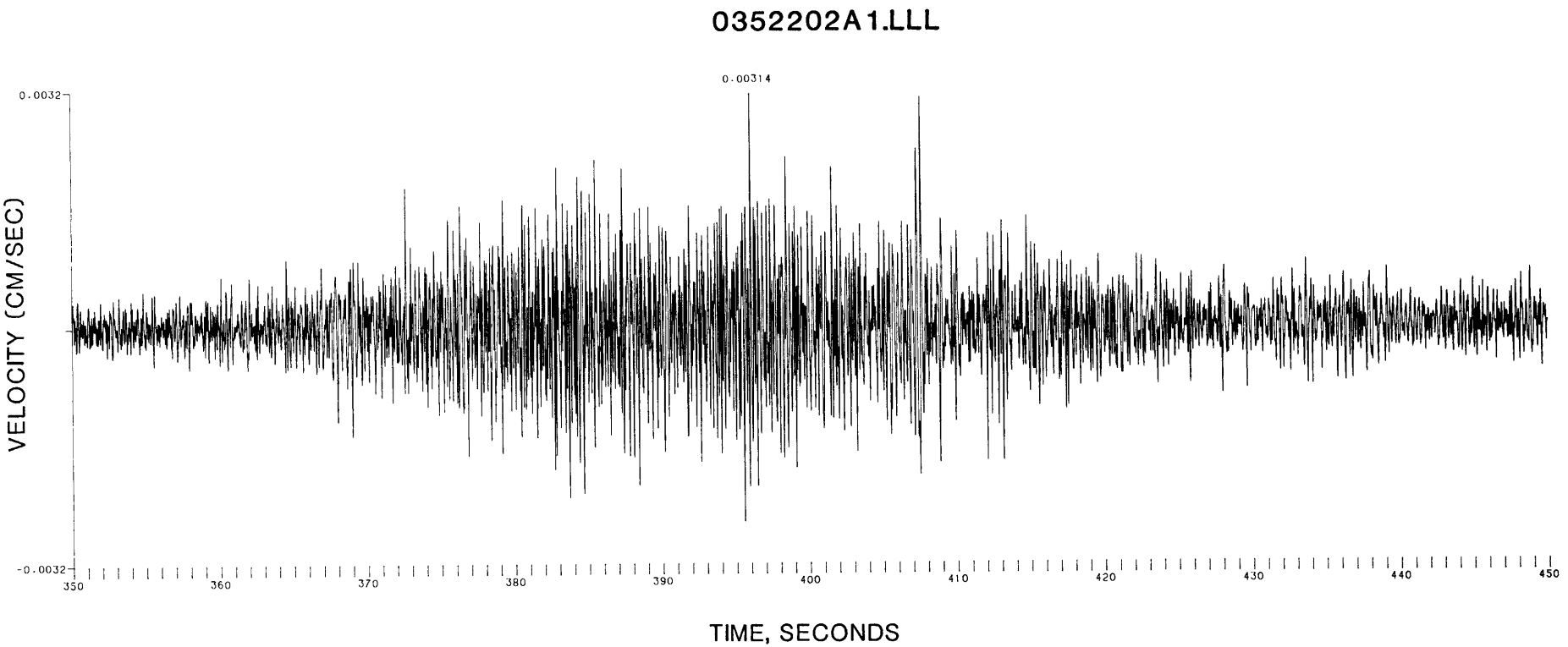

Figure 24. Seismogram recorded at station L1 showing 100 seconds of vertical ground velocity for a gas-piston event superimposed on a background of tremor at position B in the record of Figure 22.

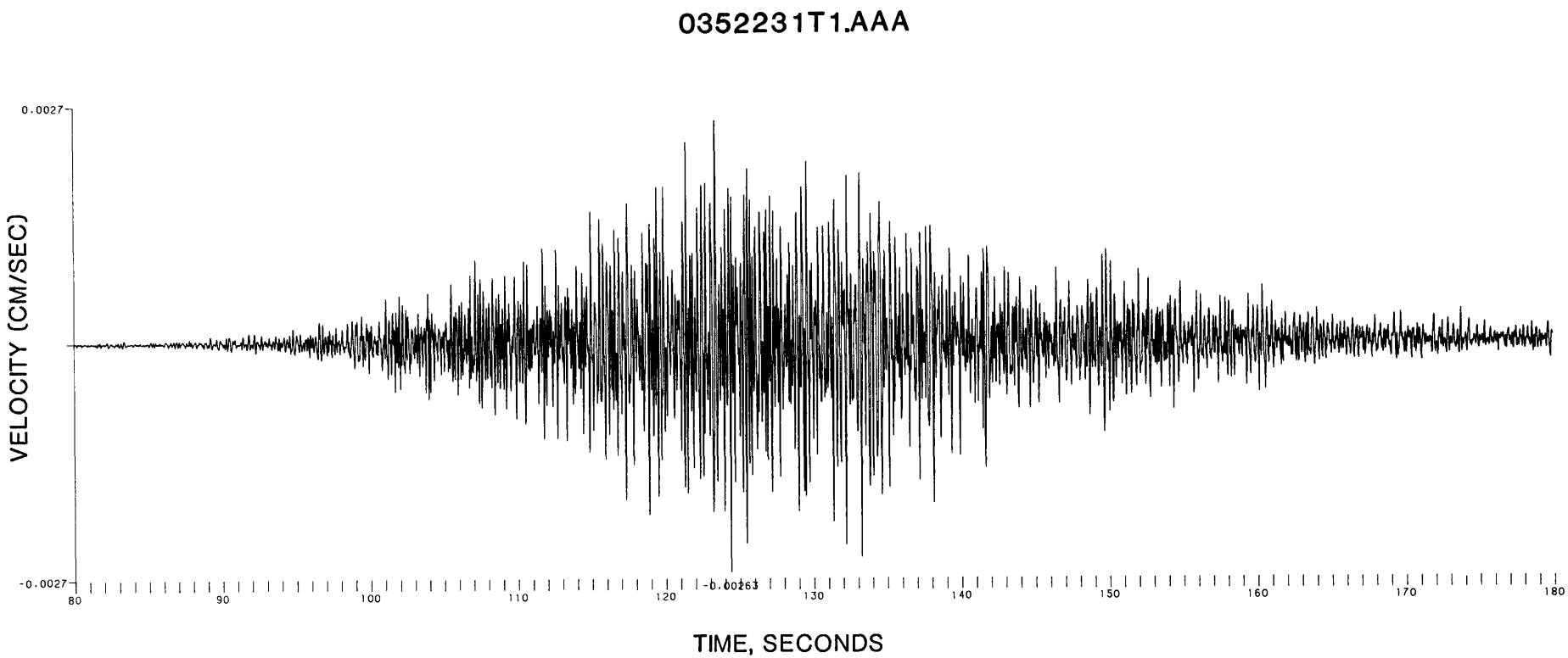

Figure 25. Seismogram recorded at station A1 showing 100 seconds of vertical ground velocity for gas-piston event at position D in the record of Figure 22.

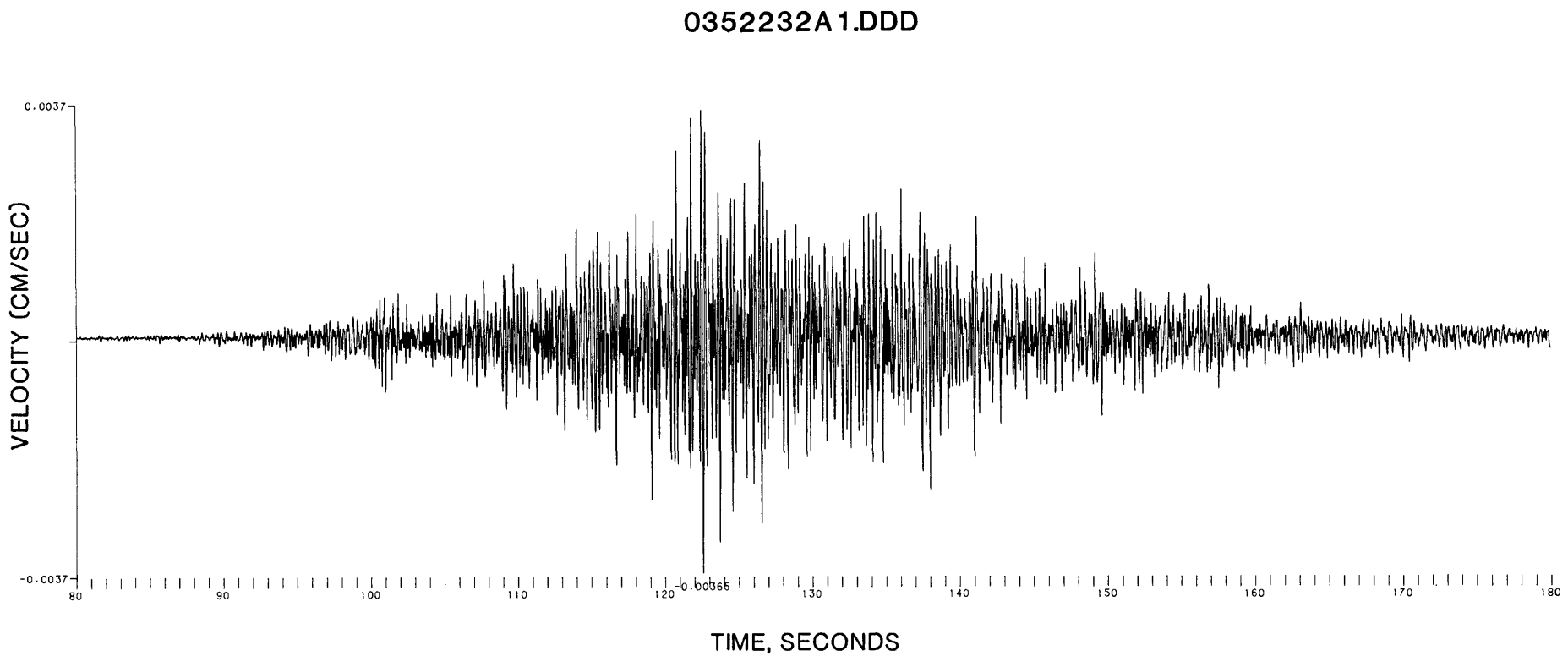

Figure 26. Seismogram recorded at station D1 showing 100 seconds of vertical ground velocity for gas-piston event at position D in the record of Figure 22.

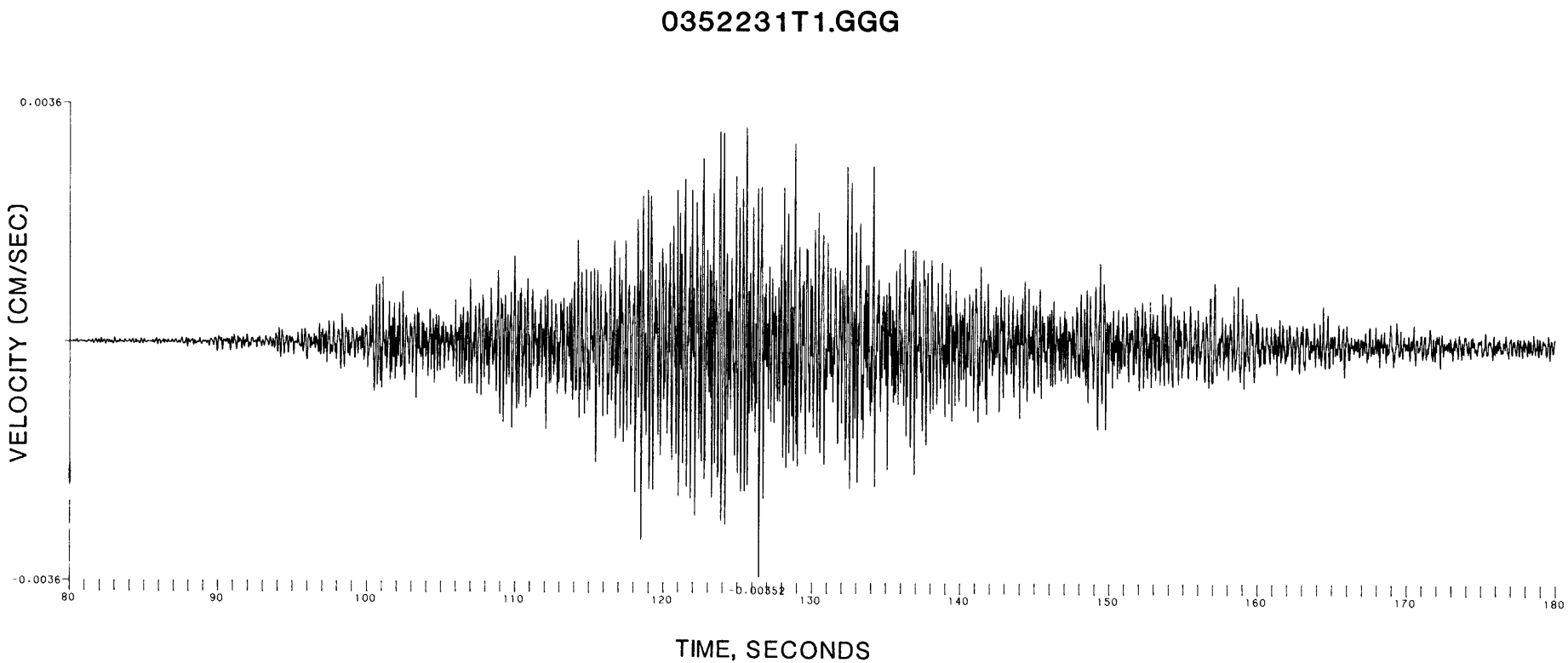

Figure 27. Seismogram recorded at station G1 showing 100 seconds of vertical ground velocity for gas-piston event at position D in the record of Figure 22.

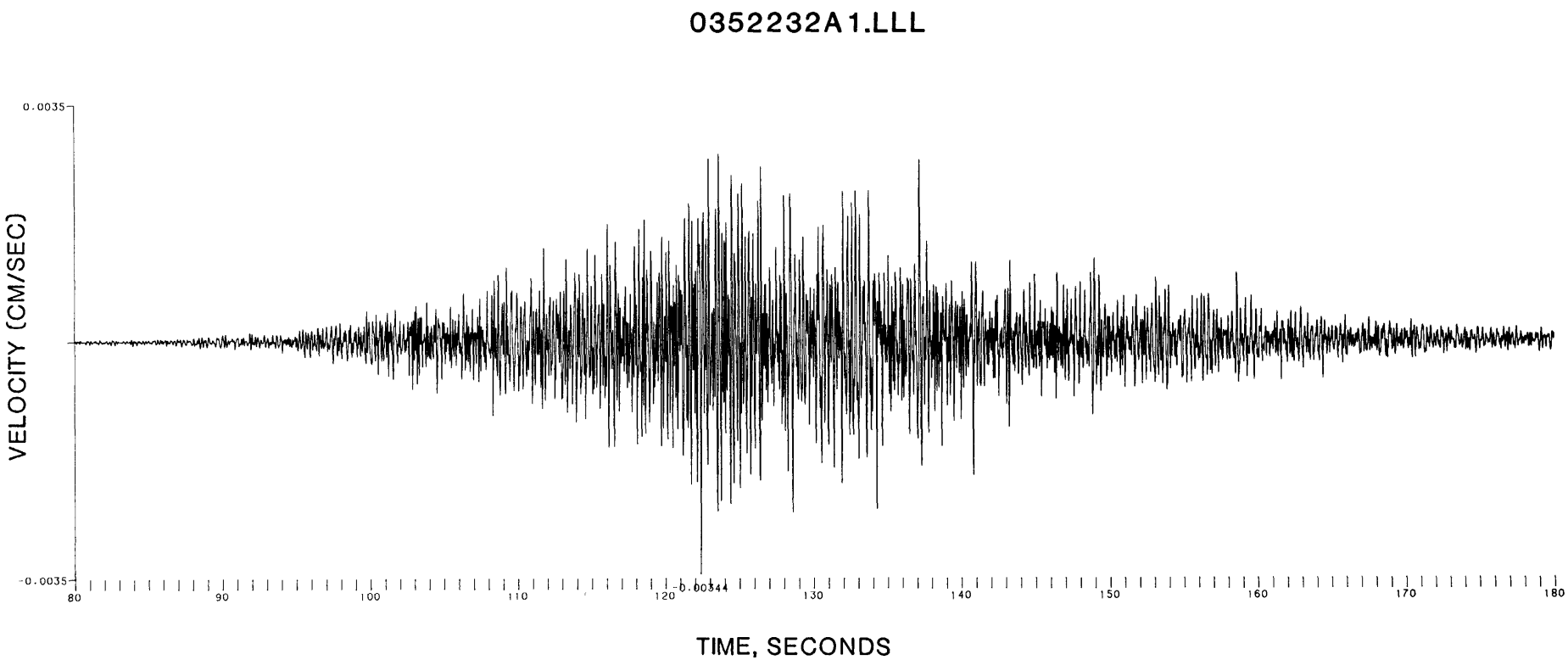

Figure 28. Seismogram recorded at station L1 showing 100 seconds of vertical ground velocity for gas-piston event at position D in the record of Figure 22.

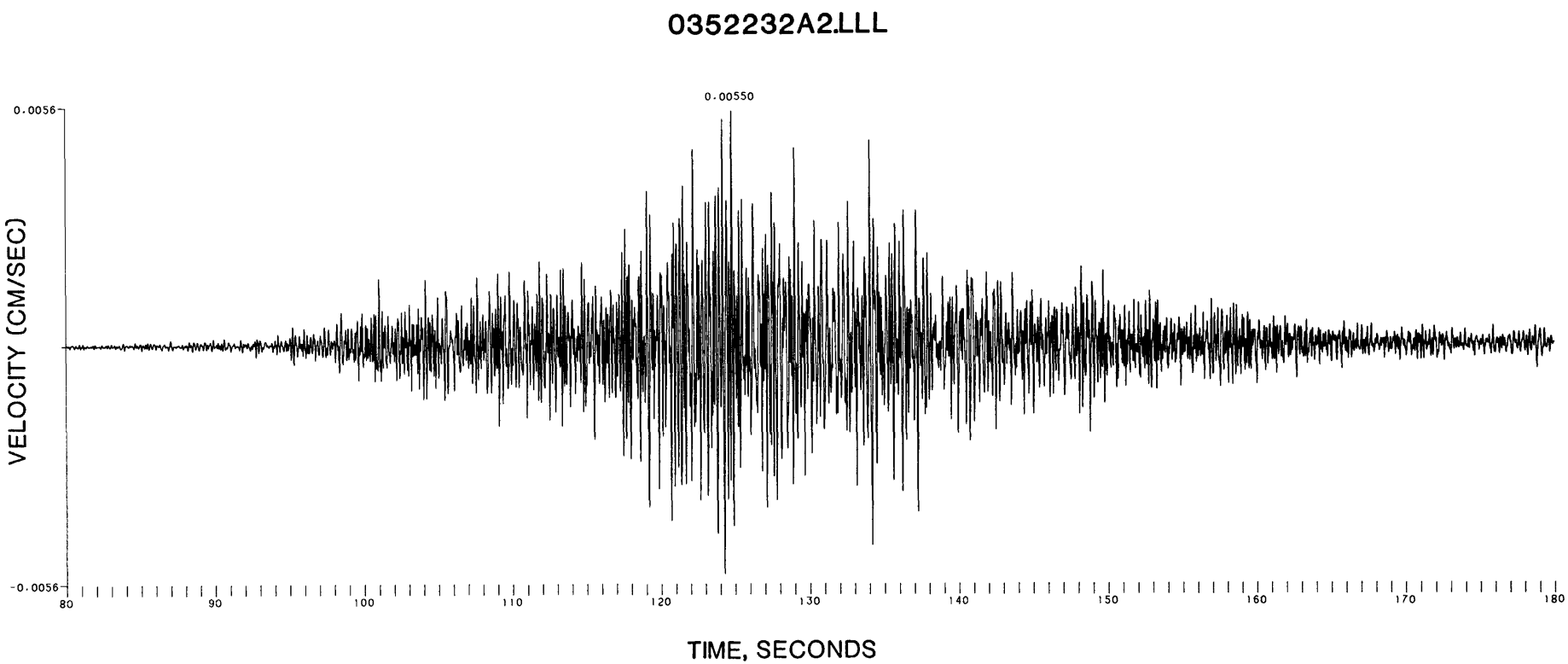

Figure 29. Seismogram recorded at station L2 showing 100 seconds of horizontal component 2 ground velocity for gas-piston event at position D in the record of Figure 22.

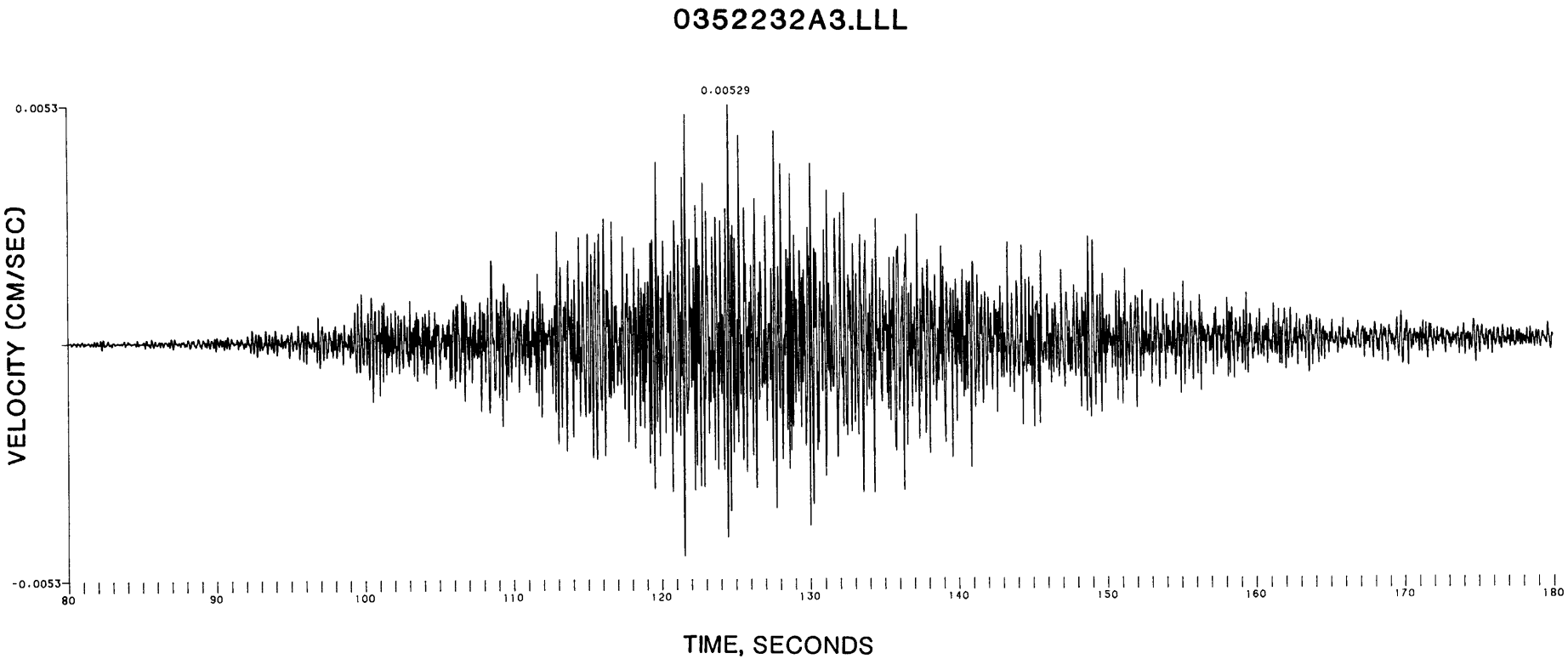

Figure 30. Seismogram recorded at station L3 showing 100 seconds of horizontal component 3 ground velocity for gas-piston event at position D in the record of Figure 22.

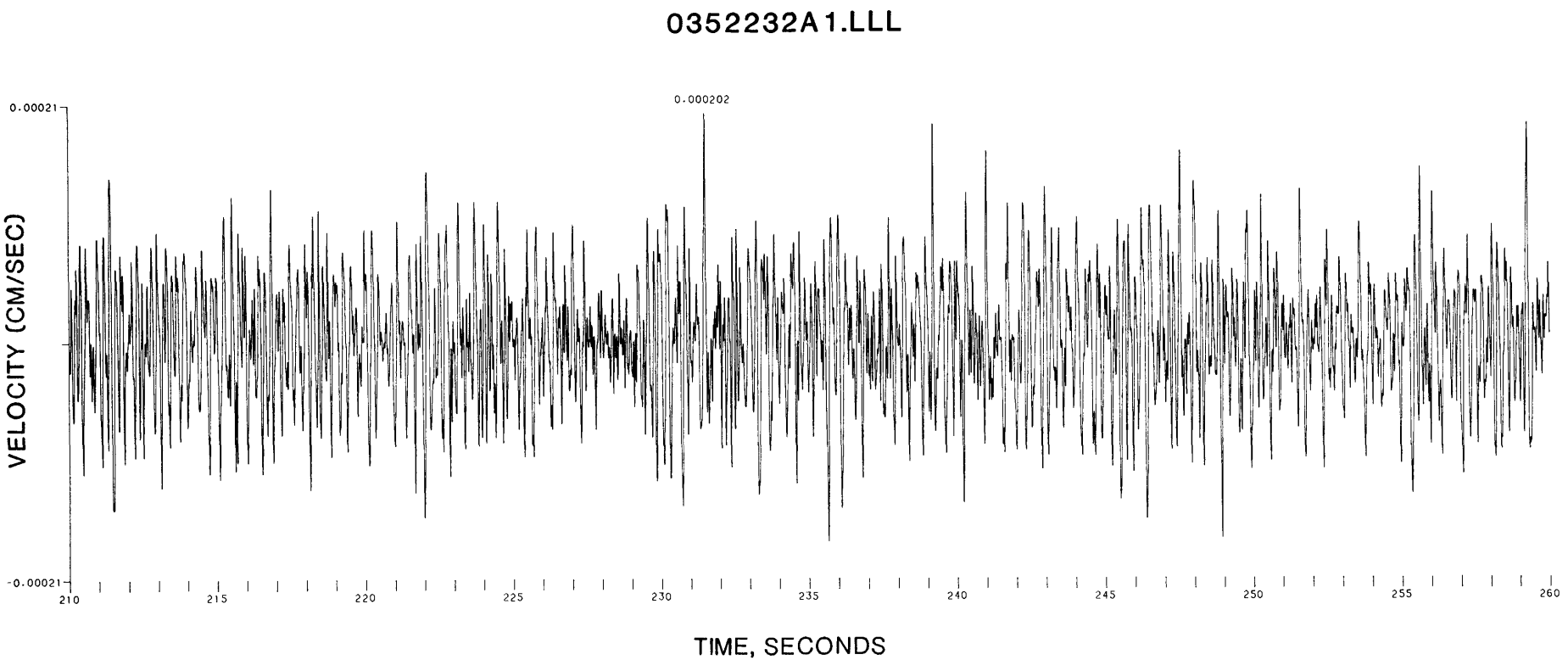

Figure 31. Seismogram recorded at station L1 showing 50 seconds of vertical ground velocity for tremor at position E in the record of Figure 22.

Figure 32. Three-component velocity seismograms recorded at station A1,2,3 on the second array showing 40 minutes of tremor and gas-piston activity observed on February 14, 1988.

04521070A.AAA

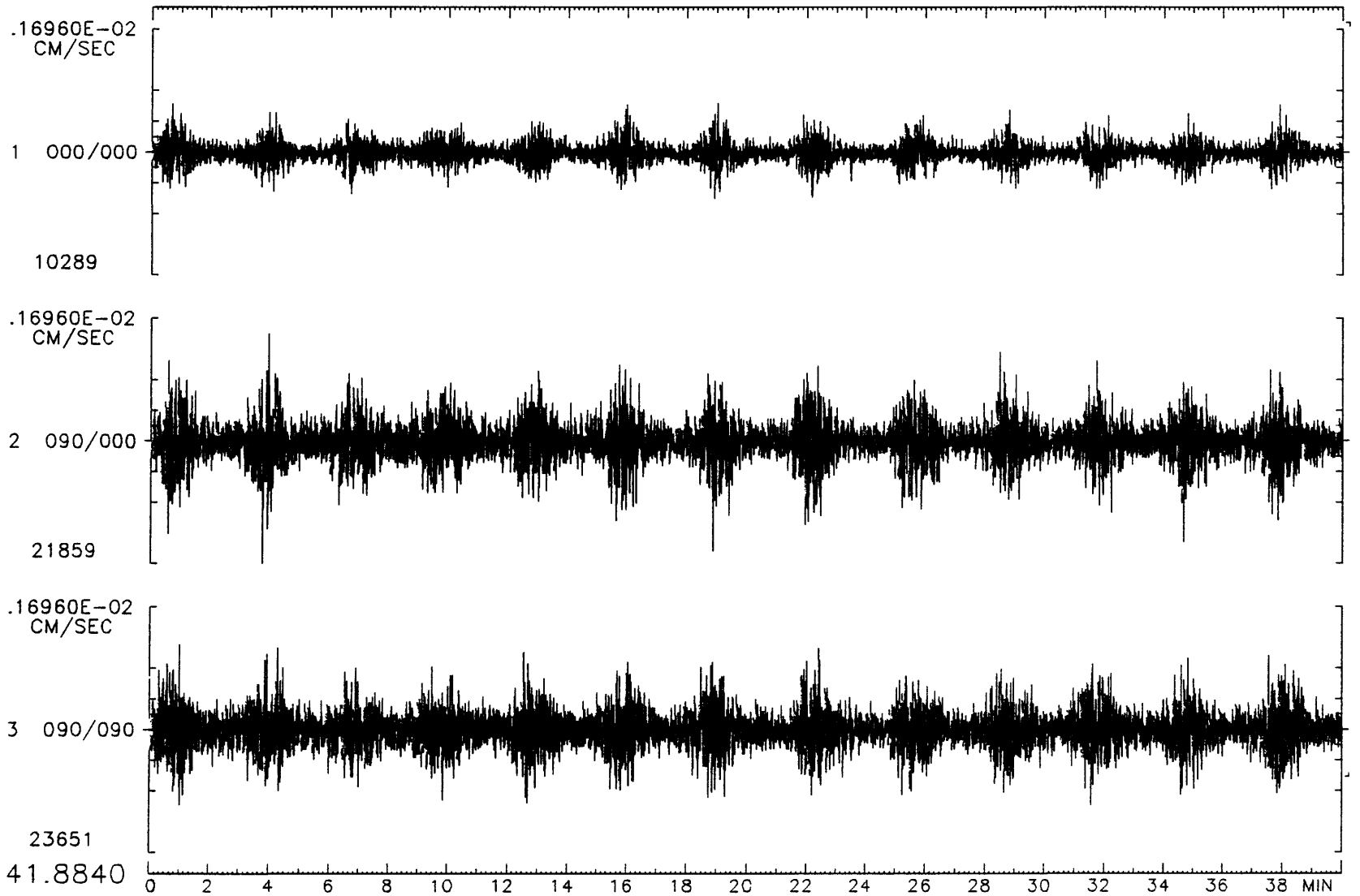

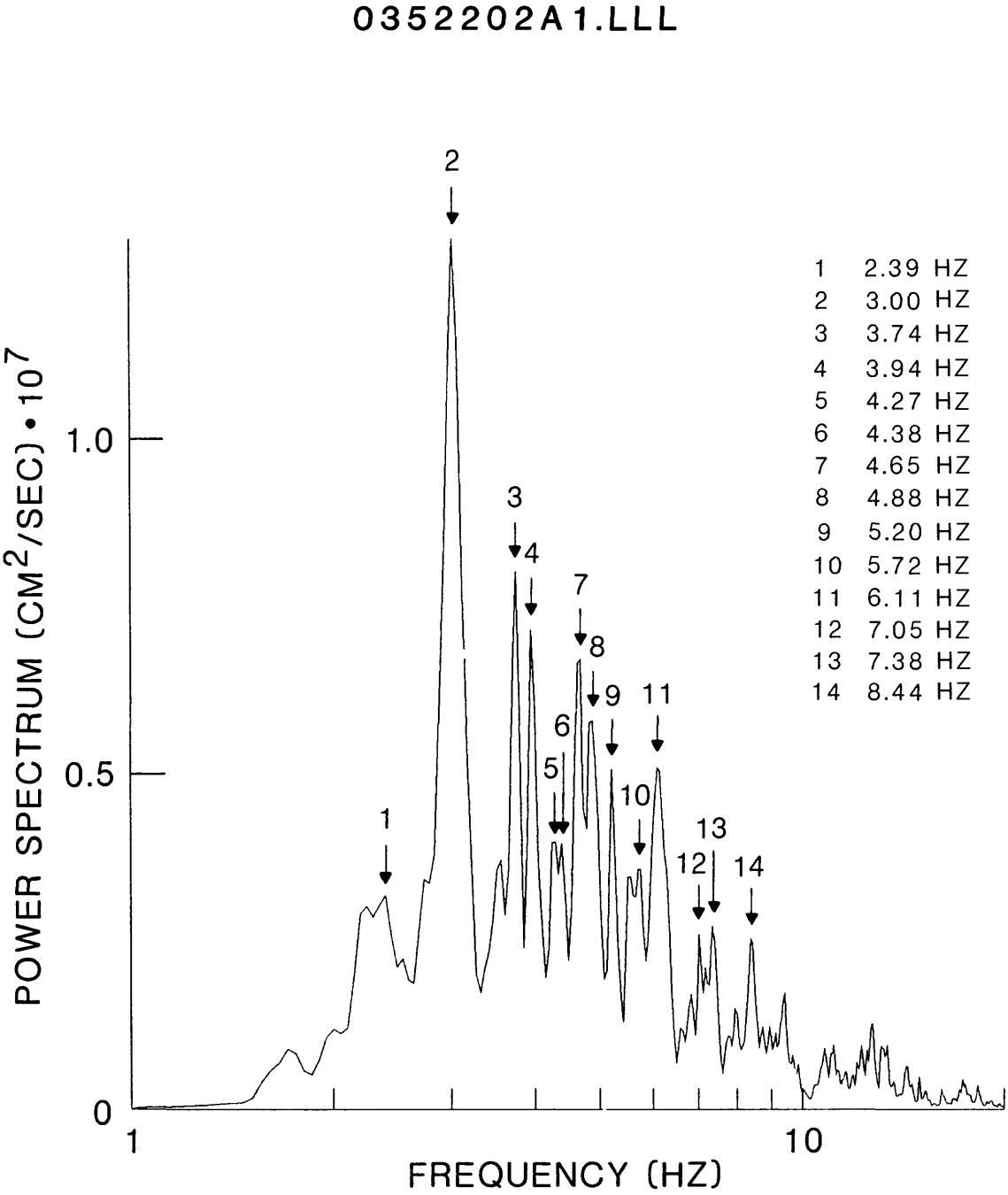

Figure 33. Power spectrum of vertical ground velocity, recorded at station L1, of tremor at position A in the record of Figure 22.

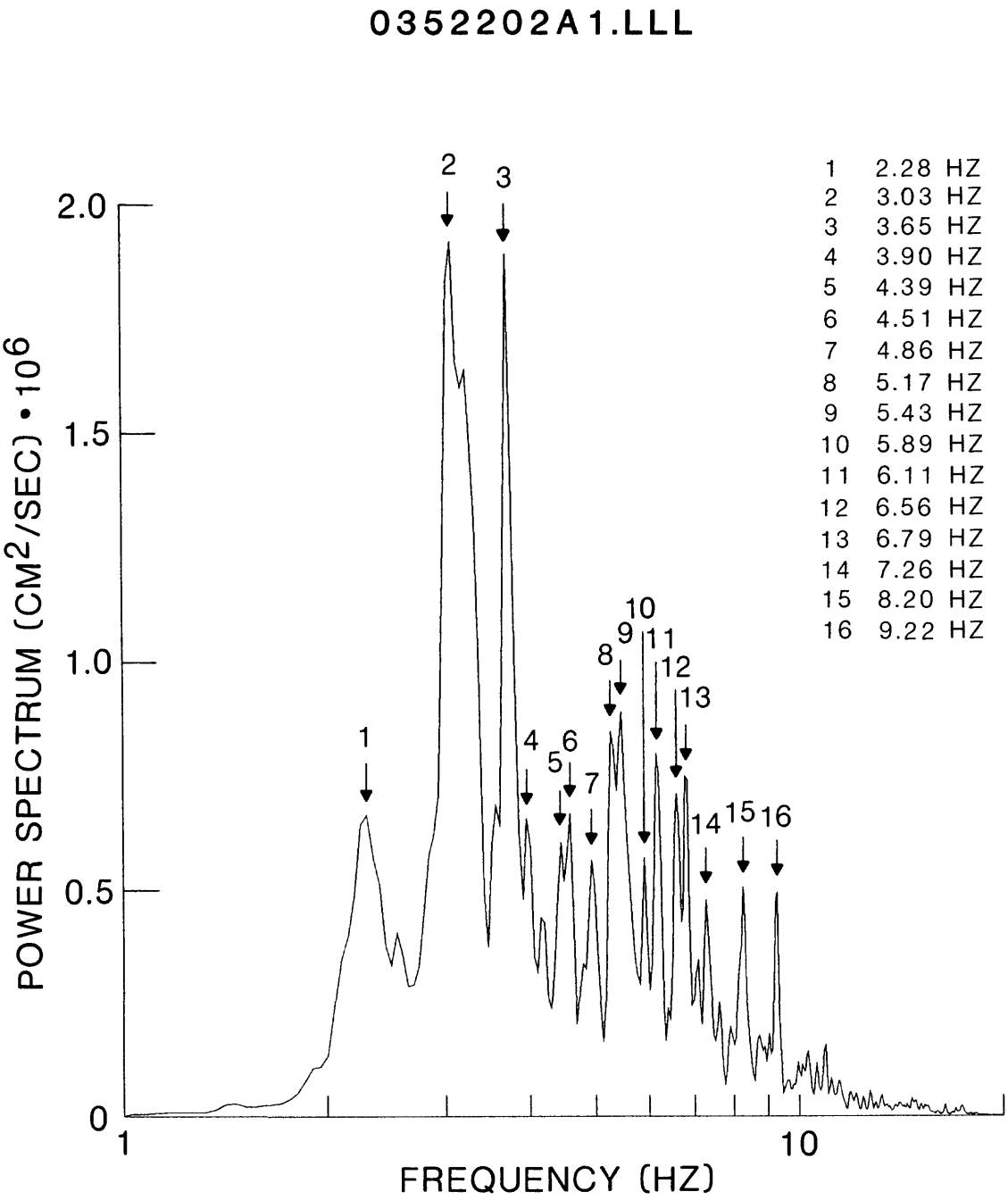

Figure 34. Power spectrum of vertical ground velocity, recorded at station L1, of gas-piston event superimposed on a background of tremor at position B in the record of Figure 22.

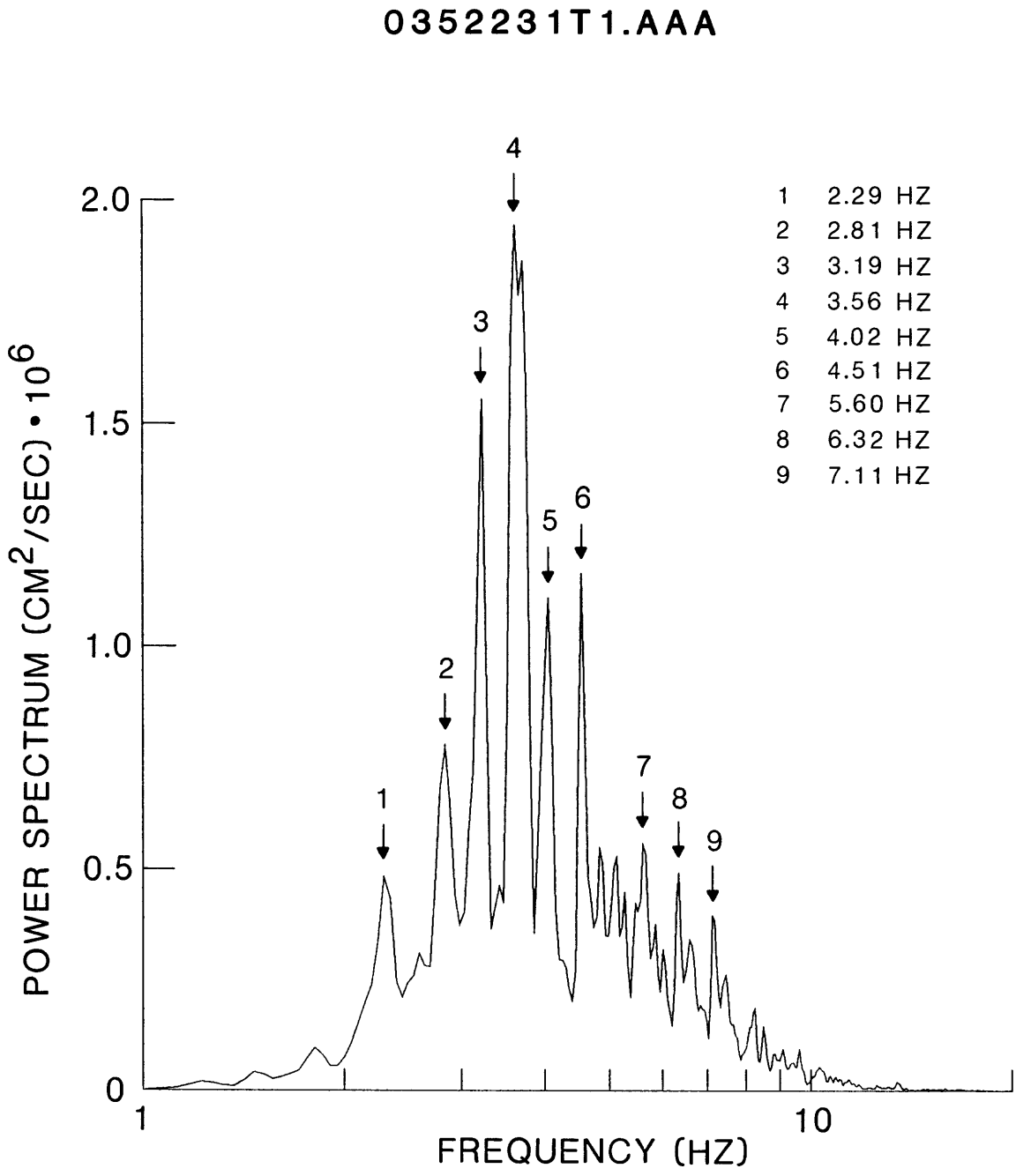

Figure 35. Power spectrum of vertical ground velocity, recorded at station A1, of gas-piston event at position D in the record of Figure 22.

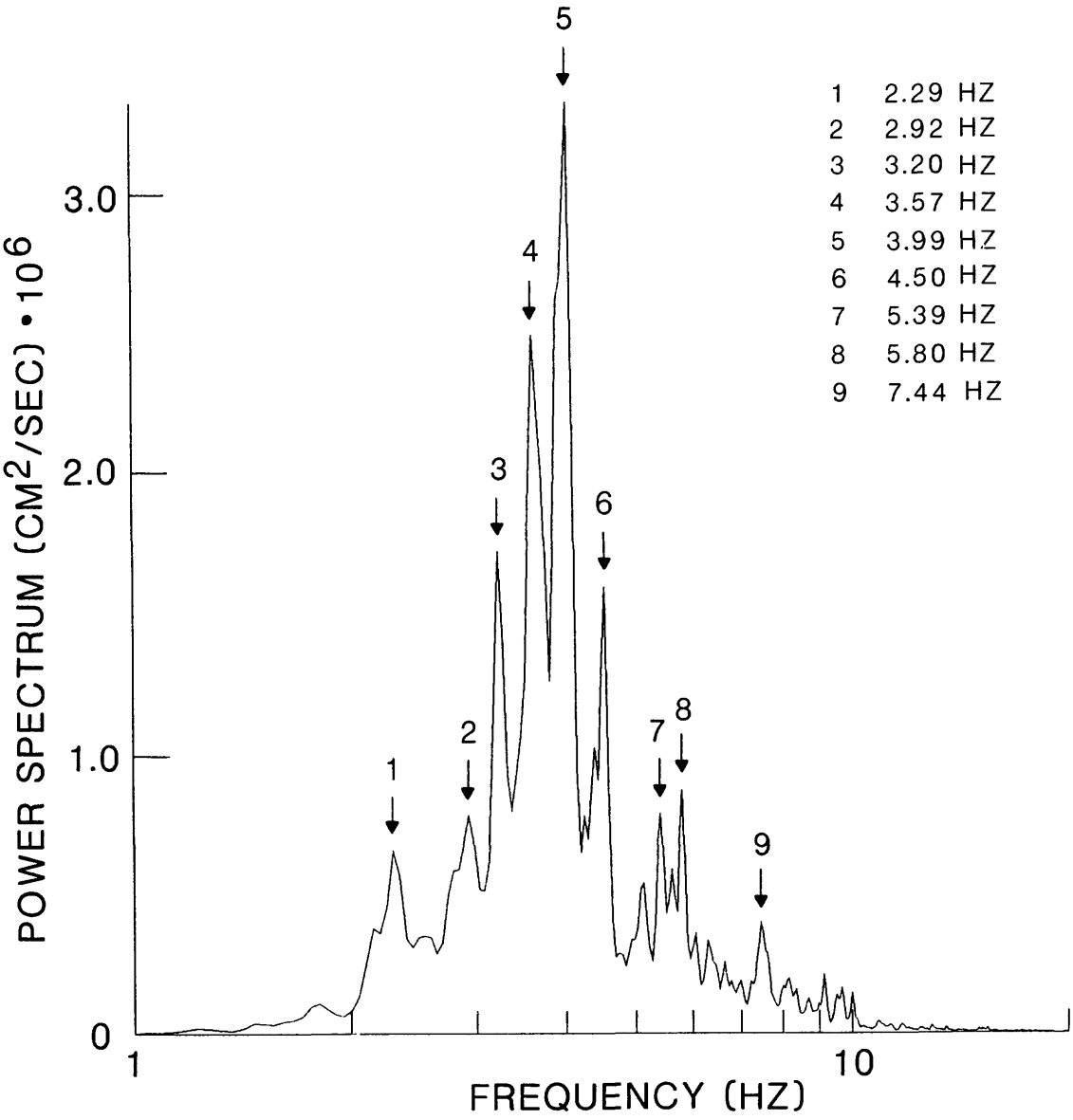

Figure 36. Power spectrum of vertical ground velocity, recorded at station D1, of gas-piston event at position D in the record of Figure 22.

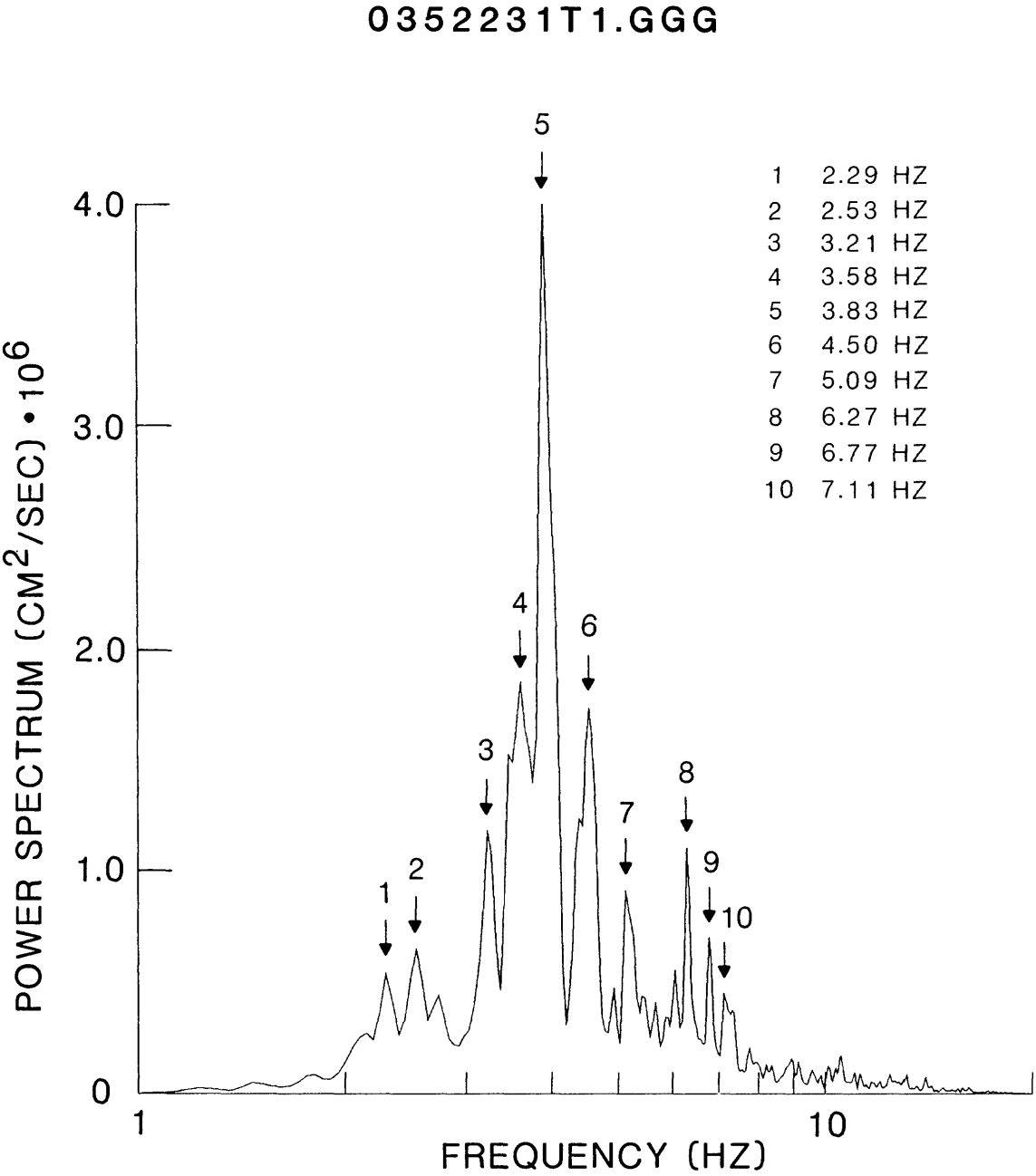

Figure 37. Power spectrum of vertical ground velocity, recorded at station G1, of gas-piston event at position D in the record of Figure 22.

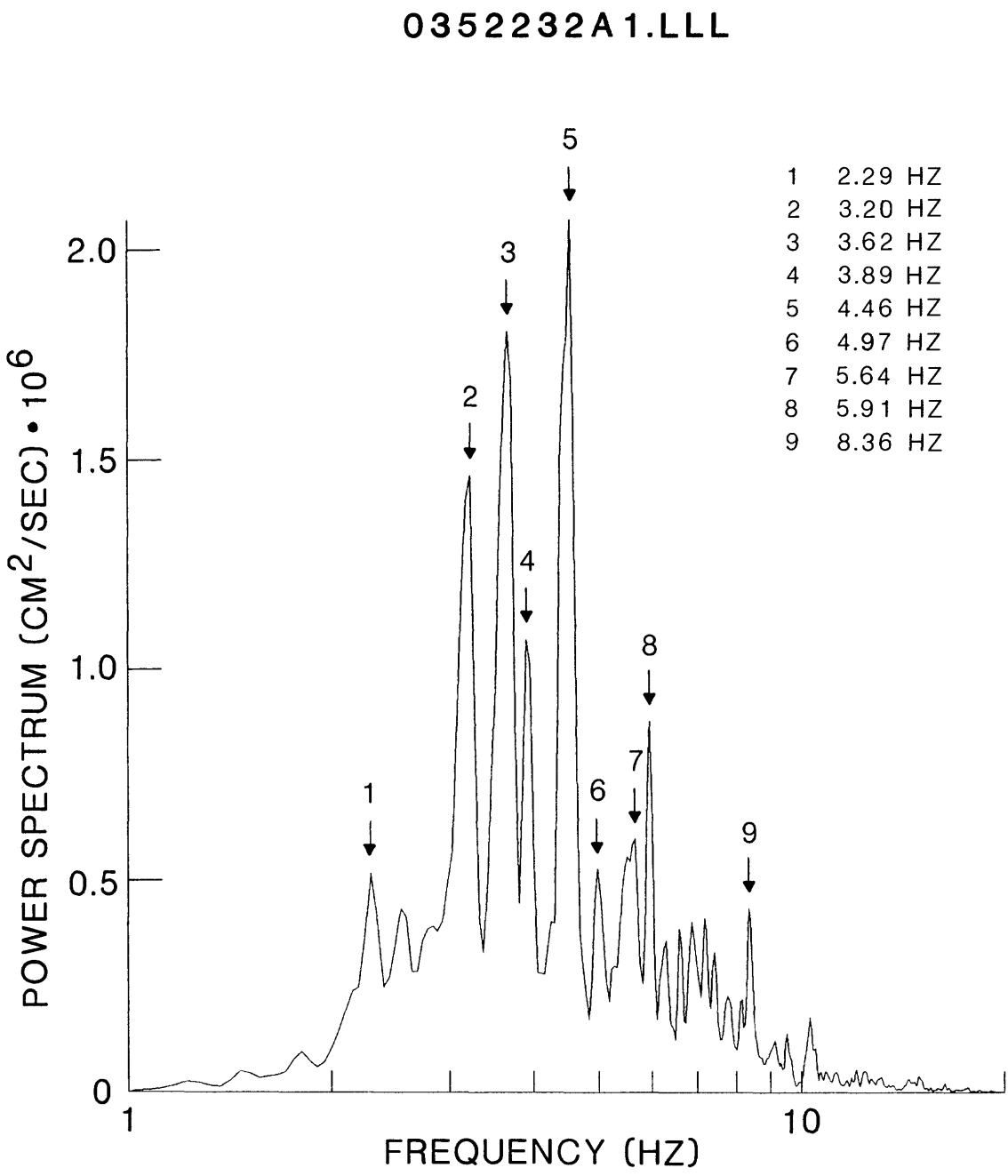

Figure 38. Power spectrum of vertical ground velocity, recorded at station L1, of gas-piston event at position D in the record of Figure 22.

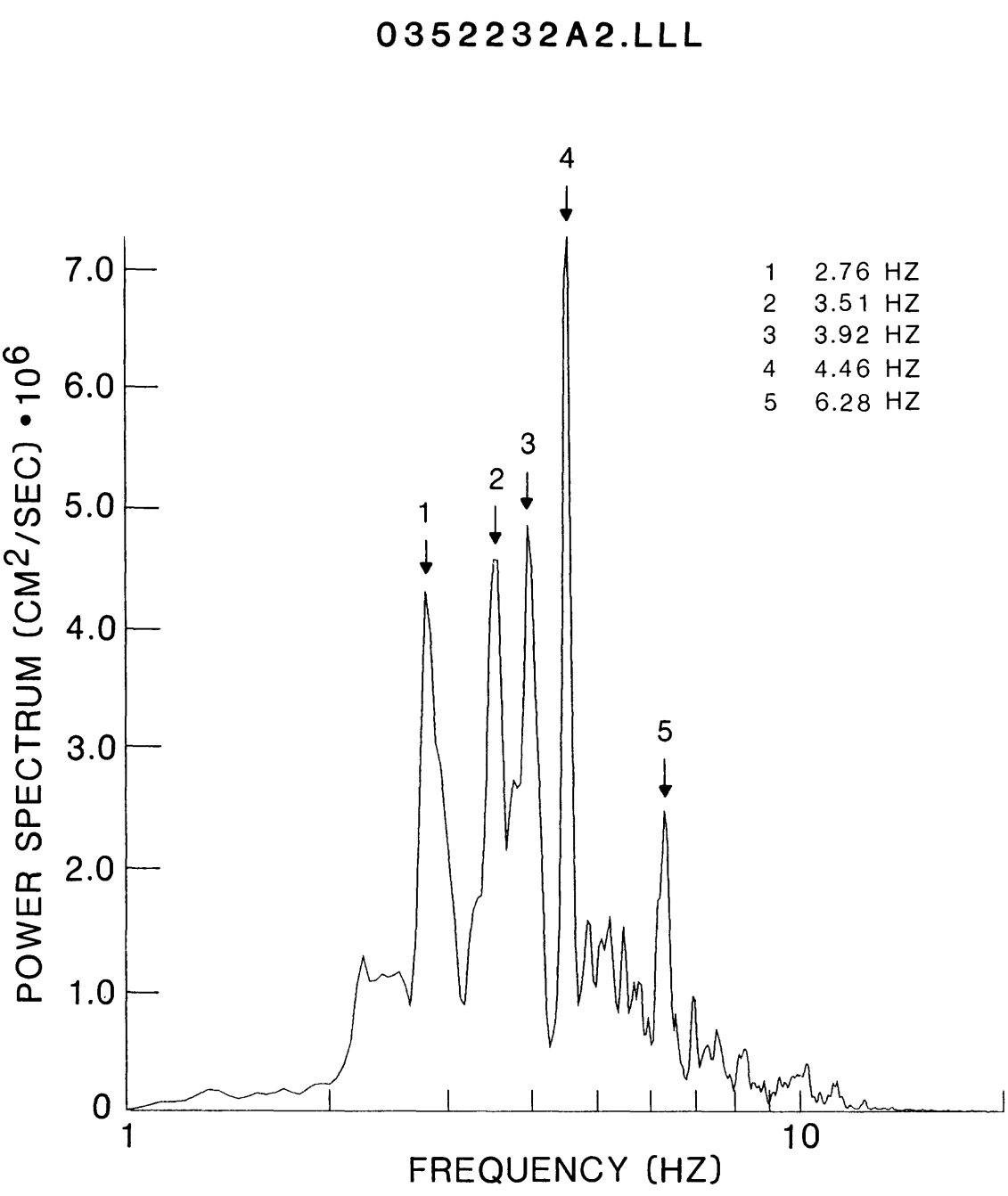

Figure 39. Power spectrum of horizontal component 2 ground velocity, recorded at station L2, of gas-piston event at position D in the record of Figure 22.

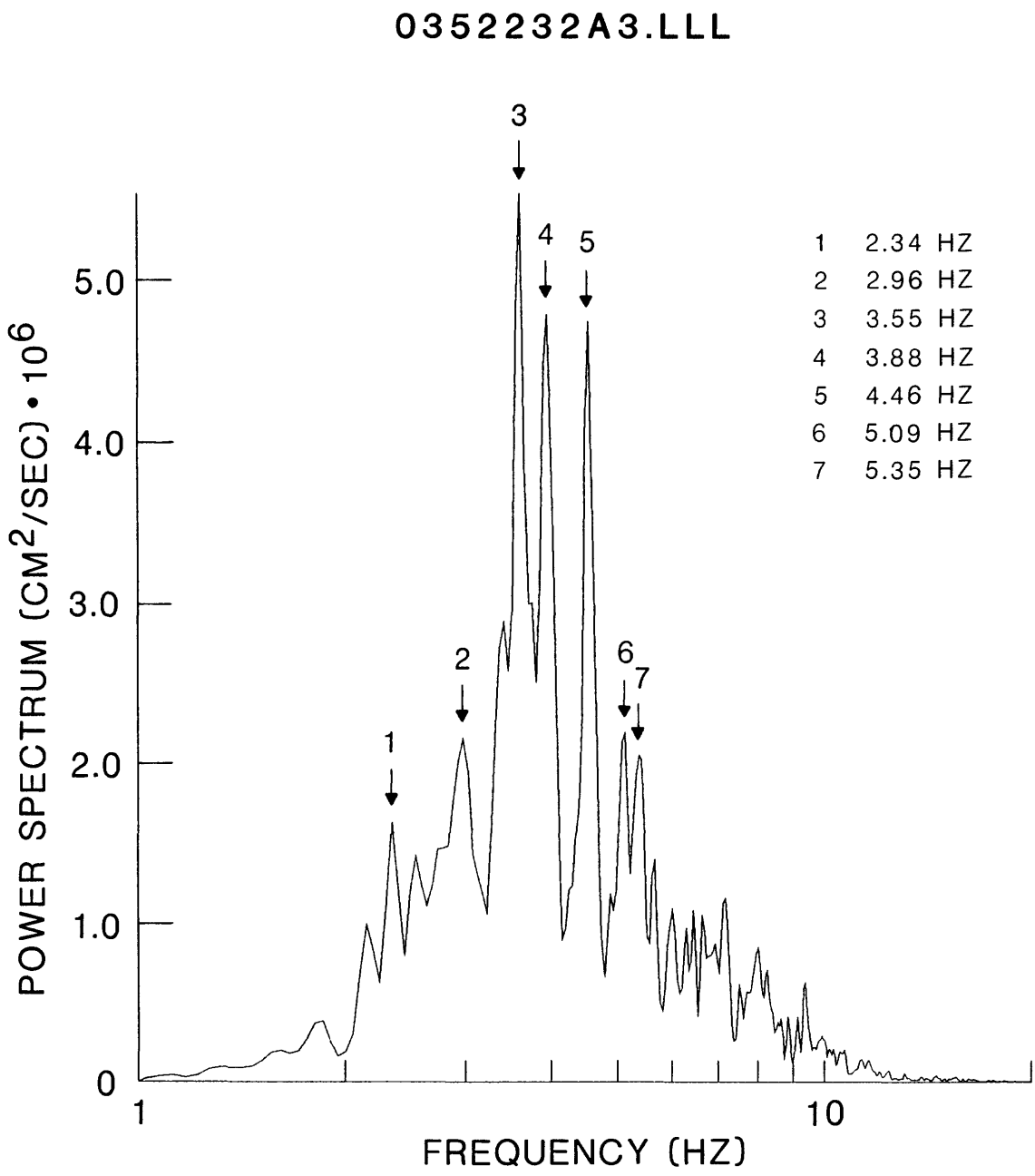

Figure 40. Power spectrum of horizontal component 3 ground velocity, recorded at station L3, of gas-piston event at position D in the record of Figure 22.

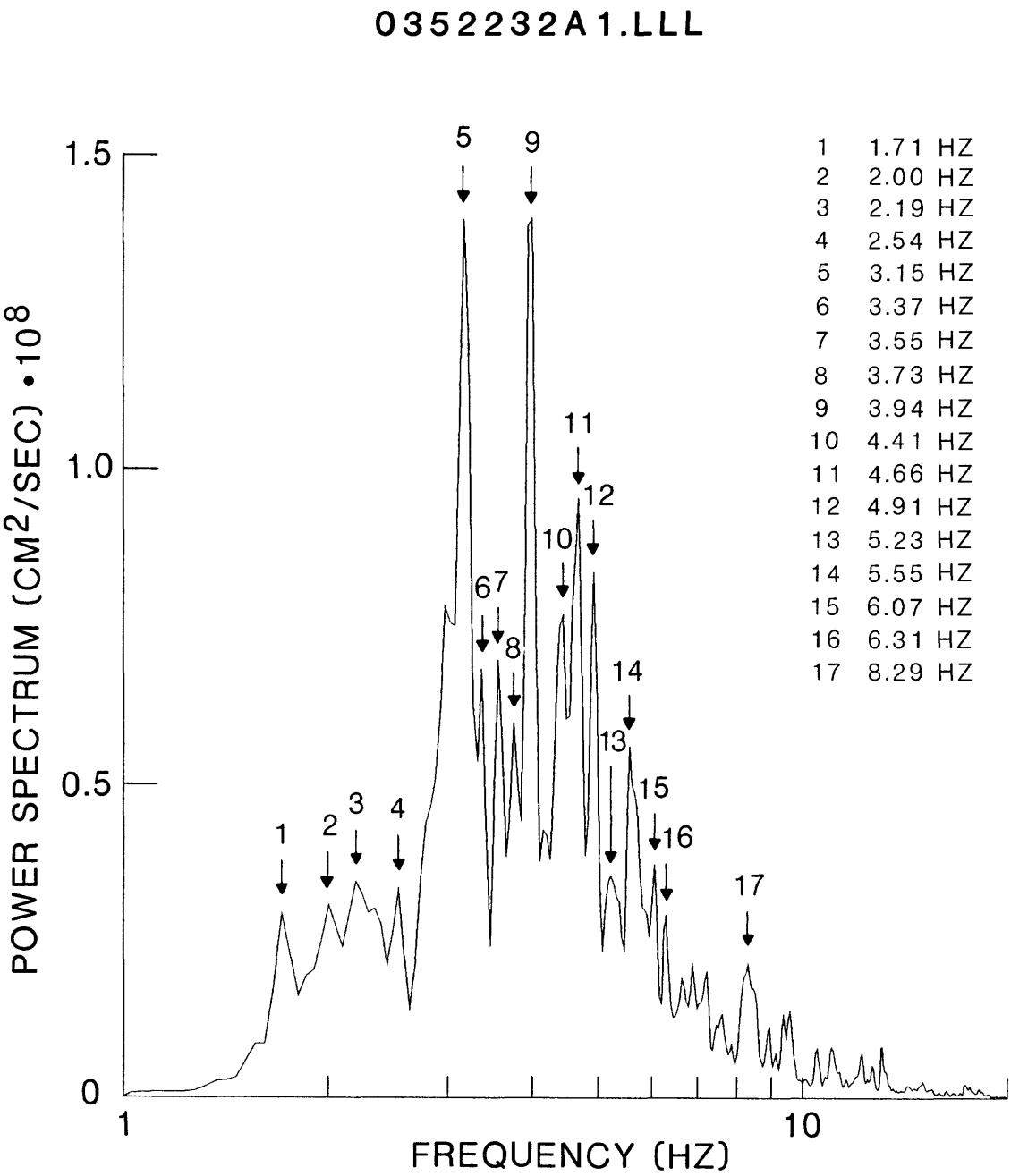

Figure 41. Power spectrum of vertical ground velocity, recorded at station L1, of tremor at position E in the record of Figure 22.

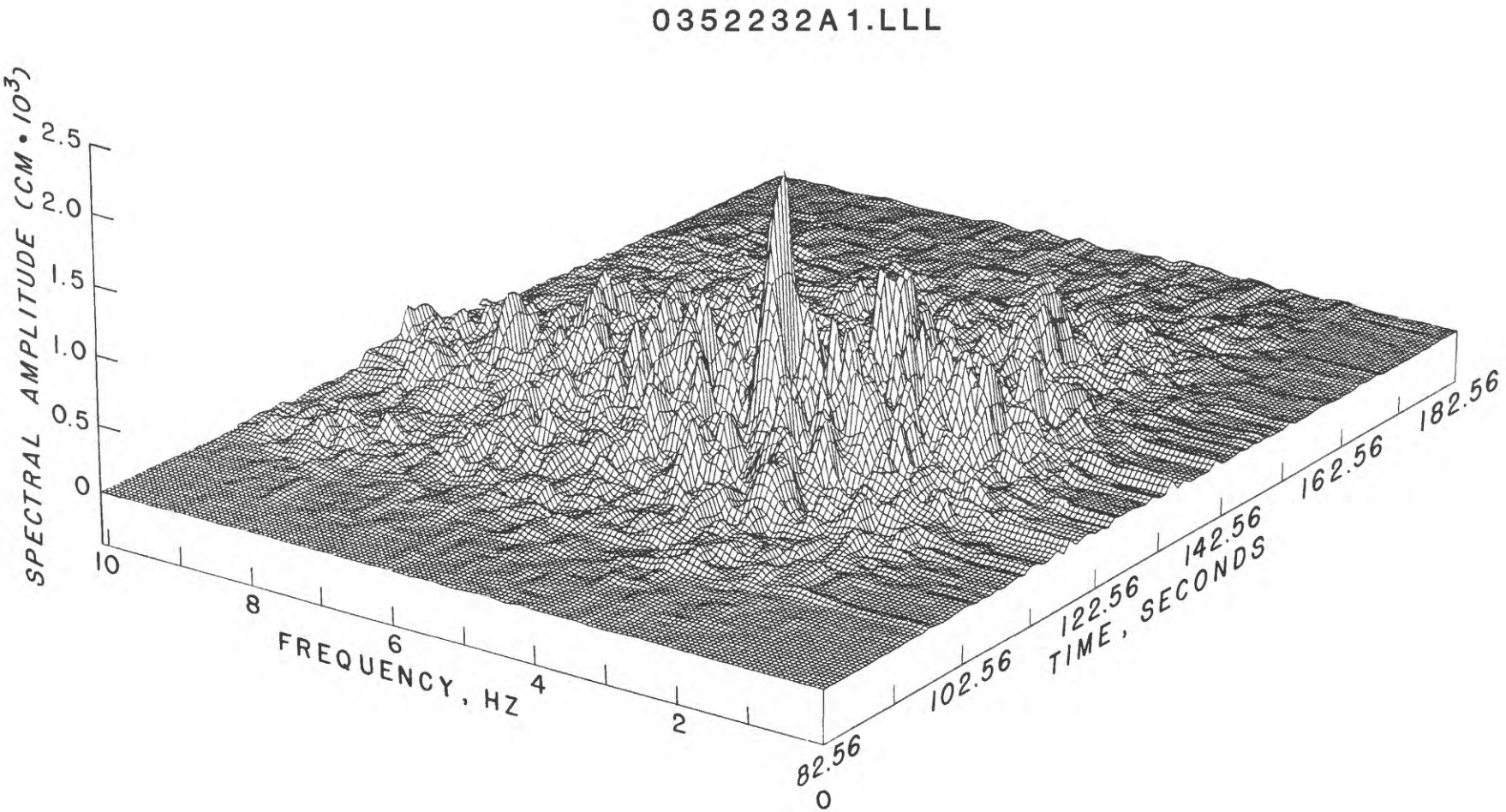

Figure 42. Three-dimensional moving window spectrum of vertical ground velocity recorded at station L1 for the gas-piston event shown in Figure 28.

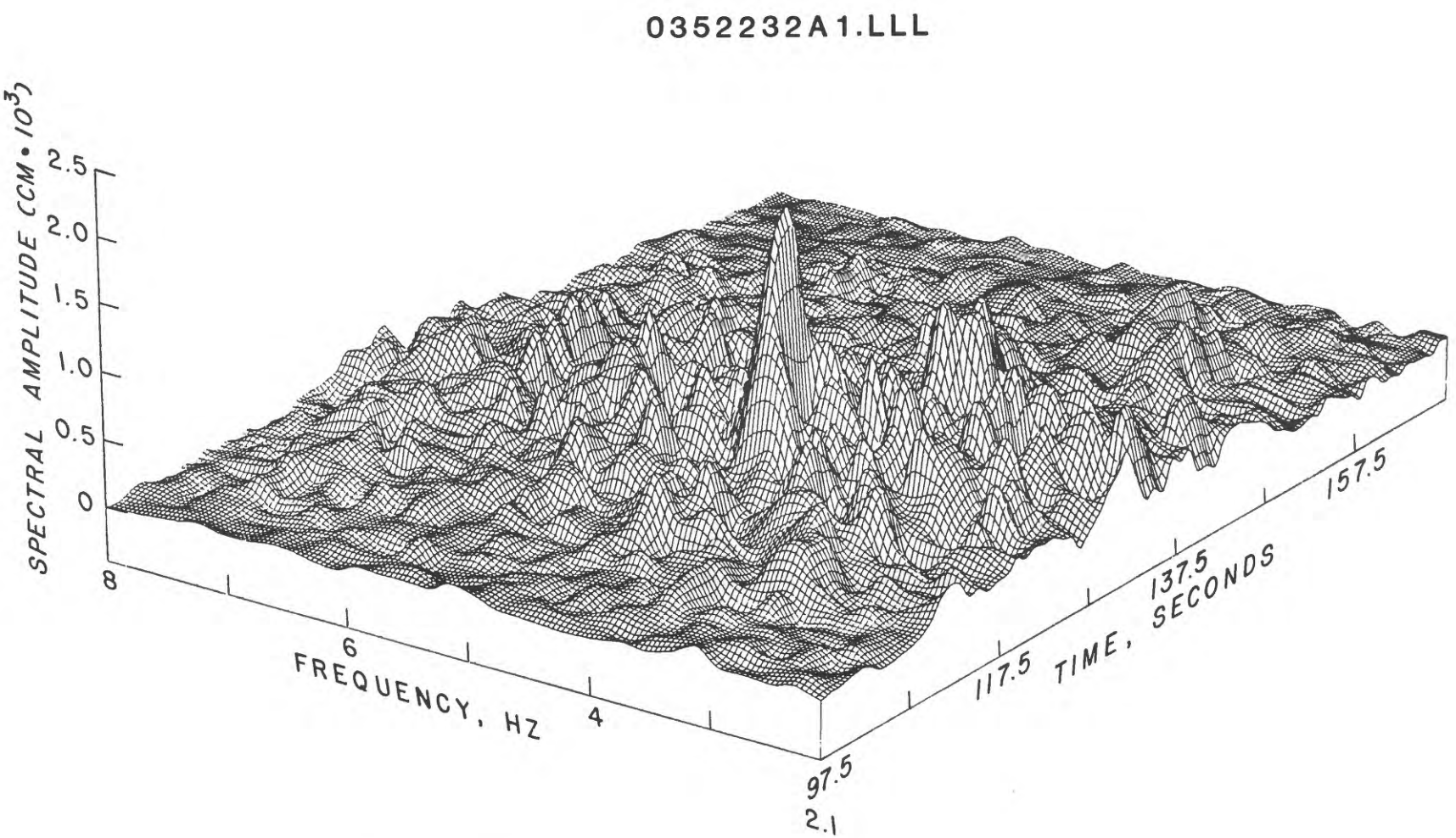

Figure 43. Three-dimensional moving window spectrum showing details of the main portion of the spectrum of Figure 42 in the window of 97.5 to 167.5 s and in the band of 2.1 to 8.0 Hz.

Figure 44. Shaded Contour plot of a moving window spectrum of vertical ground velocity, recorded at station L1, of tremor shown in Figure 23.

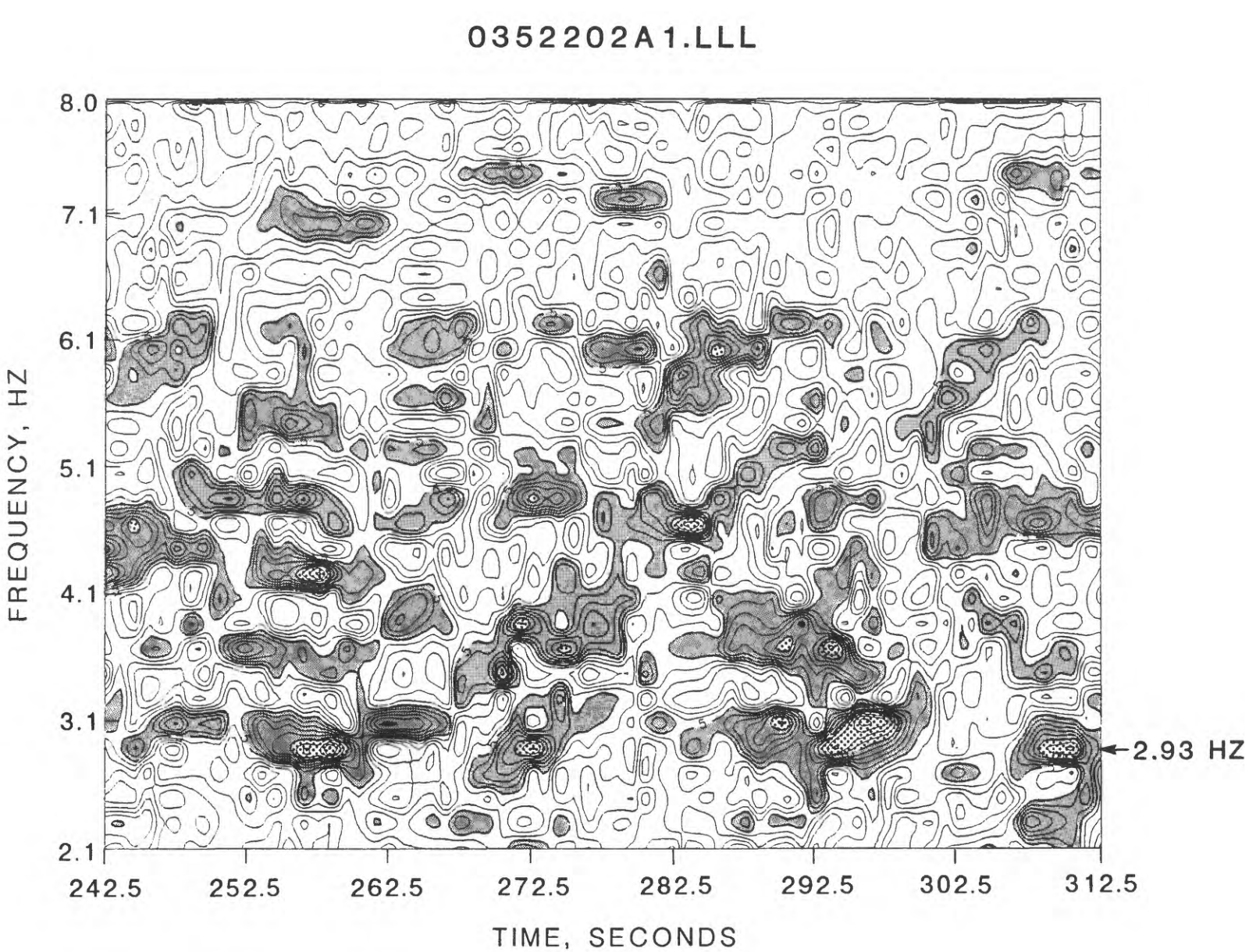
0352202A1.LLL
8.0
7.1
6.1
5.1
4.1
3.1
2.1
FREQUENCY, HZ
2.93 HZ
242.5
252.5
262.5
272.5
282.5
292.5
302.5
312.5
TIME, SECONDS

Figure 45. Shaded Contour plot of a moving window spectrum of vertical ground velocity, recorded at station L1, of a gas-piston event superimposed on a background of tremor shown in Figure 24.

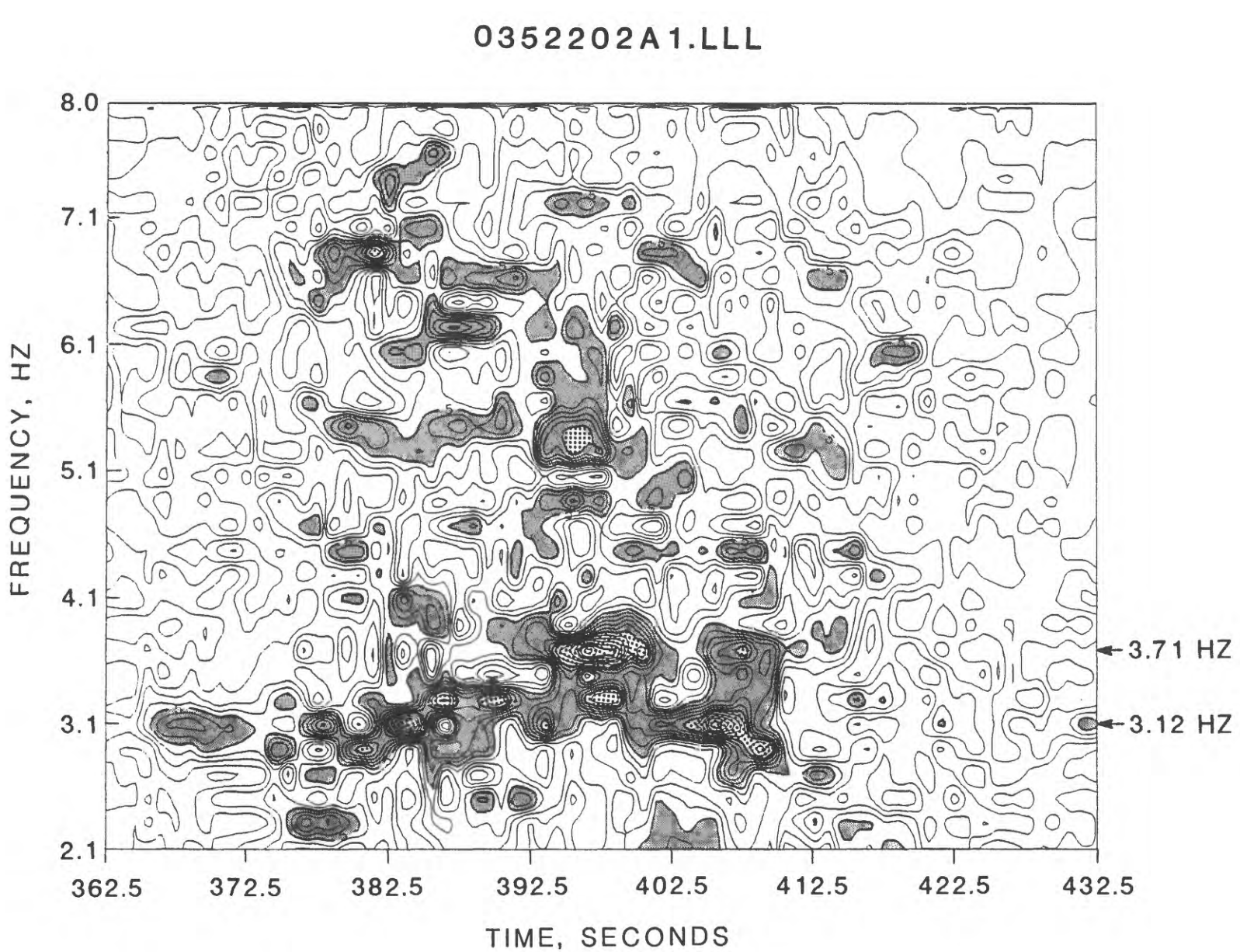
0352202A1.LLL
8.0
7.1
6.1
5.1
4.1
3.1
2.1
FREQUENCY, HZ
3.71 HZ
3.12 HZ
362.5
372.5
382.5
392.5
402.5
412.5
422.5
432.5
TIME, SECONDS

Figure 46. Shaded Contour plot of a moving window spectrum of vertical ground velocity, recorded at station A1, of the gas-piston event shown in Figure 25.

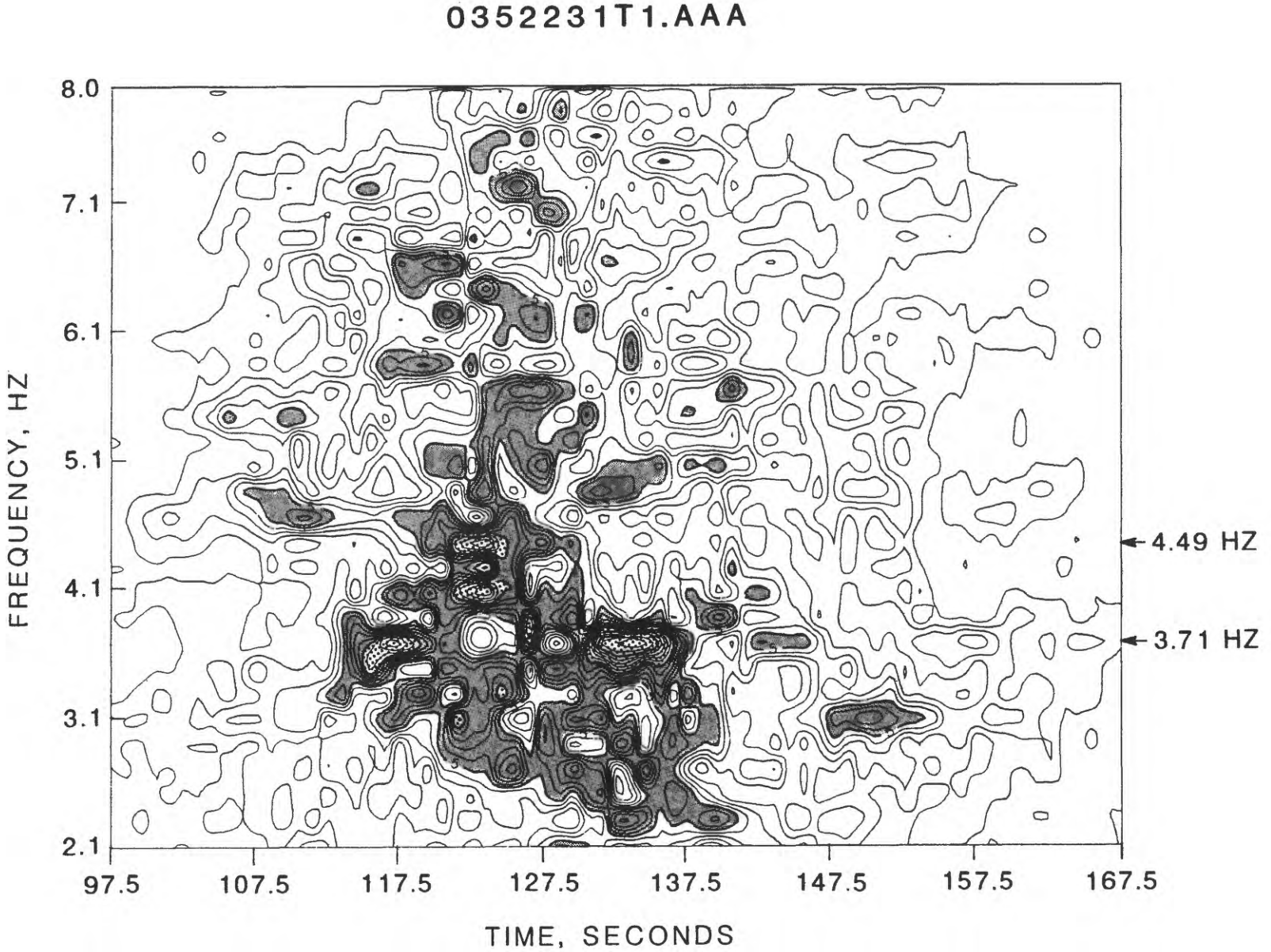
0352231T1.AAA
8.0
7.1
6.1
5.1
4.1
3.1
2.1
FREQUENCY, HZ
4.49 HZ
3.71 HZ
97.5
107.5
117.5
127.5
137.5
147.5
157.5
167.5
TIME, SECONDS

Figure 47. Shaded Contour plot of a moving window spectrum of vertical ground velocity, recorded at station D1, of the gas-piston event shown in Figure 26.

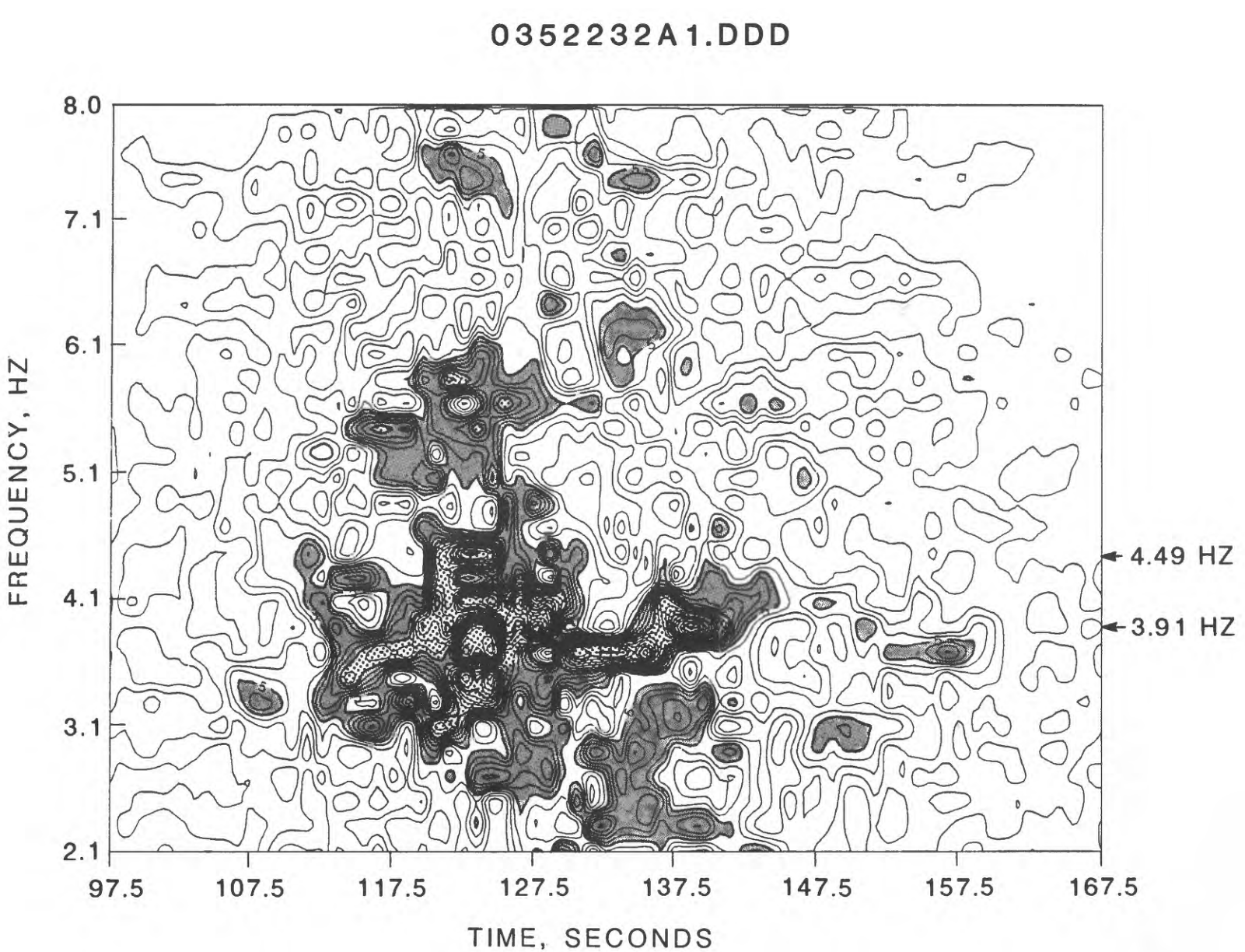
0352232A1.DDD
8.0
7.1
6.1
5.1
4.1
3.1
2.1
FREQUENCY, HZ
4.49 HZ
3.91 HZ
97.5
107.5
117.5
127.5
137.5
147.5
157.5
167.5
TIME, SECONDS

Figure 48. Shaded Contour plot of a moving window spectrum of vertical ground velocity, recorded at station G1, of the gas-piston event shown in Figure 27.

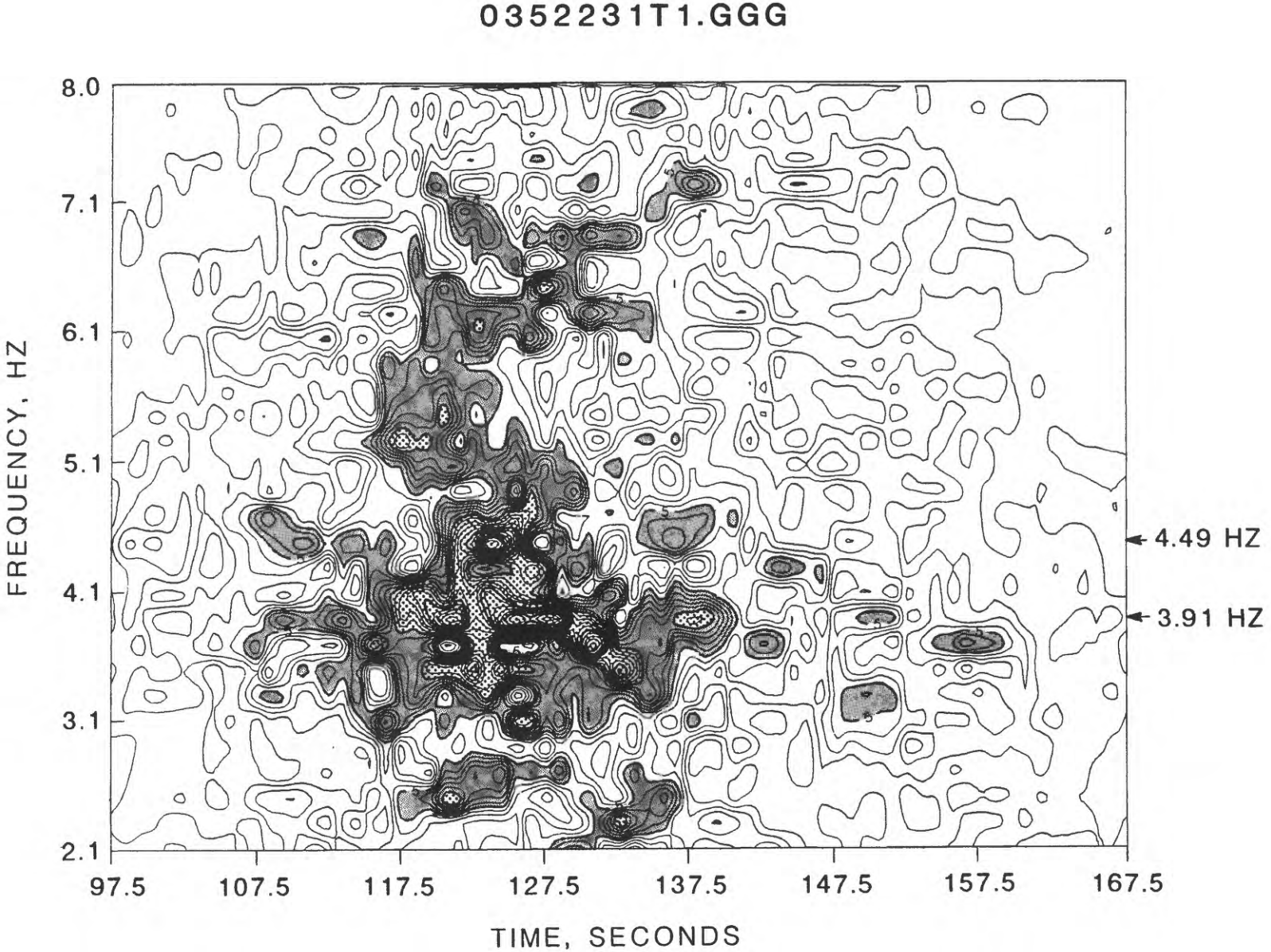
0352231T1.GGG
8.0
7.1
6.1
5.1
4.1
3.1
2.1
FREQUENCY, HZ
4.49 HZ
3.91 HZ
97.5
107.5
117.5
127.5
137.5
147.5
157.5
167.5
TIME, SECONDS

Figure 49. Shaded Contour plot of a moving window spectrum of vertical ground velocity, recorded at station L1, of the gas-piston event shown in Figure 28.

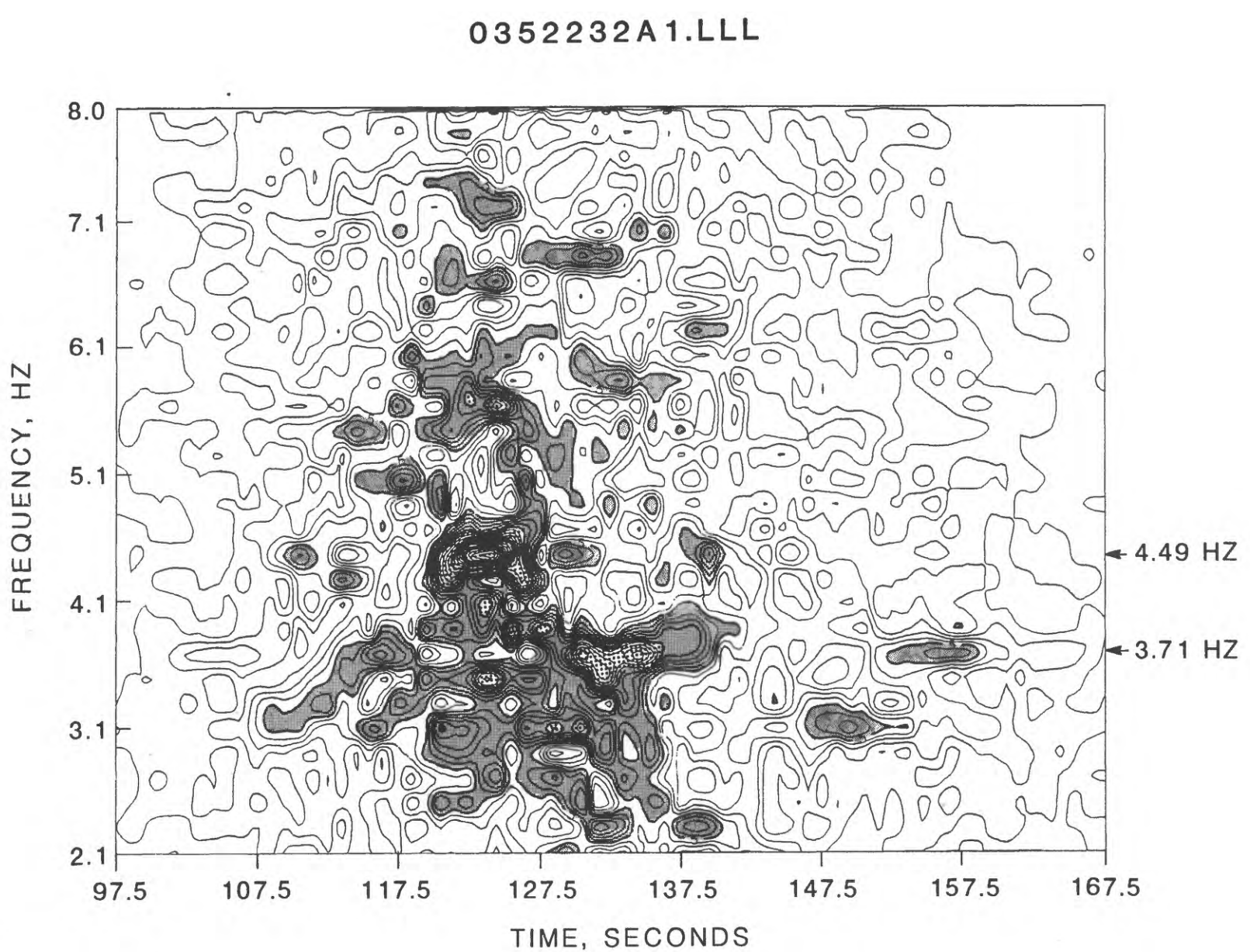
0352232A1.LLL
8.0
7.1
6.1
5.1
4.1
3.1
2.1
FREQUENCY, HZ
4.49 HZ
3.71 HZ
97.5
107.5
117.5
127.5
137.5
147.5
157.5
167.5
TIME, SECONDS

Figure 50. Shaded Contour plot of a moving window spectrum of horizontal component 2 ground velocity, recorded at station L2, of the gas-piston event shown in Figure 29.

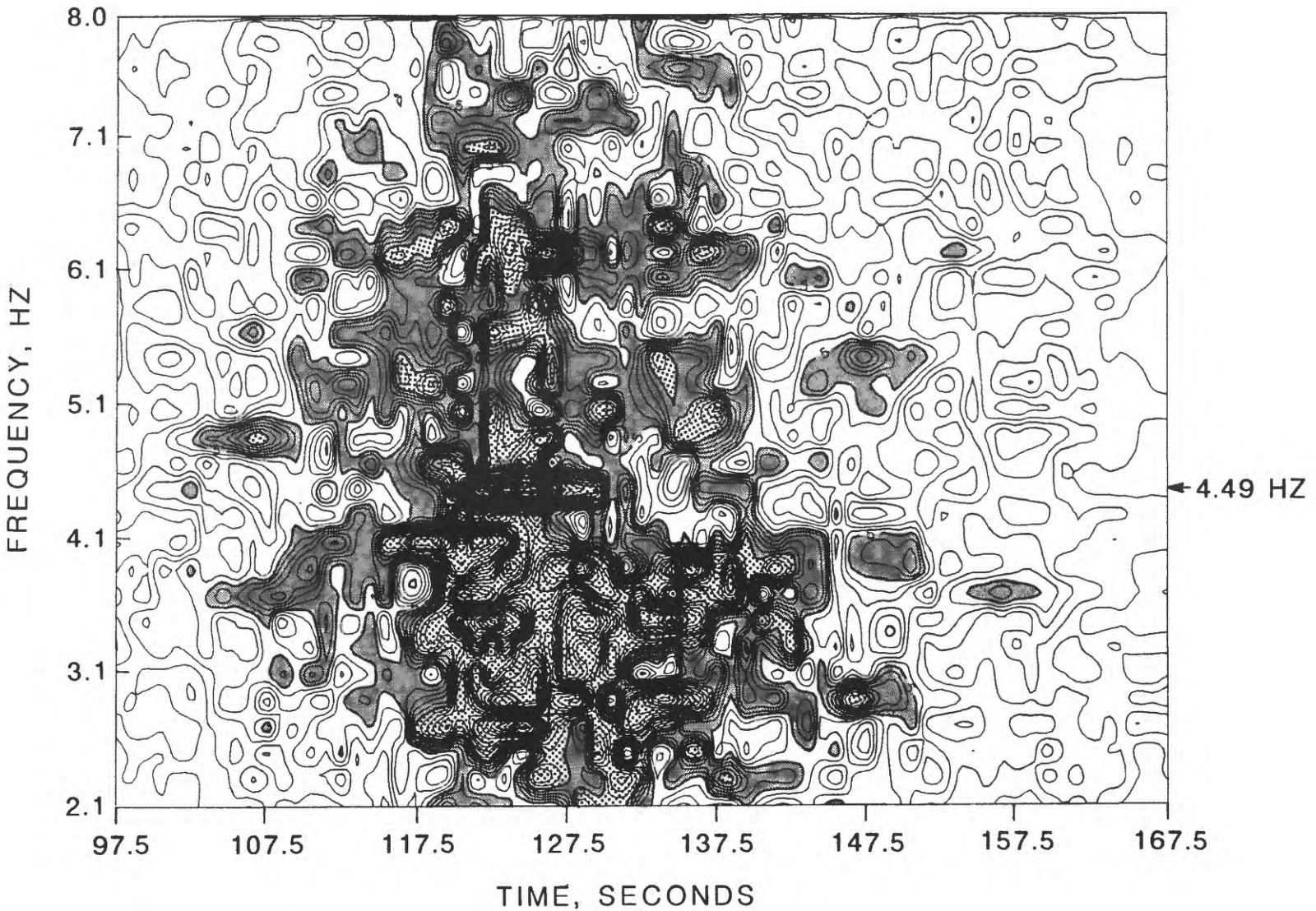
0352232A2.LLL
8.0
7.1
6.1
5.1
4.1
3.1
2.1
FREQUENCY, HZ
4.49 HZ
97.5
107.5
117.5
127.5
137.5
147.5
157.5
167.5
TIME, SECONDS

Figure 51. Shaded Contour plot of a moving window spectrum of horizontal component 3 ground velocity, recorded at station L3, of the gas-piston event shown in Figure 30.

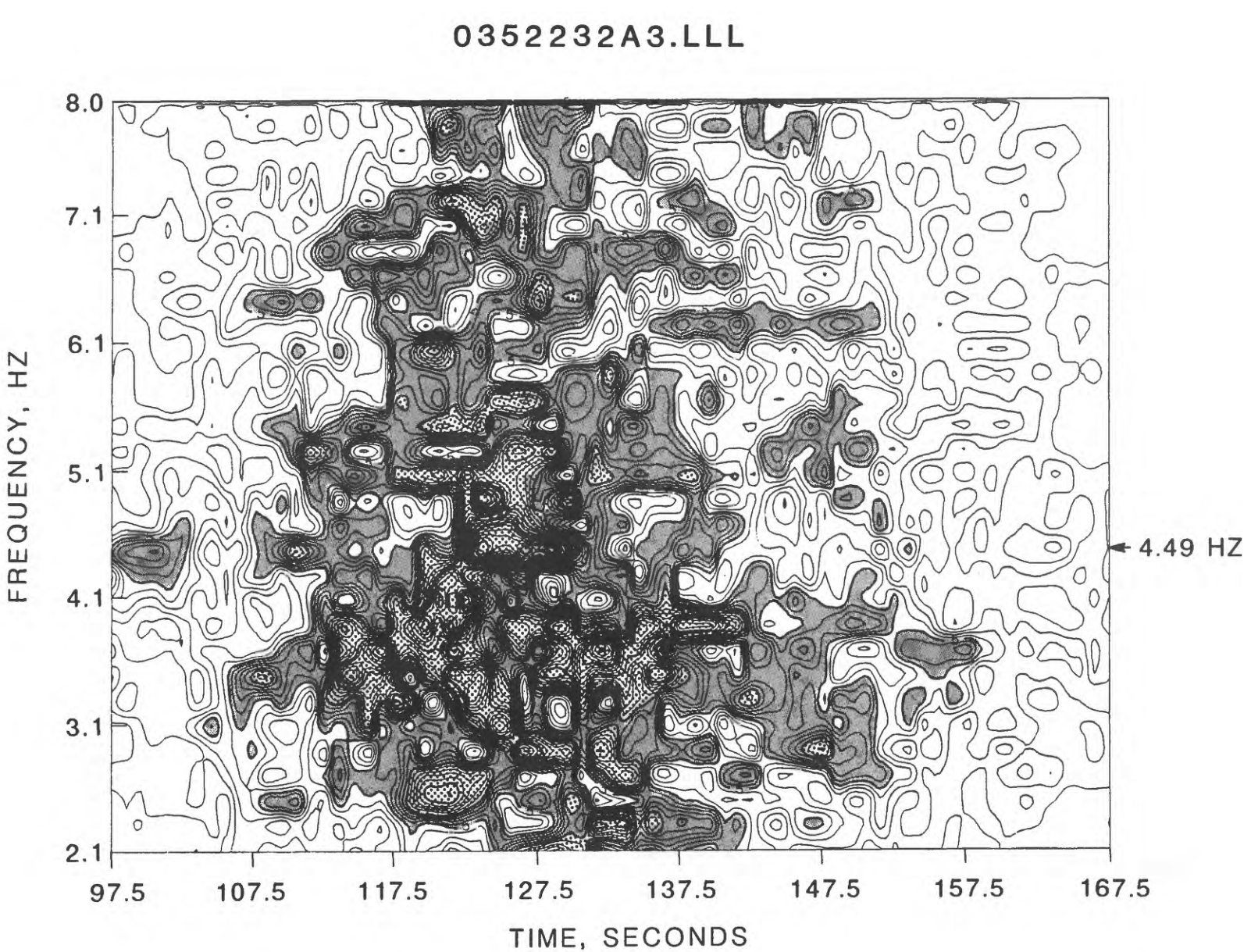
0352232A3.LLL
8.0
7.1
6.1
5.1
4.1
3.1
2.1
FREQUENCY, HZ
4.49 HZ
97.5
107.5
117.5
127.5
137.5
147.5
157.5
167.5
TIME, SECONDS

Figure 52. Shaded Contour plot of a moving window spectrum of vertical ground velocity, recorded at station L1, of tremor shown in Figure 31.

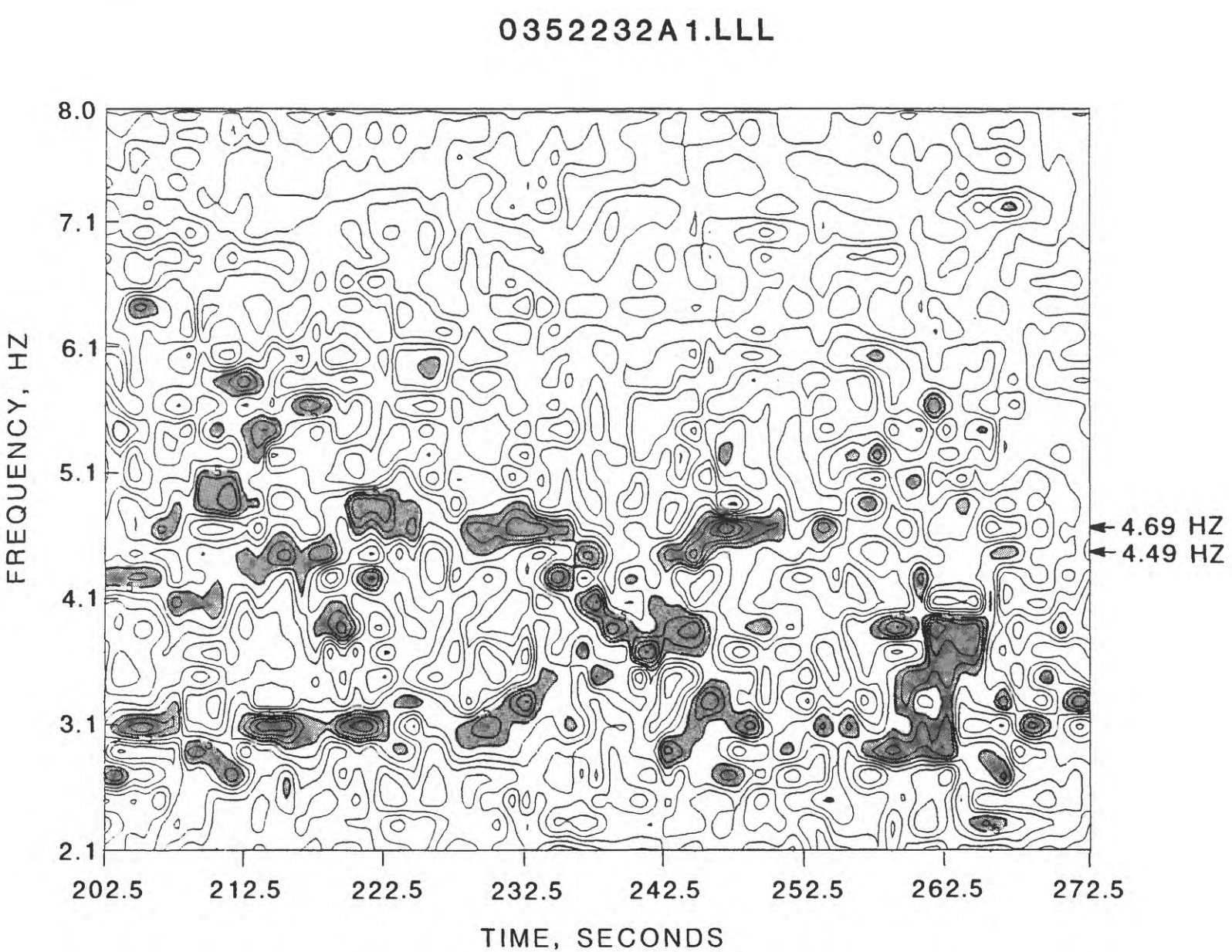
0352232A1.LLL
8.0
7.1
6.1
5.1
4.1
3.1
2.1
FREQUENCY, HZ
4.69 HZ
4.49 HZ
202.5
212.5
222.5
232.5
242.5
252.5
262.5
272.5
TIME, SECONDS

Figure 53. Comparison of power spectra of tremor and gas-piston events. Top: stacked spectra of vertical ground velocity for suites of tremor recorded at station K2 of the first array deployed at Pu'u O'o (see Fig. 2). Bottom: stacked spectra of vertical ground velocity for gas-piston events recorded at station L4 of the second array deployed at Pu'u O'o (see Fig. 3).

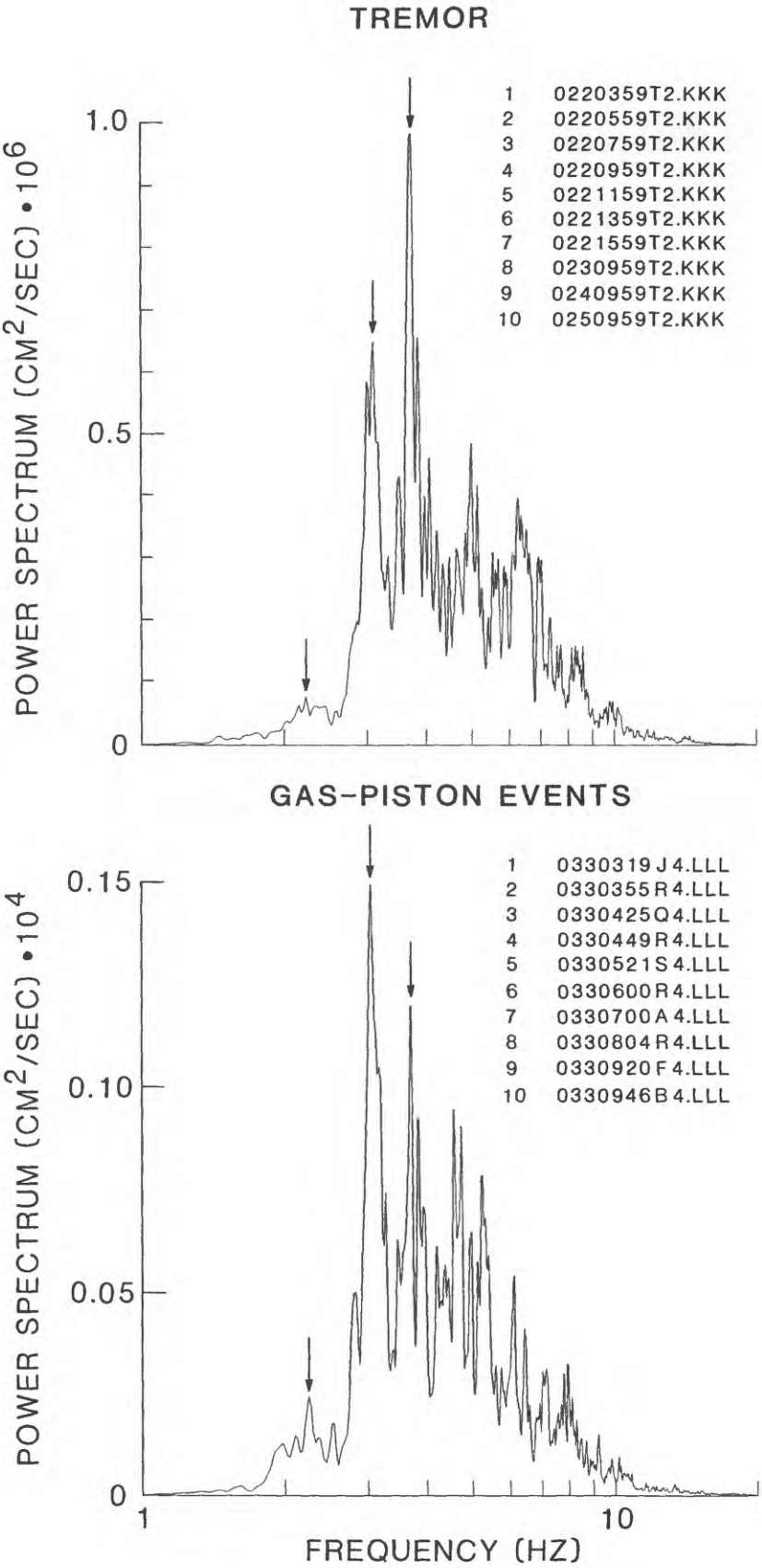
TREMOR
1 0220359T2.KKK
2 0220559T2.KKK
3 0220759T2.KKK
4 0220959T2.KKK
5 0221159T2.KKK
6 0221359T2.KKK
7 0221559T2.KKK
8 0230959T2.KKK
9 0240959T2.KKK
10 0250959T2.KKK
POWER SPECTRUM (CM2/SEC) • 10^6
1.0
0.5
0
GAS-PISTON EVENTS
1 0330319J4.LLL
2 0330355R4.LLL
3 0330425Q4.LLL
4 0330449R4.LLL
5 0330521S4.LLL
6 0330600R4.LLL
7 0330700A4.LLL
8 0330804R4.LLL
9 0330920F4.LLL
10 0330946B4.LLL
POWER SPECTRUM (CM2/SEC) • 10^4
0.15
0.10
0.05
0
1
10
FREQUENCY (HZ)

Figure 54. Power spectra obtained by stacking over 47 vertical components of ground velocity for one section of tremor and one gas-piston event. Top: stacked spectra obtained for tremor at position A in the record of Figure 22. Bottom: stacked spectra obtained for the gas-piston event at position D in the record of Figure 22.

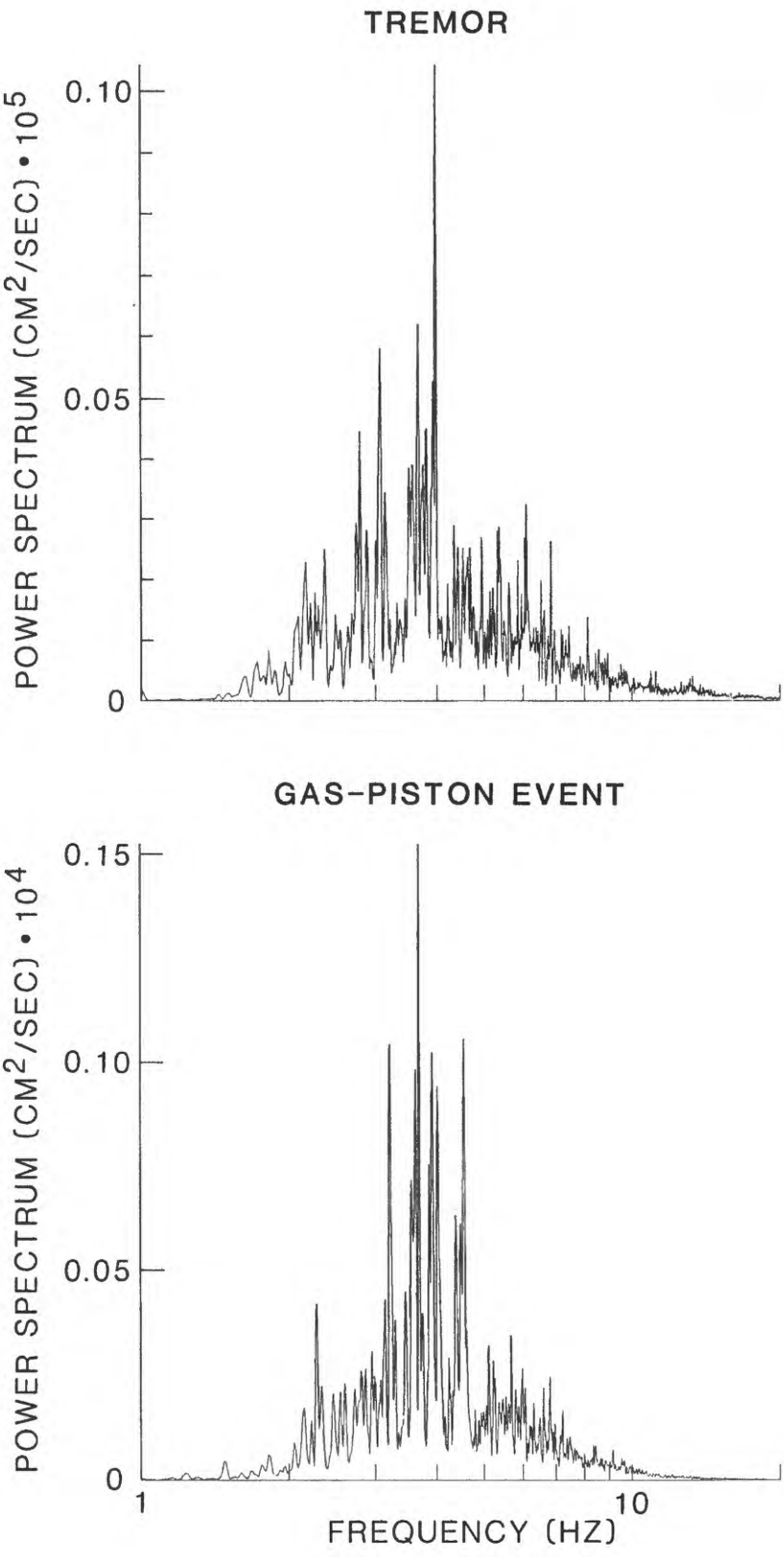
TREMOR
POWER SPECTRUM (CM2/SEC) • 10^5
0.10
0.05
0
GAS-PISTON EVENT
POWER SPECTRUM (CM2/SEC) • 10^4
0.15
0.10
0.05
0
1
10
FREQUENCY (HZ)

Figure 55. Synthetic plane wave showing the expected distortion in the shape of the elastic wavefield over the surface encompassed by the second array.

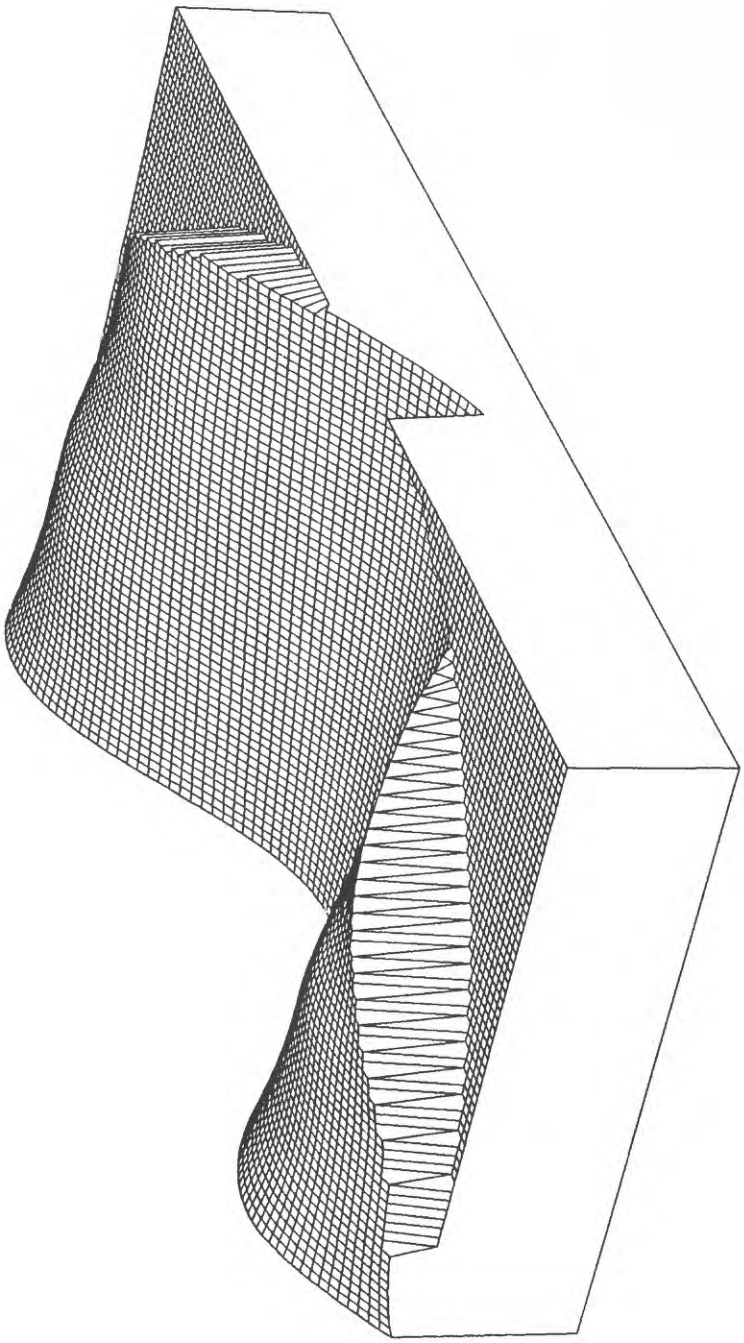

Figure 56. Snapshots of the vertical components of ground velocity over the surface encompassed by the second array. The sequence starts at 88 35 22 34 2.996 GMT and samples the elastic wavefield at constant intervals of 0.01 s during the gas-piston event depicted in Figures 25-28 (continued in Fig. 57).

88 35 22 34 2.996

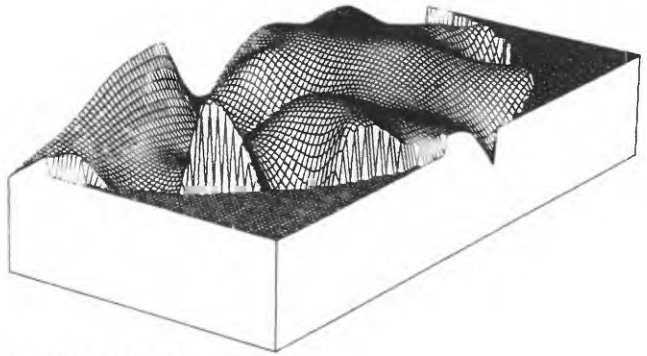

0.00 SEC

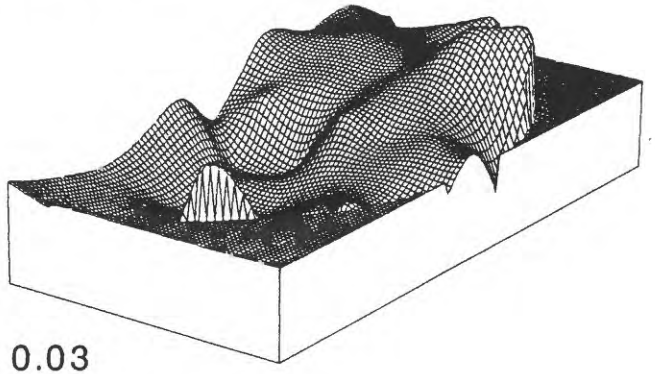

0.03

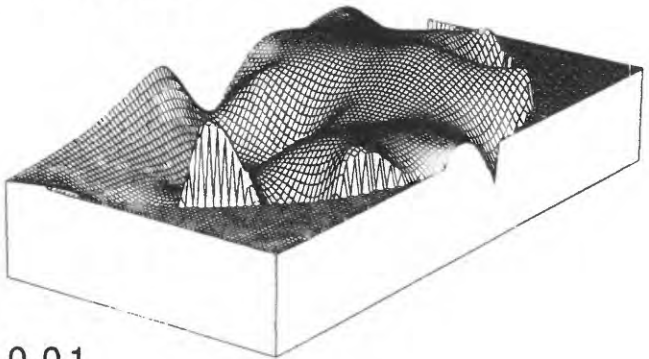

0.01

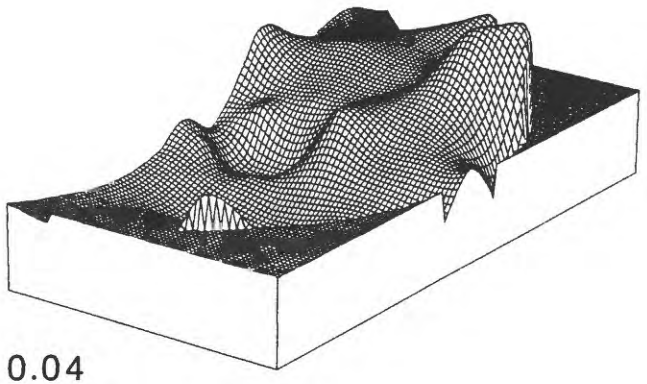

0.04

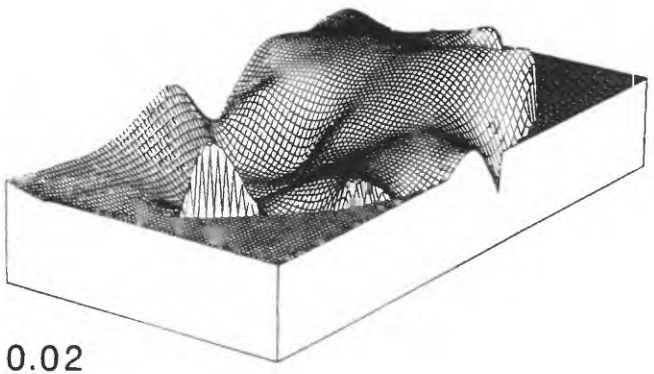

0.02

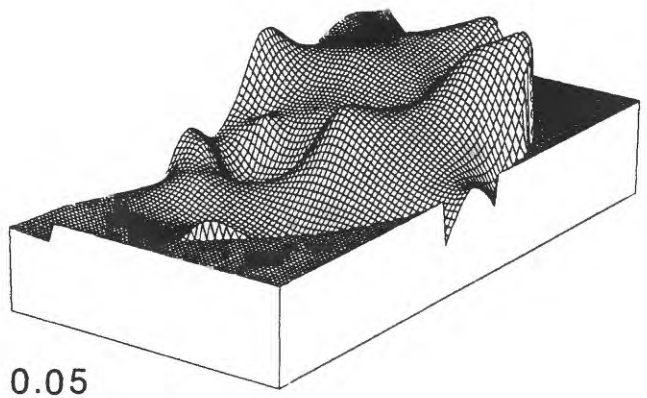

0.05

Figure 57. Continuation from sequence shown in Figure 56. The sequence starts with the last snapshot of Figure 56 at 88 35 22 34 2.996 + 0.05 and ends 0.05 seconds later.

88 35 22 34 2.996

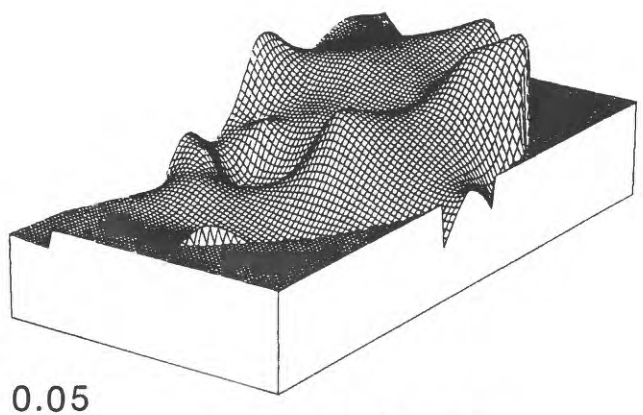

0.05

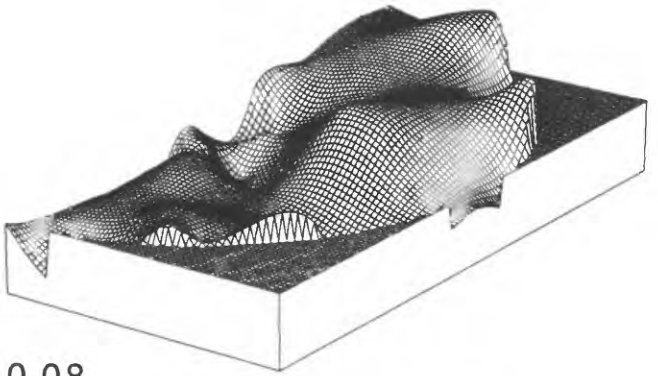

0.08

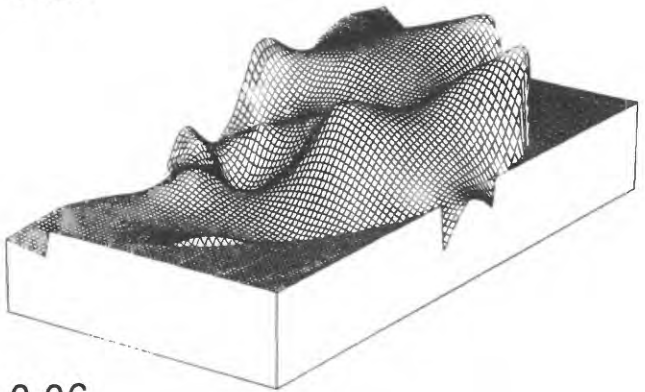

0.06

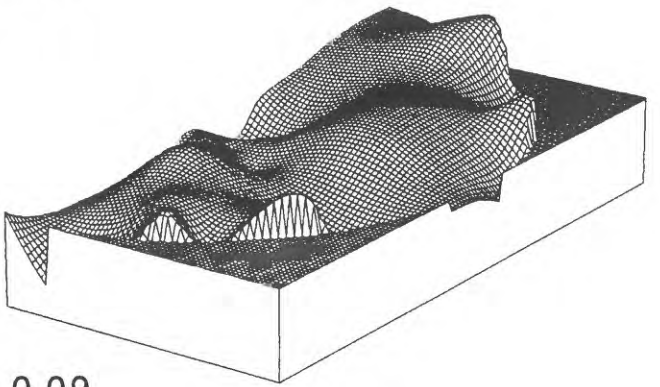

0.09

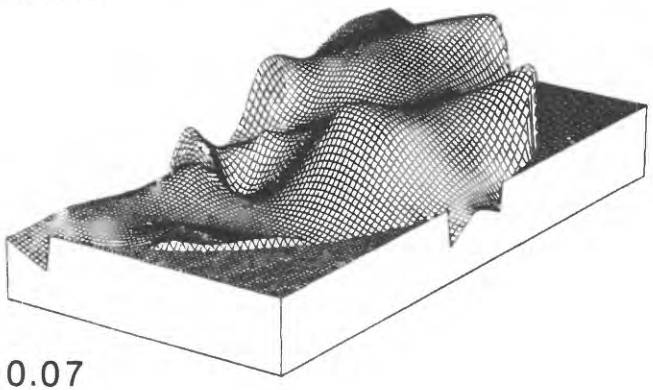

0.07

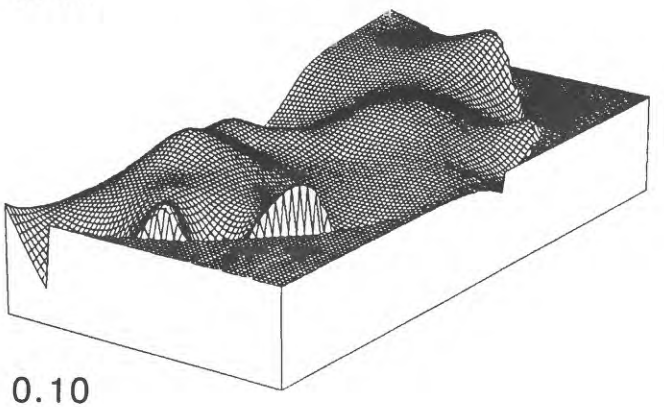

0.10

Figure 58. Snapshots of the vertical components of ground velocity over the surface encompassed by the second array. The sequence starts at 88 35 22 34 2.996 GMT and samples the elastic wavefield at constant intervals of 0.1 s during the gas-piston event depicted in Figures 25-28 (continued in Fig. 59).

88 35 22 34 2.996

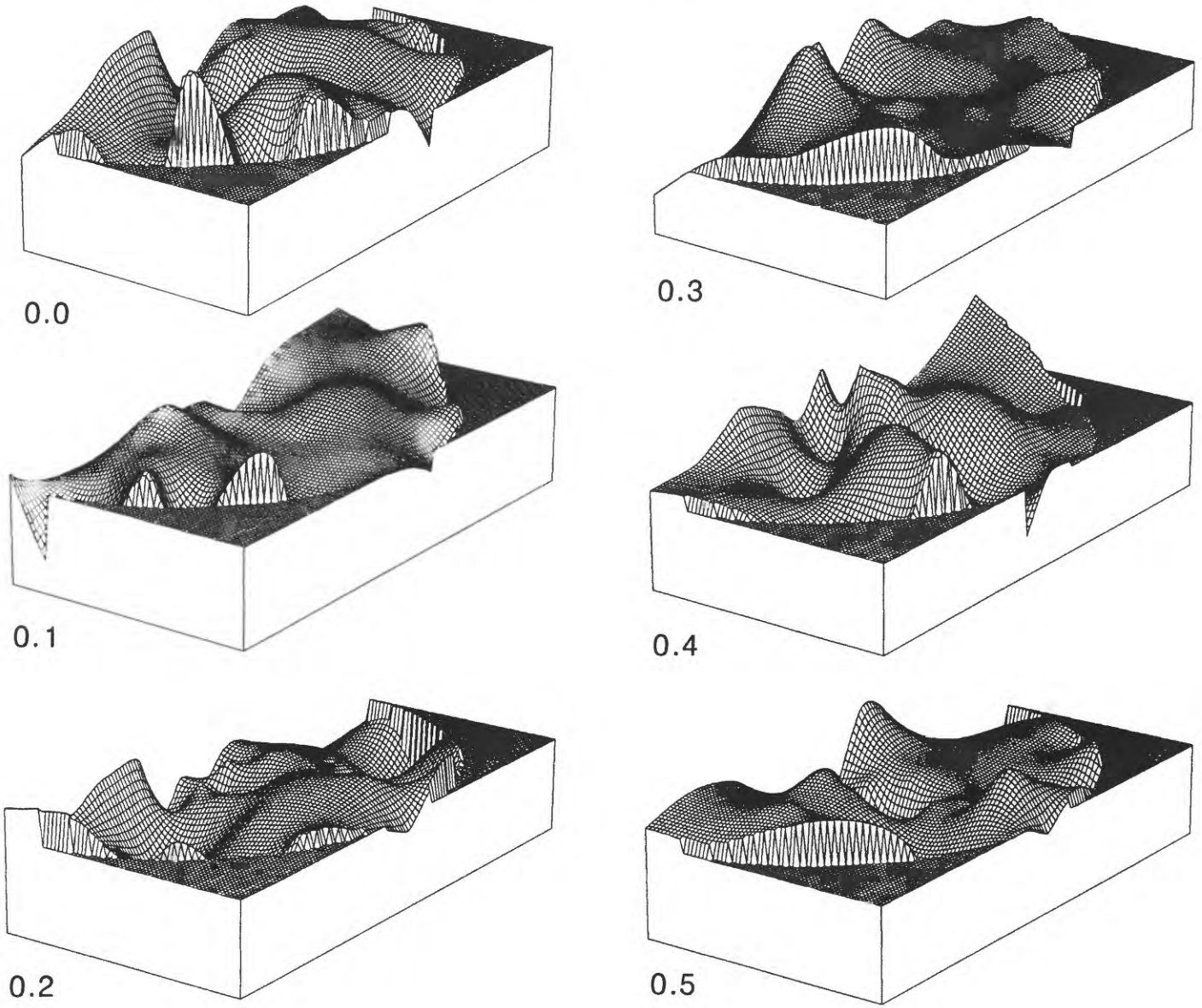

Figure 59. Continuation from sequence shown in Figure 58. The sequence starts with the last snapshot of Figure 58 at 88 35 22 34 2.996 + 0.5 and ends 0.5 seconds later.

88 35 22 34 2.996

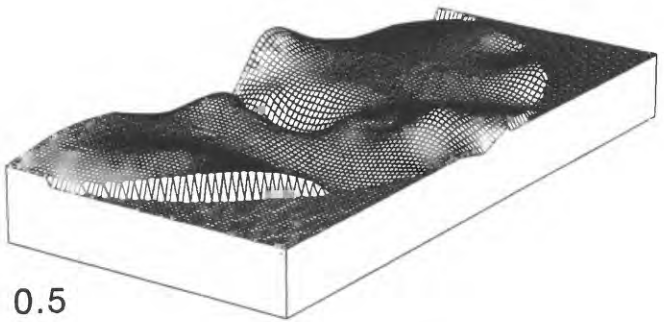

0.5

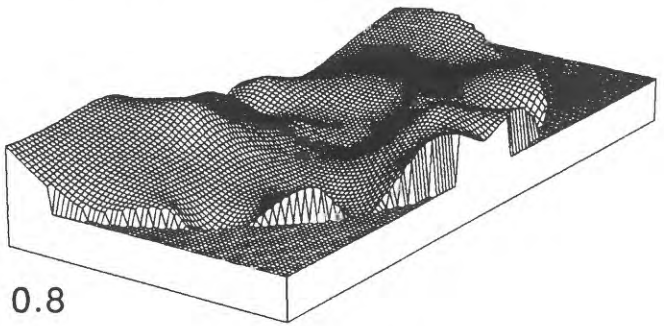

0.8

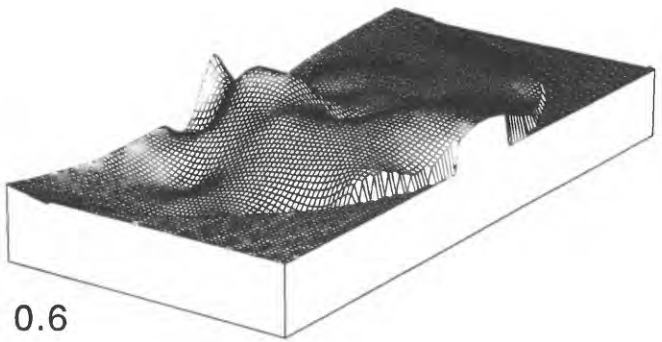

0.6

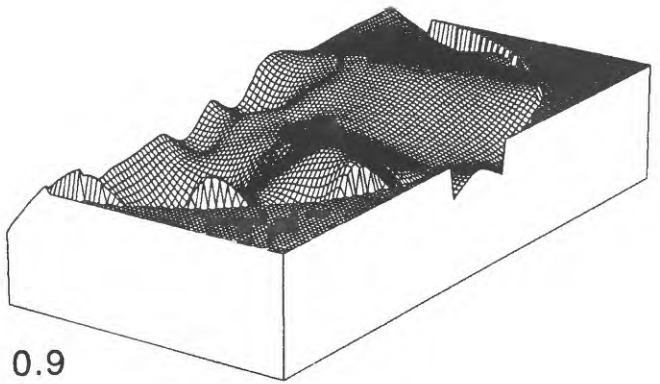

0.9

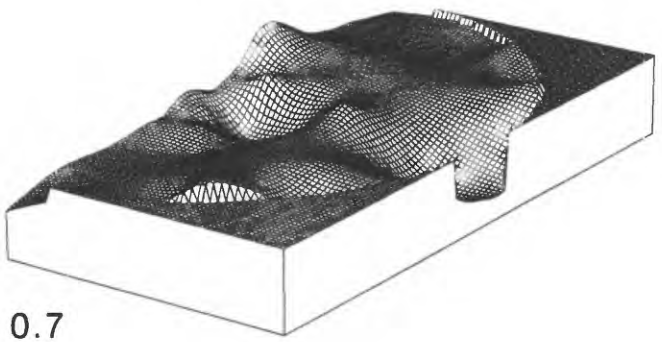

0.7

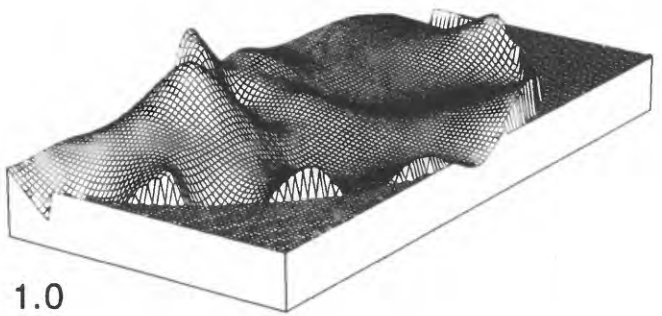

1.0

Figure 60. Continuation from sequence shown in Figure 59. The sequence starts with the last snapshot of Figure 59 at 88 35 22 34 2.996 + 1.0 and ends 0.5 seconds later.

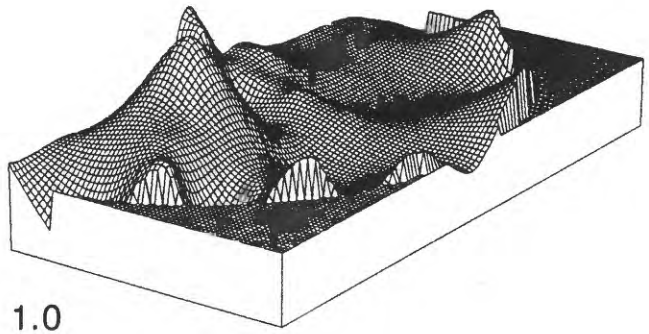

1.0

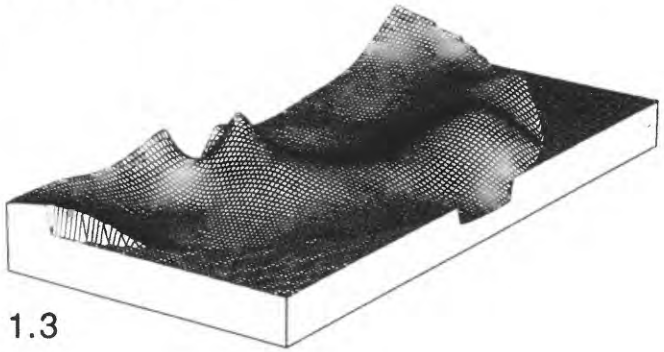

1.3

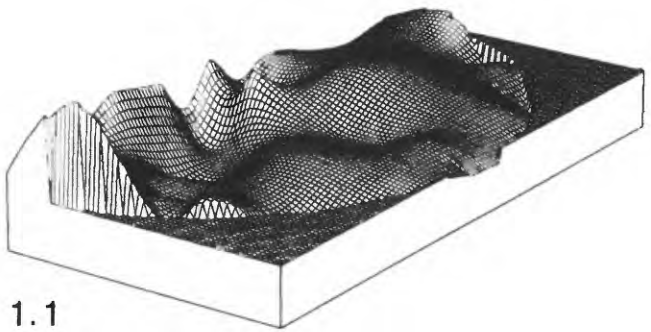

1.1

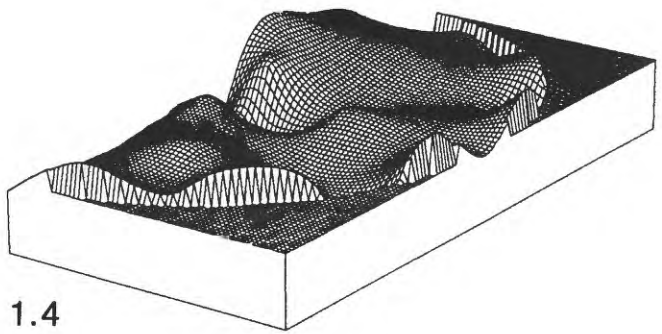

1.4

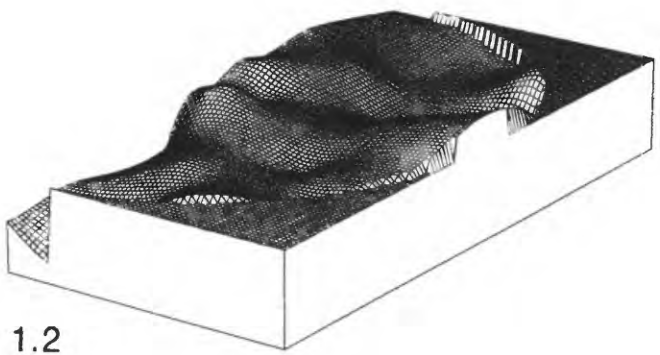

1.2

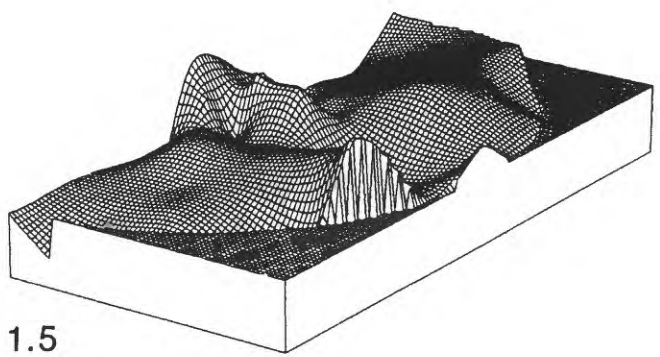

1.5

Figure 61. Continuation from sequence shown in Figure 60. The sequence starts with the last snapshot of Figure 60 at 88 35 22 34 2.996 + 1.5 and ends 0.5 seconds later.

88 35 22 34 2.996

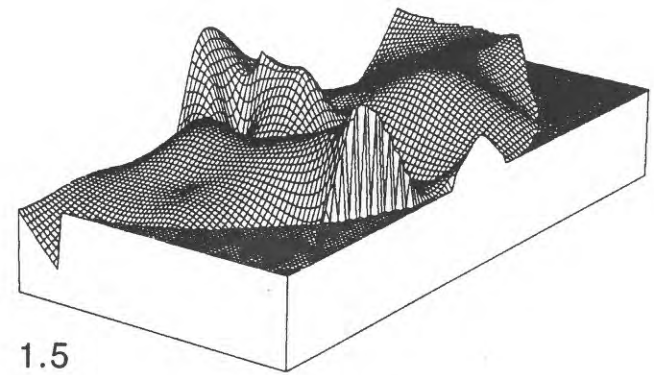

1.5

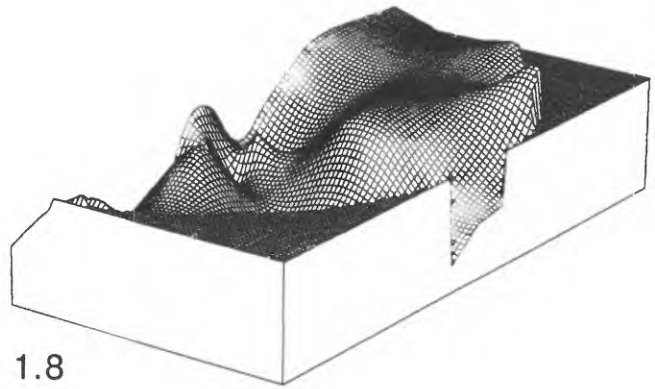

1.8

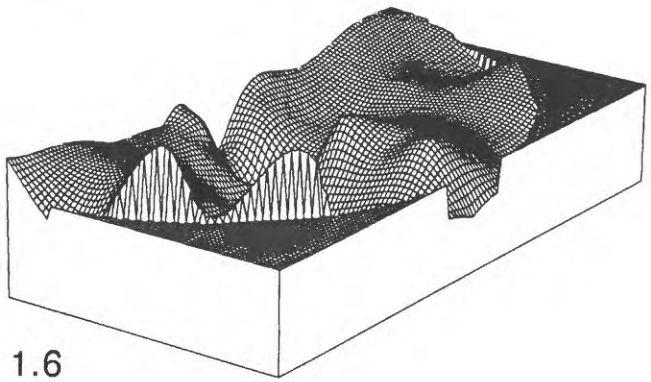

1.6

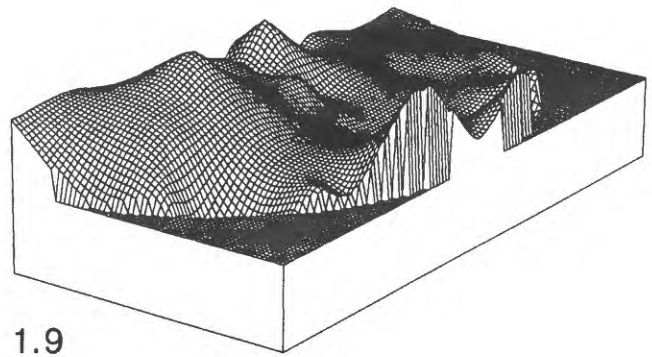

1.9

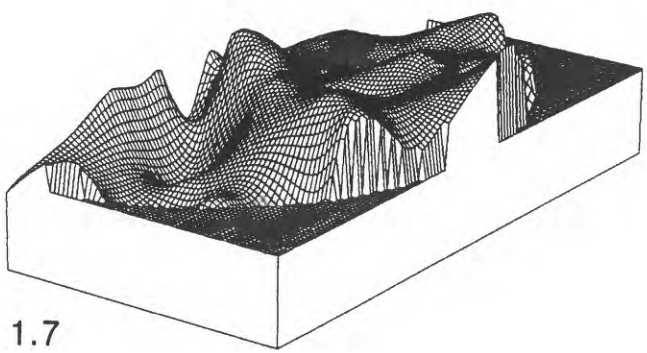

1.7

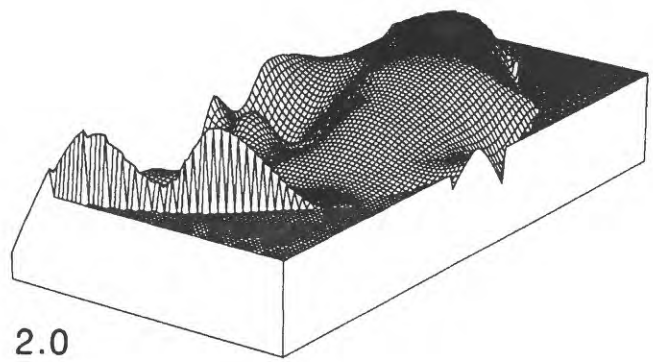

2.0

Figure 62. Continuation from sequence shown in Figure 61. The sequence starts with the last snapshot of Figure 61 at 88 35 22 34 2.996 + 2.0 and ends 0.5 seconds later.

88 35 22 34 2.996

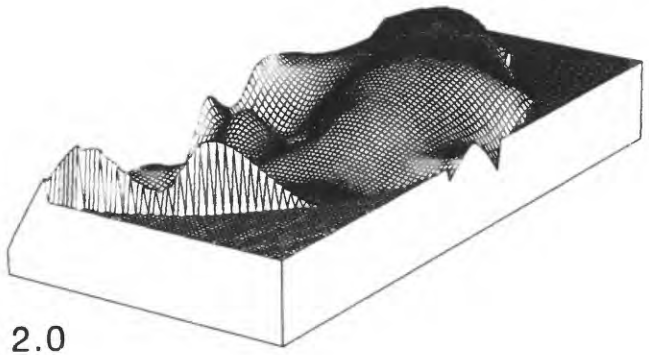

2.0

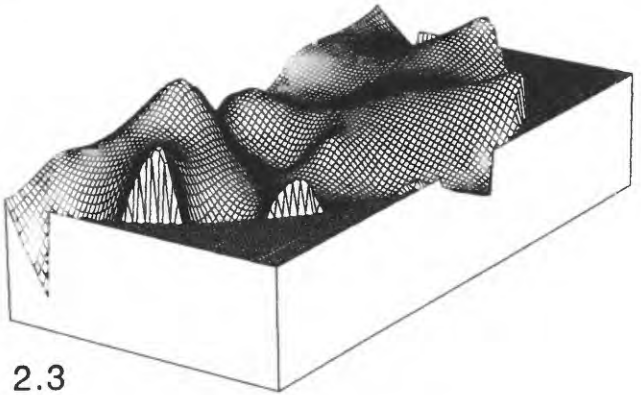

2.3

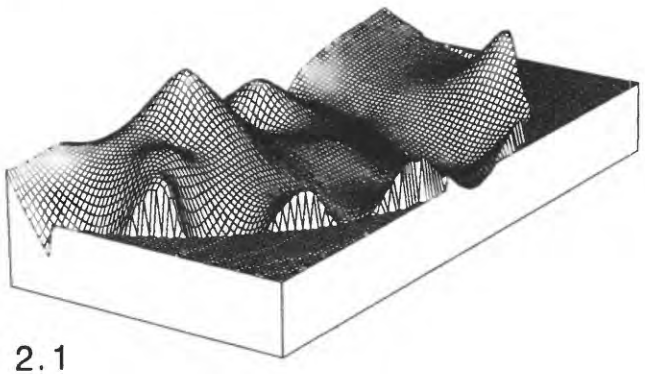

2.1

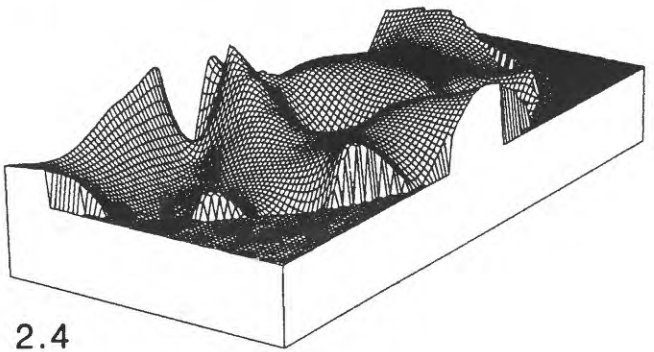

2.4

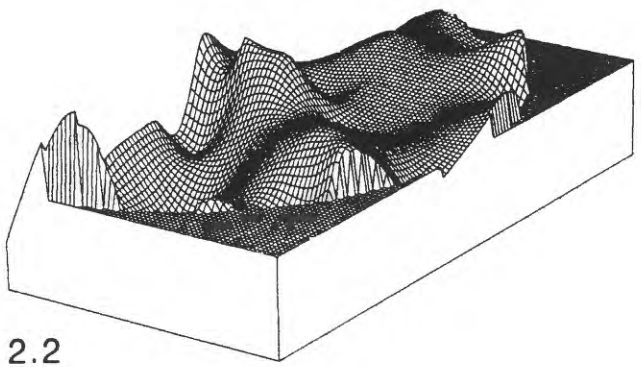

2.2

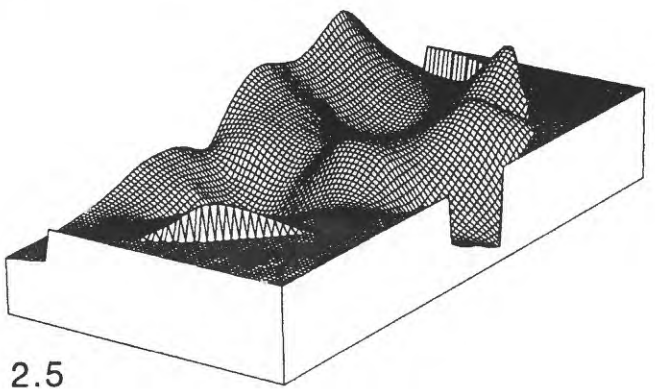

2.5

Figure 63. Continuation from sequence shown in Figure 62. The sequence starts with the last snapshot of Figure 62 at 88 35 22 34 2.996 + 2.5 and ends 0.5 seconds later.

88 35 22 34 2.996

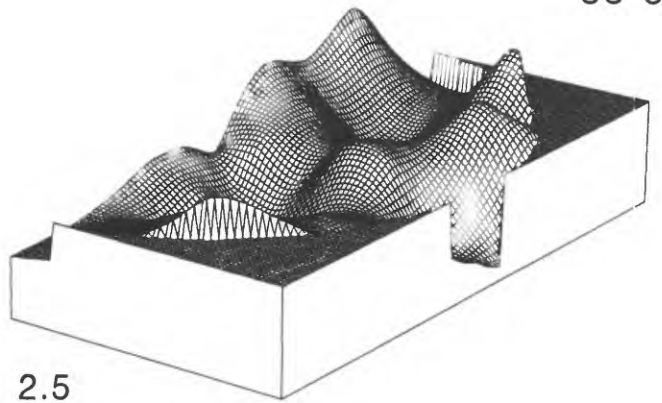

2.5

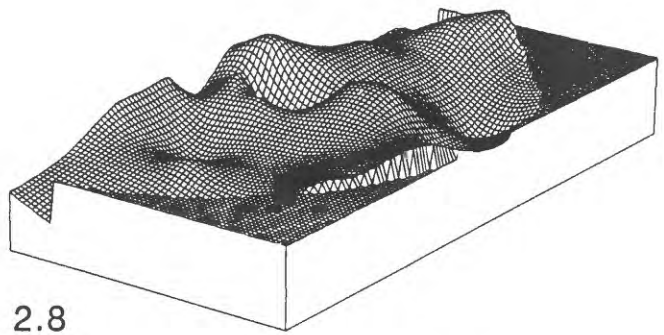

2.8

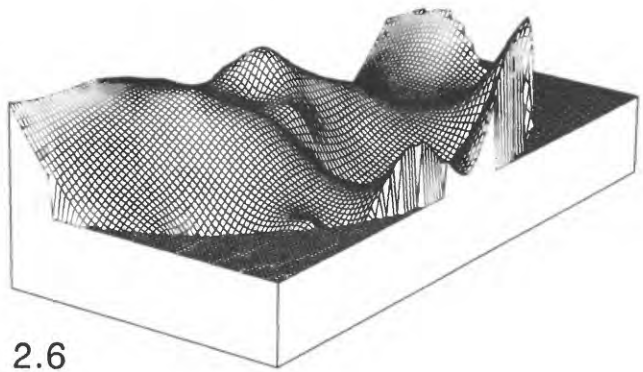

2.6

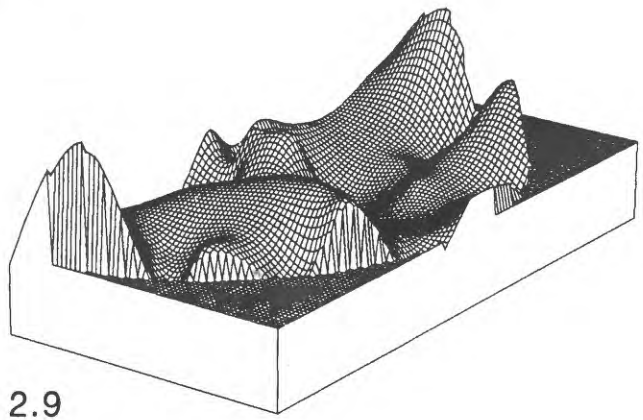

2.9

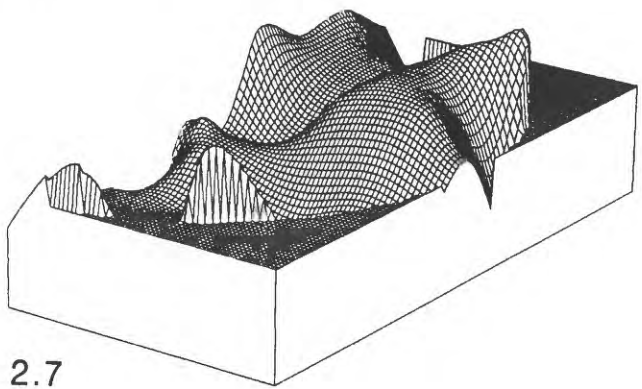

2.7

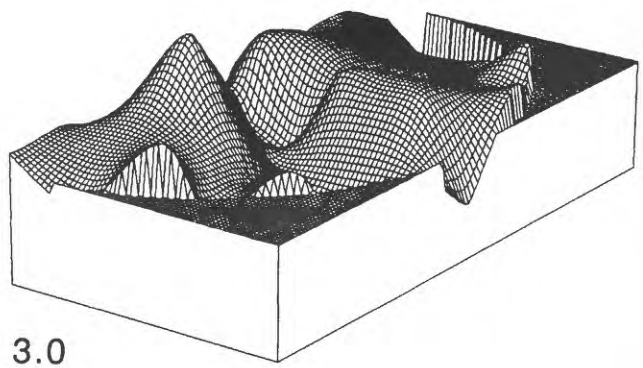

3.0

Figure 64. Three-component velocity seismograms recorded at station OUT near the south rim of Kilauea Caldera (see Fig. 1) showing 31 seconds of a Long-Period Caldera (LPC) event.

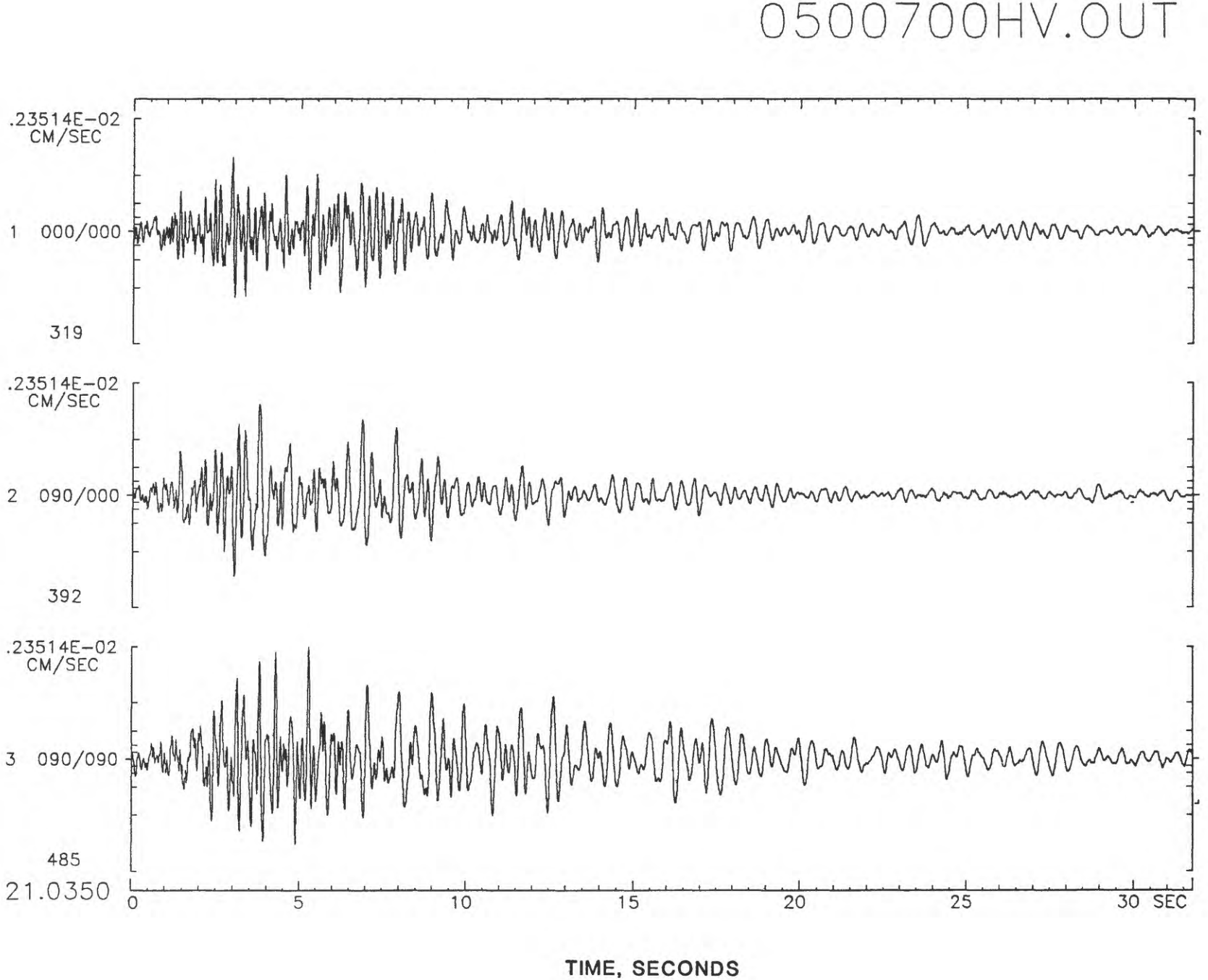
0500700HV.OUT
.23514E-02
CM/SEC
1 000/000
319
.23514E-02
CM/SEC
2 090/000
392
.23514E-02
CM/SEC
3 090/090
485
21.0350
0
5
10
15
20
25
30 SEC
TIME, SECONDS

Figure 65. Three-component velocity seismograms recorded at station OUT near the south rim of Kilauea Caldera (see Fig. 1) showing 22 seconds from a 90-minute window of low-amplitude shallow tremor.

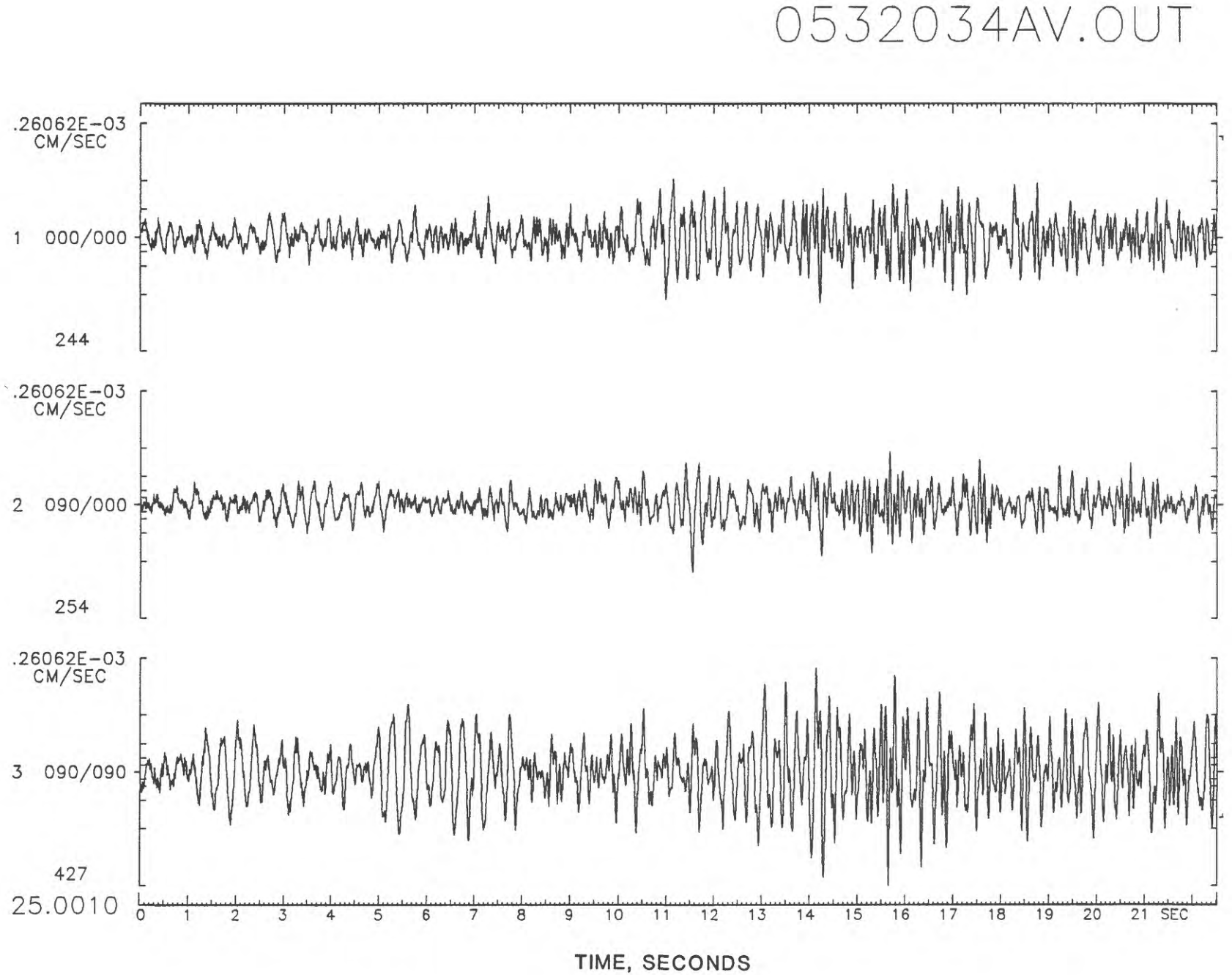
0532034AV.OUT
.26062E-03
CM/SEC
1 000/000
244
.26062E-03
CM/SEC
2 090/000
254
.26062E-03
CM/SEC
3 090/090
427
25.0010
0 1 2 3 4 5 6 7 8 9 10 11 12 13 14 15 16 17 18 19 20 21 SEC
TIME, SECONDS

Figure 66. Record section showing 30 seconds of ground velocity for a M 2.8 earthquake recorded on the four GEOS summit stations (see Fig. 1). Each trace is labeled at the left with its 3-letter station code followed by a number identifying the component of motion, where 1 is vertical motion, 2 is north-south horizontal motion, and 3 is east-west horizontal motion.

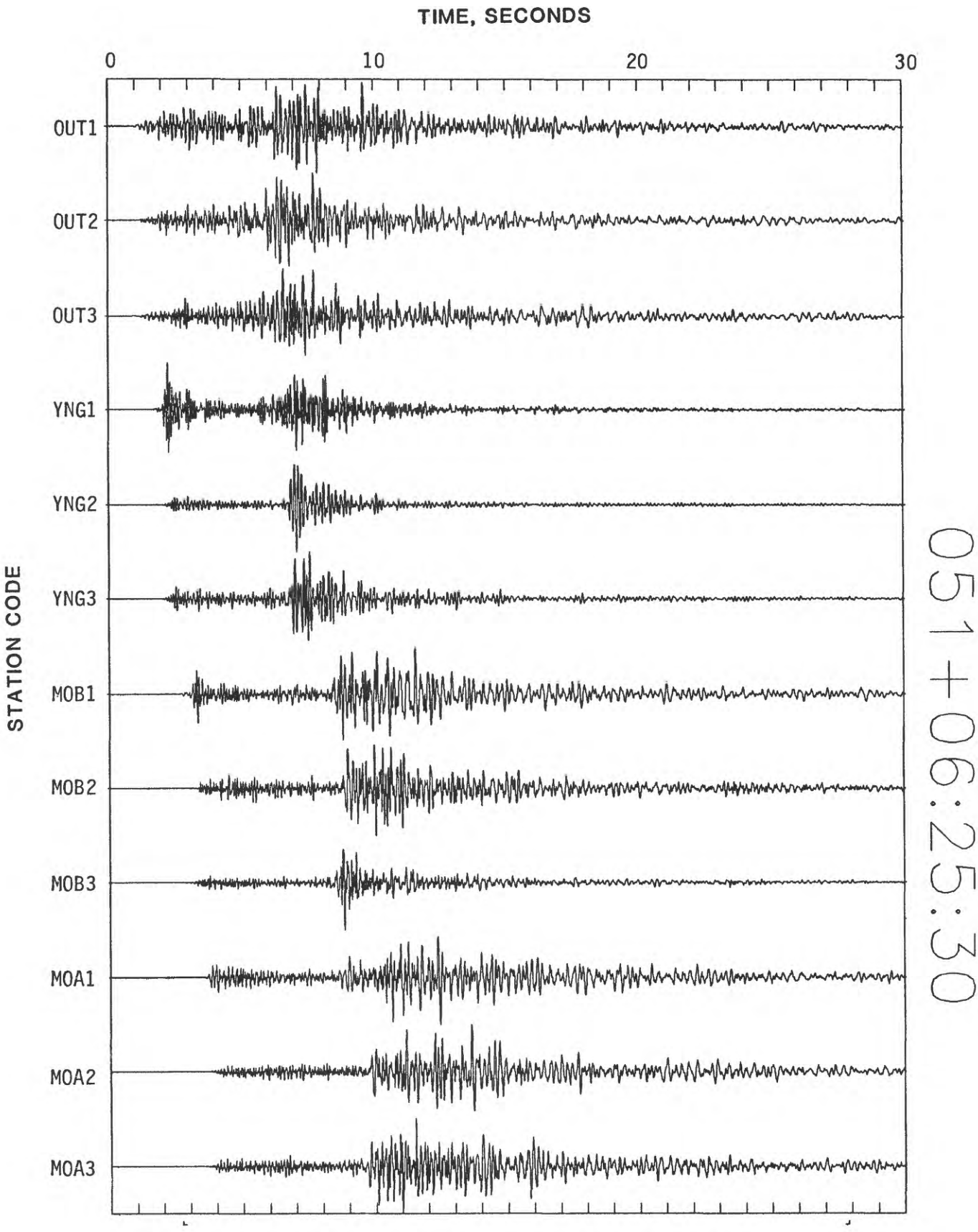
TIME, SECONDS
0
10
20
30
STATION CODE
OUT1
OUT2
OUT3
YNG1
YNG2
YNG3
MOB1
MOB2
MOB3
MOA1
MOA2
MOA3
051 +06:25:30

Figure 67. Map showing the epicenters of 28 earthquakes taken from an HVO CUSP listing and correlated with earthquakes recorded on at least three of the four GEOS summit stations. The M 2.1 earthquake listed in Table 12 (59:14:37 GMT) falls outside the map boundary.

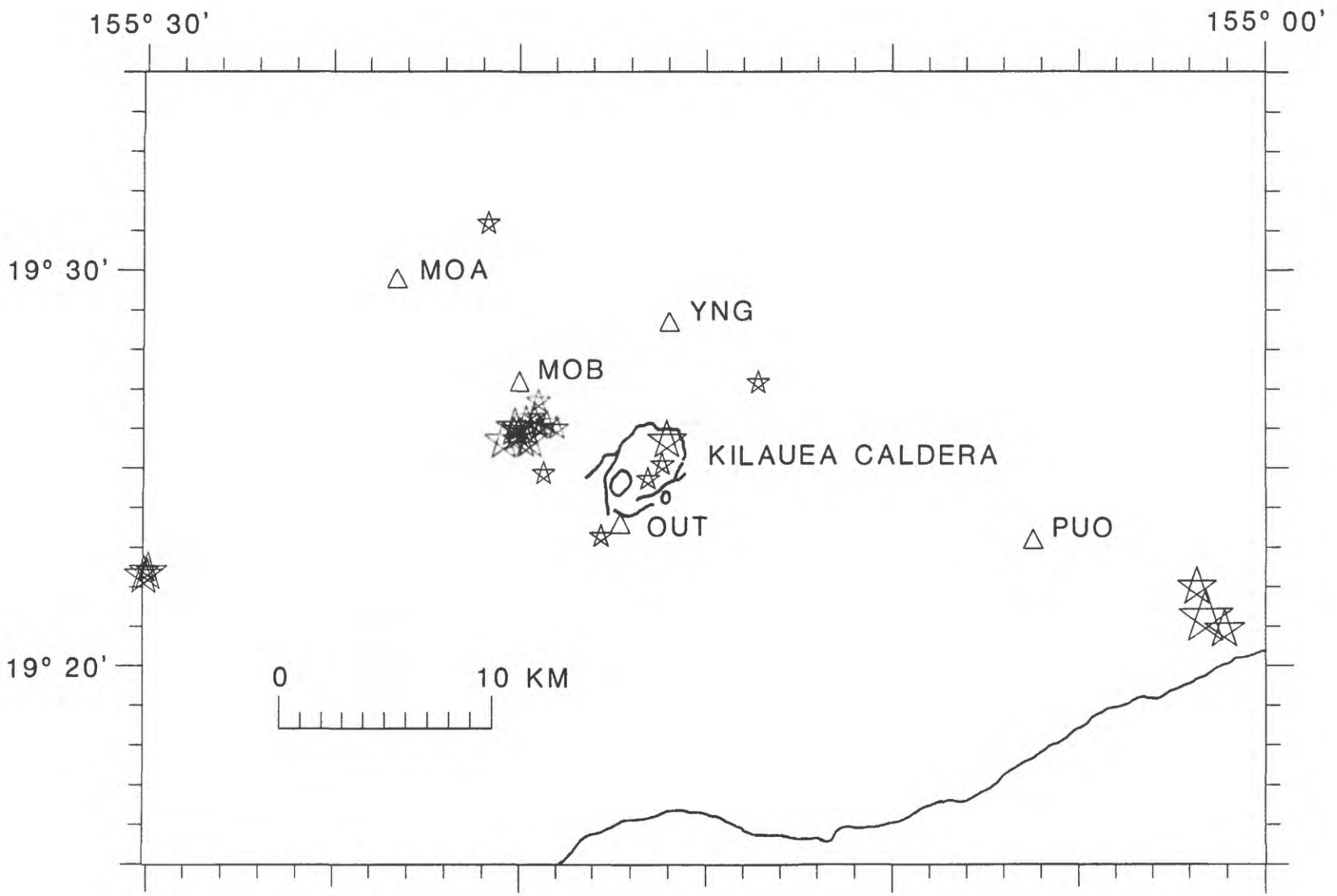
155° 30'
155° 00'
19° 30'
19° 20'
MOA
YNG
MOB
KILAUEA CALDERA
OUT
PUO
0
10 KM

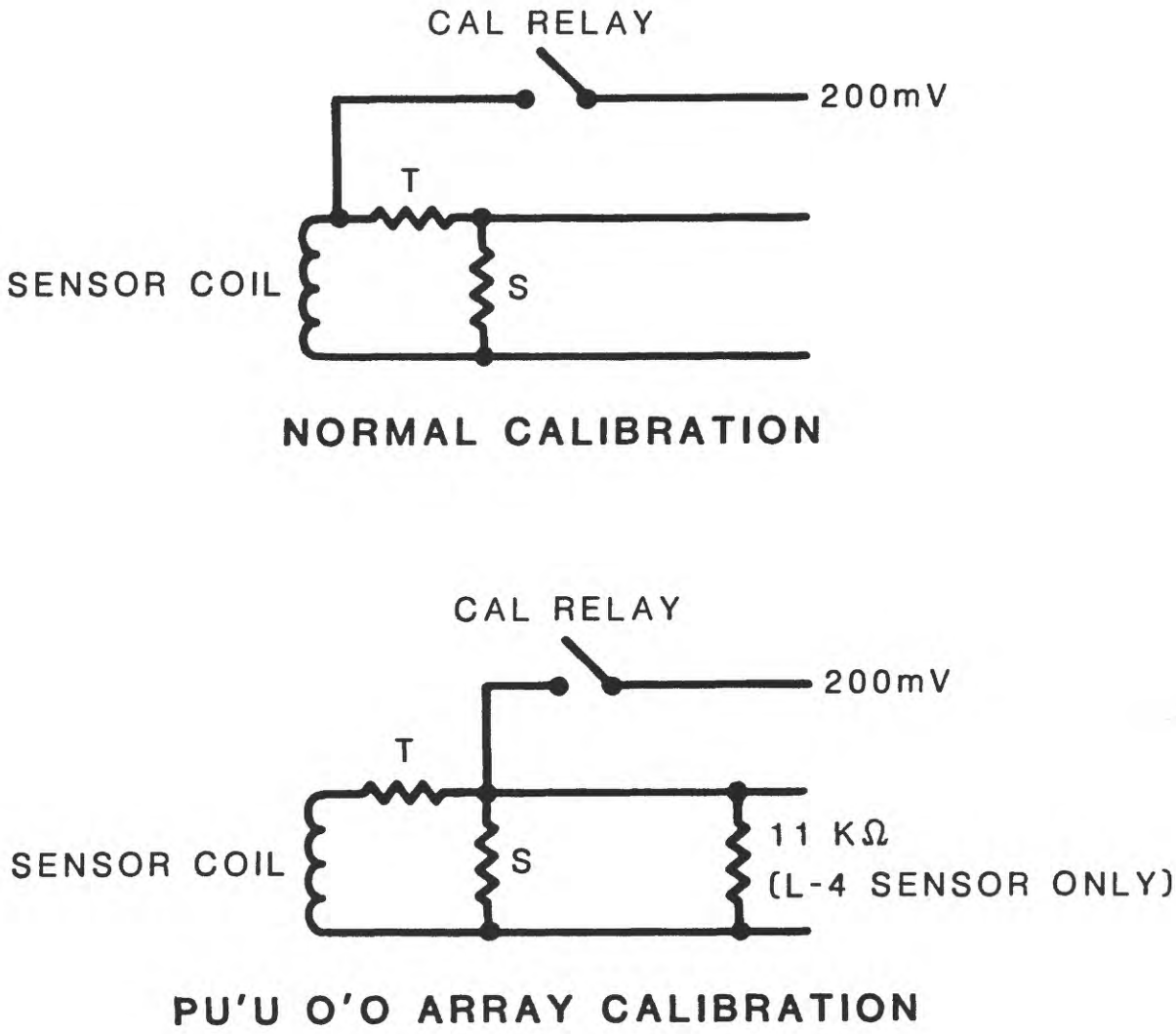

Figure 68. Schematic diagrams showing the position of the S and T shunt resistors in relation to the sensor coil for the GEOS instruments, and showing the locations of the GEOS calibration input signal for normal calibration (top) and for the Pu'u O'o array calibration (bottom).

Figure A1. Side and front panel view of the General Earthquake Observation System (GEOS) with two set of three-component sensors, and a WWVB antenna (cylinder between sensors and GEOS).

Figure A2. Left: Fourier amplitude spectra of the recorder-sensor velocity response for stations J1, J2, and J3 (top to bottom) of the second array deployed near Pu'u O'o. Right: Fourier amplitude spectra of recorder response on the three channels of the GEOS unit at stations J1, J2, and J3 (top to bottom).

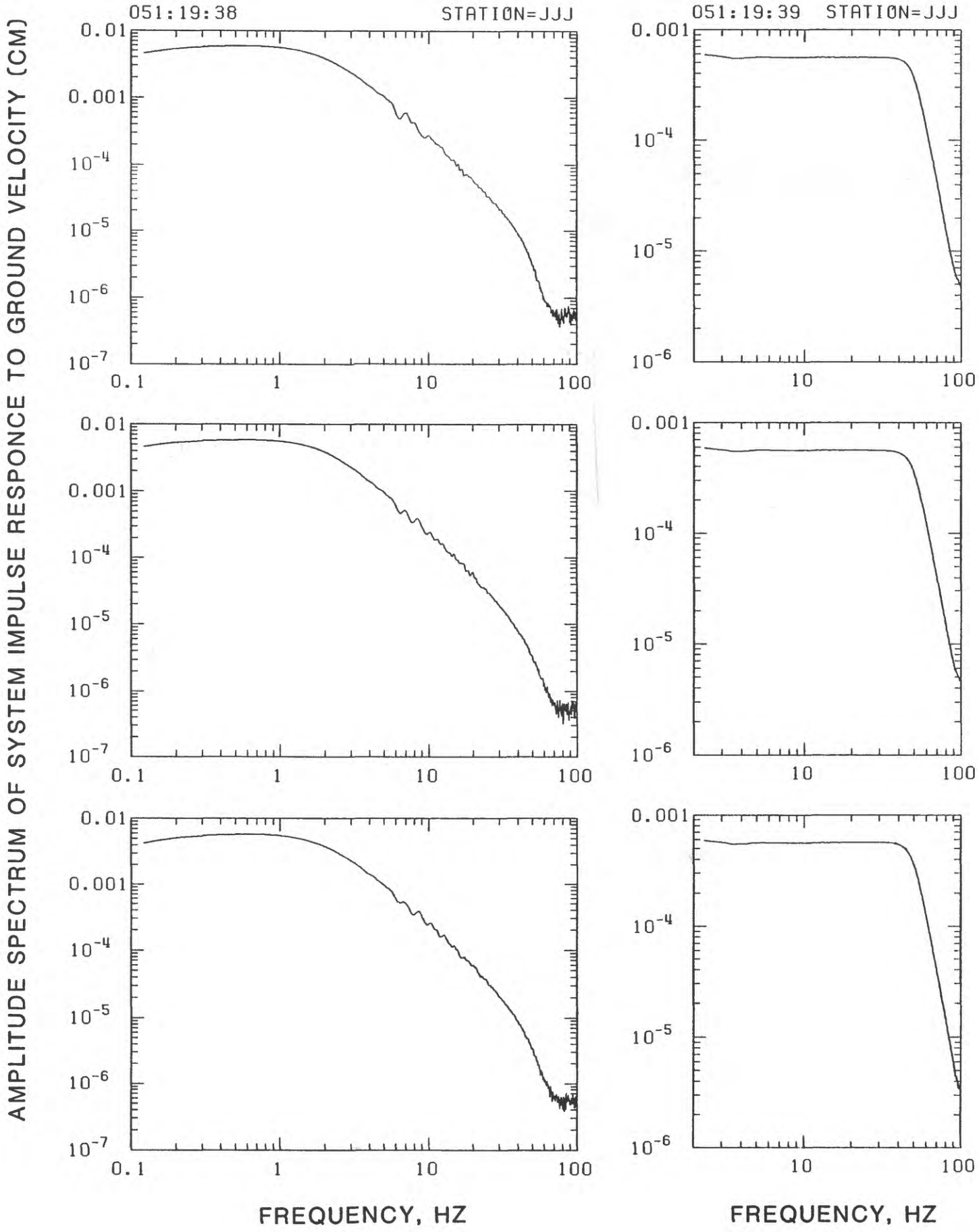
051:19:38 STATION=JJJ
051:19:39 STATION=JJJ
AMPLITUDE SPECTRUM OF SYSTEM IMPULSE RESPONCE TO GROUND VELOCITY (CM)
0.01
0.001
10^{-4}
10^{-5}
10^{-6}
10^{-7}
0.1
1
10
100
FREQUENCY, HZ
FREQUENCY, HZ